

AD-A080 368

AIR FORCE INST OF TECH WRIGHT-PATTERSON AFB OH SCHOO--ETC F/G 17/8
PHASE SEQUENCE ESTIMATION FOR LASER LINE-SCAN IMAGERY IN THE PR--ETC(U)
DEC 79 D E MEER

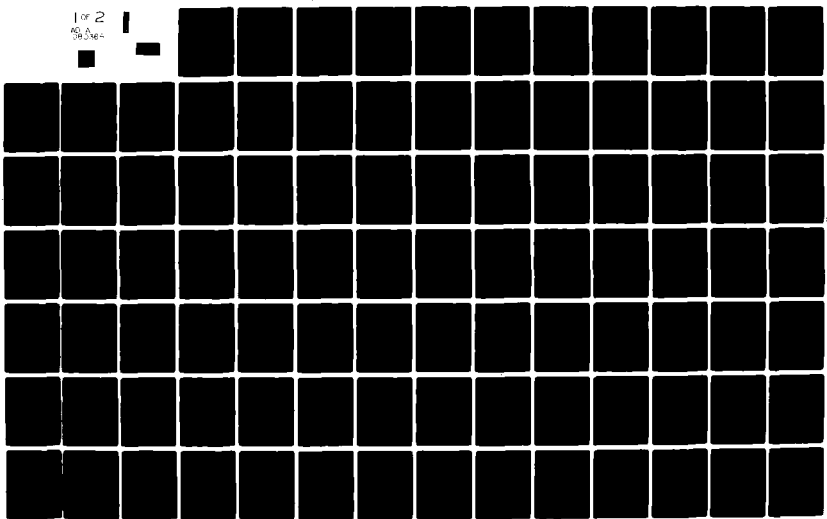
UNCLASSIFIED

AFIT/6E/EE/79D-24

NL

1 of 2

80 01 04



AFIT/GE/EE/79D-24

6 PHASE SEQUENCE ESTIMATION FOR LASER
LINE-SCAN IMAGERY IN THE
PRESENCE OF RAYLEIGH FADING.

9 Master's THESIS,

14 AFIT/GE/EE/79D-24

10
David E. Meer
Captain USAF

11 Dec 79

12 126

Approved for public release; distribution unlimited.

012225

AFIT/GE/EE/79D-24

PHASE SEQUENCE ESTIMATION FOR LASER
LINE-SCAN IMAGERY IN THE
PRESENCE OF RAYLEIGH FADING

THESIS

Presented to the Faculty of the School of Engineering
of the Air Force Institute of Technology

Air University

in Partial Fulfillment of the
Requirements for the Degree of
Master of Science

by

David E. Meer, B.S.E.E.

Captain USAF

Graduate Electrical Engineering

December 1979

Approved for public release; distribution unlimited

Preface

This study was prompted by a phase estimation problem of a fading signal in a laser line-scan imagery system. The system is sponsored by the Air Force Avionics Laboratory and it is designed to produce a three dimensional image of the ground surface when operated from an aircraft.

The problem of nonlinear phase estimation in a fading environment is quite general and there are possible applications in many areas for a phase estimator which is insensitive to amplitude fluctuations. The wide application of this estimation problem has made it particularly interesting and stimulating to me.

I would like to extend my thanks to my thesis advisor, Capt. Stanley Robinson, PhD, MSEE, BSEE, for his guidance and assistance on this project over the last nine months; and to my committee members Professor Peter Maybeck, PhD, BSEE, and Major Gary Reid, PhD, MS, BS for their very useful comments and suggestions. A very special thank you is also due my wife, Maripat, for her time, encouragement, suggestions, and typing throughout this project. Her help has meant a great deal to me.

David E. Meer

Contents

Preface	ii
List of Figures	v
Abstract.viii
I. Introduction	1
Background	2
Phase Estimation Problem	3
Methods of Phase Detection	6
Scope and Assumptions.	7
Overview	7
II. Theoretical Background	8
Signal Model	8
Optical Detector Output	8
Signal Model.	12
Phase Statistics.	13
Phase Sequence Estimation	17
Viterbi Algorithm.	21
III. Performance Analysis	26
Mean-Squared Error	26
Probability of Error Path.	34
Minimum Free Distance.	36
Linear Phase Transition	37
Step Transition	43
Random Variable Amplitude.	47
Linear Phase Transition	53
Step Phase Transition	54
Bias	57
Performance Analysis Comments.	60
IV. Estimator Simulation	61
Simulation Setup	61
Simulation Results	65
Confidence of Sample Statistics	65
Sample Estimation	67
Ambiguous Decisions	72
Parameter Variations.	72

V.	Comparison with Other Estimators	95
	Cramer Rao Lower Bound	95
	Phase-Locked-Loop, Constant Amplitude.	98
	Phase-Locked-Loop, Rayleigh Amplitude.	100
	Comments	100
VI.	Implementation Considerations.	103
	Storage Requirements	103
	Complexity	104
	Modulo- 2π Data Interpretation.	105
VII.	Conclusions and Recommendations.	108
	Conclusions.	108
	Recommendations for Further Study.	110
	Bibliography.	112
	Vita.	114

List of Figures

Figure

1	Geometry of the Laser Line-scan System	3
2.	Block Diagram of Laser Line-scan Imagery System. .	4
3.	Shifted Spectrum of Terrain Information.	10
4.	Quadrature Demodulator	18
5.	Phase Trellis, $M=5$	27
6.	Error Event.	33
7.	Minimal Error Path β	39
8.	Predicted MSEN, Linear Transition, Constant A. . .	41
9.	Lower Bound on MSEN, Linear Transition, Constant A	42
10.	Predicted MSEN, Linear Transition, Constant A. . .	44
11.	Lower Bound on MSEN, Linear Transition, Constant A	45
12.	Predicted MSEN, Step Transition, Constant A. . . .	48
13.	Lower Bound on MSEN, Step Transition, Constant A .	49
14.	Predicted MSEN, Step Transition, Constant A. . . .	50
15.	Lower Bound on MSEN, Step Transition, Constant A .	51
16.	Predicted MSEN versus M , Linear Transition, Random Variable A	55
17.	Predicted MSEN versus \bar{E}/N_0 , Linear Transition, Ran- dom Variable A	56
18.	Predicted MSEN versus M , Step Transition, Random Variable A	58
19.	Predicted MSEN versus \bar{E}/N_0 , Step Transition, Ran- dom Variable A	59
20.	Tactical Phase Signal	63

21.	Number of Runs	66
22.	Sample Estimation	68
23.	Ensemble Mean-Squared Error	69
24.	Sample Estimation	70
25.	Ensemble Mean-Squared Error	71
26.	MSEN, Varying Levels, A, ϕ	74
27.	MSEN, Varying Levels, ϕ, A_c	75
28.	MSEN versus E/N_0 , Varying Levels, Tactical ϕ, A .	76
29.	MSEN versus \bar{E}/N_0 , Varying Levels, Tactical ϕ, A_c .	77
30.	MSEN, Varying VARPH, ϕ, A	79
31.	MSEN, Varying VARPH, ϕ, A_c	80
32.	MSEN, Varying VARPH, Tactical ϕ, A	81
33.	MSEN, Varying VARPH, Tactical ϕ, A_c	82
34.	MSEN, Varying Depth, A, ϕ	84
35.	MSEN, Varying Depth, A_c, ϕ	85
36.	MSEN, Varying Depth, A Tactical ϕ	86
37.	MSEN, Varying Depth, A_c Tactical ϕ	87
38.	MSEN, Varying Coherence Times, A_c, ϕ	88
39.	MSEN, Varying Coherence Times, A_c , Tactical ϕ . . .	89
40.	MSEN versus \bar{E}/N_0 , In Phase Amplitude Estimation Disturbance	91
41.	MSEN versus \bar{E}/N_0 , Quadrature Amplitude Estimation Disturbance	92
42.	MSEN versus \bar{E}/N_0 , Correlated Phase, Varying VARPH, A_c	93
43.	CR Lower Bound and ML Estimator Performance . . .	97
44.	Simulated Estimator Performance versus PLL, Con- stant A	99

45.	Simulated Estimator Performance versus PLL, Slowly Fading A	101
46.	Display Mapping Functions	106

Abstract

An airborne laser line-scan imaging system can determine the relative range to a target by power modulating the illuminating laser and detecting the relative phase of the reflected signal with respect to the modulation phase reference. The amplitude of the reflected signal may fluctuate greatly due to such factors as speckle noise and the varying reflectivity of the target, resulting in the severe degradation of performance of commonly used phase detection circuitry.

In this report, a maximum-a posteriori (MAP) phase sequence estimator is developed based upon the Viterbi algorithm. The signal is observed in additive, zero mean, white Gaussian noise and the statistics of the amplitude are assumed to be Rayleigh. Perfect knowledge of each realization of the signal amplitude is assumed and the sensitivity to errors in the amplitude estimate is investigated. Expressions for approximate mean-squared error and a lower bound on mean-squared error are developed and verified by a Monte Carlo simulation of the estimator.

For quantization of the phase estimates to 15 levels and for a signal with constant amplitude, the estimator outperforms a first order phase-locked loop (PLL) by 2-6 dB over the range of input signal to noise ratios of 3-17 dB.

For the case when the amplitude is rapidly fading, the

estimator outperforms a first order PLL by greater than 10 dB. This performance margin is based on the Viterbi estimator's performance for a rapidly fading signal compared to PLL performance for a slowly fading signal. Note that as the amplitude fading bandwidth of the PLL signal is increased, the PLL will lose lock completely, so that the improvement margin presented is extremely conservative.

The Viterbi estimator is shown to be insensitive to errors in the estimate of the signal amplitude for input signal to noise ratios larger than 2(3dB). The MAP sequence estimator is also shown to reduce its mean-squared error with increasing decision depth (fixed lag of the Viterbi algorithm), and increasing number of discrete phase levels. The performance depends weakly on the match between the variance of the actual phase and the variance assumed by the estimator.

PHASE SEQUENCE ESTIMATION
FOR LASER LINE-SCAN IMAGERY
IN THE PRESENCE OF RAYLEIGH FADING

I. Introduction

A laser line-scan imagery system is currently being developed by the Air Force Avionics Laboratory and the Environmental Research Institute of Michigan. It is designed for airborne use and will provide a three dimensional image of the earth's surface. Slant range information is obtained by modulating the incident laser beam with a periodic signal and then comparing the phase of the reflected signal with a known reference. The slant range to the surface (assumed to be flat earth) can be combined with the two dimensional reflected signal power image to provide intelligence data to a human operator or to automatic cueing equipment.

The signal reflected from the ground target is perturbed in amplitude by the spatially varying reflectivity of the target and speckle noise (to be defined subsequently) (Ref6:4-5).

This amplitude variation detrimentally affects phase estimation. For example, a linearized first order phase-locked-loop will lose lock as the fading bandwidth of the signal is increased (Ref 13).

The purpose of this thesis is to develop a phase estimator

which is insensitive to amplitude variations. The performance of the estimator will be calculated and results will be verified by a simulation of the estimator algorithm.

Background

The geometry of the line-scan imagery system is depicted in Figure 1. The aircraft carrying the scanning system is shown flying in the Y direction while the laser beam is swept across the ground in the X direction. When the beam reaches the end of a scan, it is pointed to the start of the next scan and a new strip of ground is illuminated as the beam scans in the X direction.

The beamwidth of the laser, speed of the aircraft, speed of the sweep, and altitude of the aircraft must be interrelated to allow the scanner to sweep contiguous strips of ground and cover the entire area. For a typical beamwidth of one milliradian (Ref3:2) and an altitude of 1000 feet, the illuminated area is a spot one foot in diameter. The time that a point is illuminated by the beam is the dwell time. If the scan length extends to 1000 feet on either side of the ground track of the aircraft, and if the aircraft has a speed of 600 knots, the dwell time is approximately 0.5 microseconds.

A block diagram of the scanner system is shown in Figure 2. The modulator provides a reference signal to the phase estimator, in addition to modulating the power of the laser source. The scan optics sweep the incident beam across a

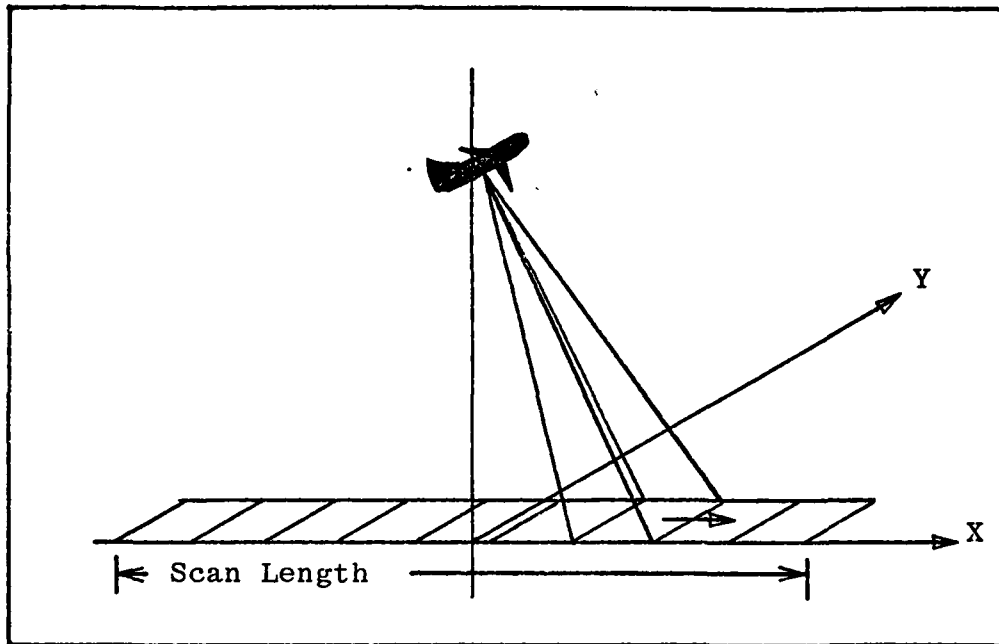


Fig. 1. Geometry of the Laser Line-Scan System

strip of ground and focus the reflected signal onto the optical detector. Either direct optical detection or heterodyne detection is suitable for the receiver, and speckle noise is present in the detected signal of each (Ref 6).

Signal processing encompasses any amplification, frequency translation, or filtering required before the signal is routed to the phase estimator and the image forming circuit.

Phase Estimation Problem

As described previously, amplitude fluctuations in the received signal adversely affect the task of phase estimation. These variations in amplitude arise from three main sources.

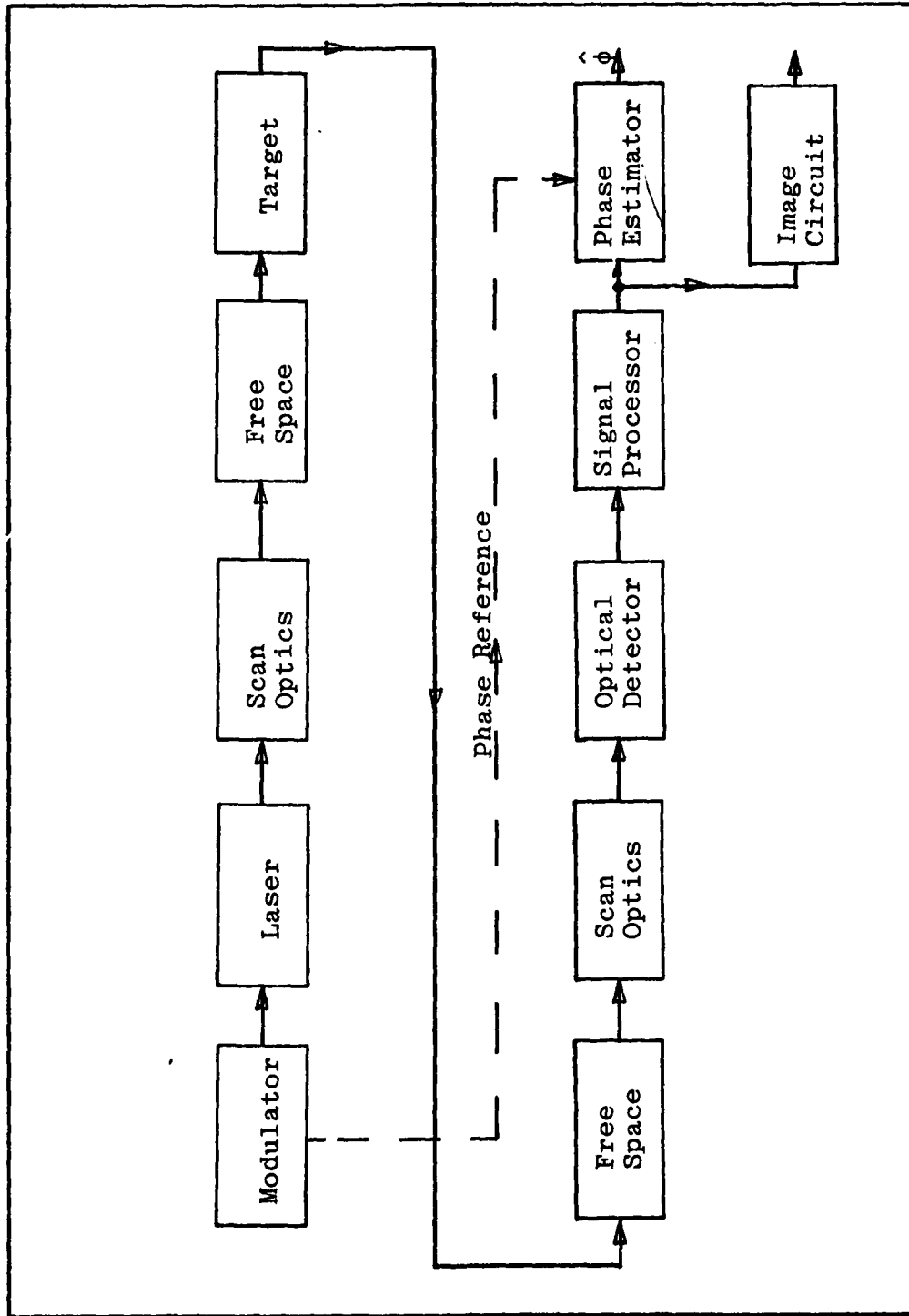


Fig. 2. Block Diagram of Laser Line-Scan Imagery System

The first is the reflectivity of the target surface. As the illuminated spot scans from lightly colored objects to dark objects, the energy in the reflected signal will vary.

The second cause of amplitude variations is speckle noise. When light is reflected from a surface which is rough with respect to the wavelength of the incident light, a random amplitude distortion is produced. When the reflected light is used for image formation, the distortion manifests itself as varying intensities across the image. This is called speckle noise (Ref 6:4-5).

The third cause of phase estimation errors is the receiver hardware itself. The signal of interest has a large dynamic range due to the reflectivity of the target and due to speckle noise. Typically, receivers designed to accommodate a large dynamic range have nonlinearities in their phase and amplitude response curves. These nonlinearities can distort the phase input to the estimator and cause additional amplitude variations. Also, amplitude modulation (AM) at the input to the receiver may be converted into phase modulation (PM) directly by AM to PM conversion.

The first two causes of estimation problems, reflectivity and speckle, are inherent in the nature of an actively illuminated system. It is essential, therefore, to use a phase estimation scheme which is robust with respect to amplitude fluctuations.

Phase estimation problems caused by imperfections in the

receiver are under the control of the system designer; however, an estimator which is insensitive to amplitude variations is still desirable. The problem of a receiver design with good amplitude and phase characteristics can be treated as a separate problem.

Methods of Phase Detection

The current system detects the zero crossings of the received signal and the reference. The relative phase is determined by measuring the time between zero crossings. This type of estimator will not operate below a threshold set by the parameters of the circuit, and there is no provision for making a "reasonable" estimate during periods when the estimator is below threshold.

Phase-locked-loop (PLL) performance is well known for phase estimation applications and it is useful as a benchmark against which other estimators can be measured. A PLL exhibits a threshold effect too, usually two to four db lower than that of a zero crossing phase estimator. Prior statistics of the phase process may be available; however, PLL estimators do not usually make use of this prior information.

Both zero crossing and PLL estimators are sensitive to amplitude fluctuations. Amplitude limiters are typically used to condition the input signal before the phase is estimated.

The phase estimator developed in this thesis is one which produces the maximum a posteriori (MAP) estimate of the phase

sequence after some fixed delay. The algorithm is an application of discrete smoothing and employs the Viterbi algorithm (dynamic programming) for actual computation of the MAP sequence.

Scope and Assumptions

In this thesis, the amplitude of the received signal will be considered a random variable with Rayleigh distribution and independent from sample to sample. The amplitude of the signal (before addition of noise) will be assumed known. Noise in the received signal will be assumed to be white and gaussian. Phase sequence estimation will be made on a scan by scan basis. The phase sequence in the X direction of Figure 1 will be assumed first order Gauss-Markov. In the Y direction, the phases are assumed independent.

Overview

This report begins with a description of the underlying system constraints and the nature of the phase estimation problem. Chapter II develops the phase model and algorithm for a MAP phase sequence estimator utilizing the Viterbi algorithm. The performance of the estimator is calculated in Chapter III and simulation results verifying the calculations are given in Chapter IV. Comparisons with the performance of other phase estimators are made in Chapter V and comments on the implementation of this estimator are given in Chapter VI. Finally, conclusions are reviewed and recommendations for further study are given in Chapter VII.

II. Theoretical Background

In this chapter, the theoretical background of a modulo- 2π MAP phase sequence estimator is presented. The material is logically divided into two sections. The first develops a model of the continuous phase process to be estimated and the discrete representation of that process. Statistics of the process are determined and an expression for the MAP likelihood of a sequence is proposed. Because the likelihood measure can be computed recursively, the sequence estimation problem can be solved efficiently through the use of the Viterbi algorithm (Ref 9). The application of the algorithm to this estimation problem is discussed in the second section of this chapter.

Signal Model

In order to develop a model of the phase process, it is useful to begin by looking at the signal available from the direct optical power detector.

Optical Detector Output. The output of a direct optical detector for the proposed system configuration can be modeled by (Ref 10:6)

$$y(t) = P_0 \int_{-\infty}^{\infty} \rho(x) b(x-vt) m\left(t - \frac{2r(x)}{c}\right) dx \quad (1)$$

where P_0 is the peak optical power including fixed optical losses, $\rho(x)$ is the terrain reflectivity including fluctuations due to speckle, $b(x)$ is the beam filtering function

(Ref 10:6), $m(t)$ is the periodic modulation function, $r(x)$ is the slant range to the target, v is the sweep velocity, and c is the speed of light. Since $m(t)$ is periodic, it can be expressed as a Fourier series expansion:

$$m(t) = \sum_{n=-\infty}^{\infty} C_n e^{j2\pi n f_m t} \quad (2)$$

where f_m is the fundamental frequency of $m(t)$ and the C_n 's are the Fourier series coefficients. By substituting equation (2) into equation (1) and taking the Fourier transform, the frequency domain expression for $Y(f)$ can be obtained.

$$Y(f) = \mathcal{F}\{y(t)\} = P_0 \sum_{n=-\infty}^{\infty} \frac{C_n}{|v|} B^* \left[\frac{f - n f_m}{v} \right] D_n \left[\frac{f - n f_m}{v} \right] \quad (3)$$

In equation (3), $B^*(f)$ is the transform of $b(x)$ and $D_n(f)$ is the transform of $\rho(x) \exp\left[\frac{j4\pi n f_m r(x)}{c}\right]$, the terrain information. The spectrum of the terrain information is shifted to multiples of f_m , the fundamental frequency of the modulation signal, as shown in Figure 3.

In general, the lobes of the spectra can overlap, causing aliasing errors; however, in this report it is assumed that there is no aliasing error. It should be noted that this assumption of no aliasing error usually implies that filters with "steep" skirts must be used in the receiver. For many

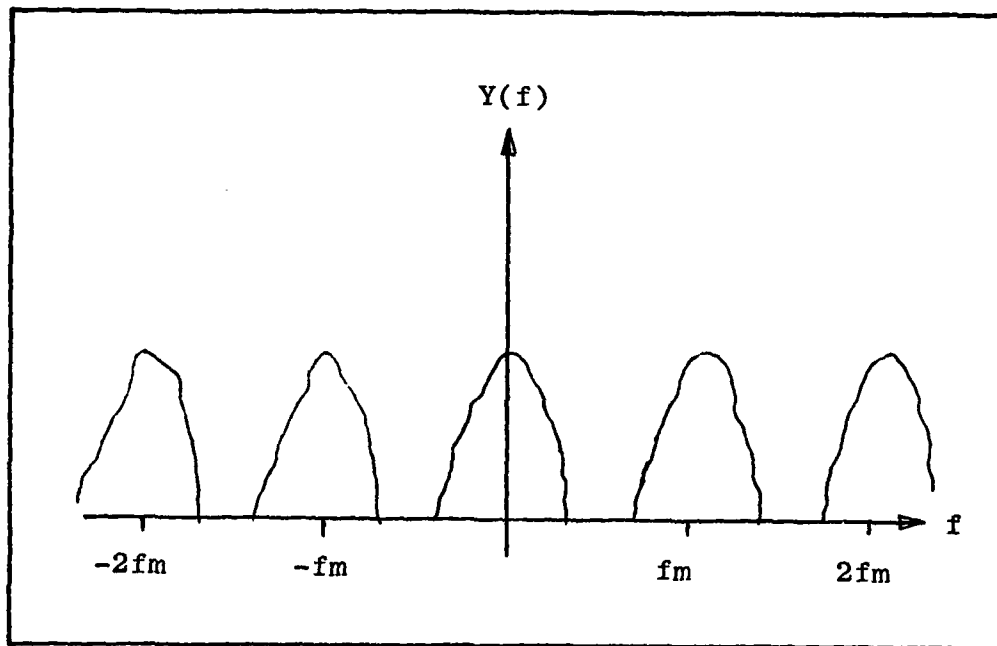


Fig. 3. Shifted Spectra of Terrain Information

analog filter designs, this means that there will be phase distortion introduced by these filters.

If the signal $y(t)$ is passed through an ideal band-pass filter centered at nf_m , the output $y'(t)$ can be described as:

$$y'(t) = P_0 \sum_{\pm n} C_n \int_{-\infty}^{\infty} \rho(x) b(x-vt) \exp \left[j2\pi n f_m \left(t - \frac{2r(x)}{c} \right) \right] dx \quad (4)$$

(Ref 10:7)

The filtered signal, $y'(t)$, can be viewed as the real part of a complex signal:

$$y'(t) = \text{Re} \left[A(t) e^{j\phi(t)} e^{j2\pi n f_m t} \right] \quad (5)$$

The complex signal can be related to equation (4) by

$$\begin{aligned}
 y'(t) &= A(t)\cos[\phi(t)+2\pi n f_m t] \\
 &= P_0 \int_{-\infty}^{\infty} \rho(x)b(x-vt) |C_n| 2\cos\left[n2\pi f_m \left(t - \frac{2r(x)}{c}\right) + \theta_n\right] dx
 \end{aligned}
 \tag{6}$$

where

$$C_n = |C_n| e^{j\theta_n} \tag{7}$$

The complex signal representation will be useful in the development of the likelihood ratio derived later in this chapter. Without loss of generality, the first harmonic of f_m can be selected so that $n=1$.

Because the modulating signal $m(t)$ is periodic, the phase $\phi(t)$ can be measured modulo- 2π with respect to the reference signal. Since the slant range to the target is calculated from $\phi(t)$, the range estimate will have an ambiguity interval of:

$$r_{\text{amb}} = \frac{c}{2f_m} \quad (\text{Ref 3:19}) \tag{8}$$

The range estimate will give a measure of the range within the ambiguity interval, but it will not describe in which ambiguity interval the absolute range lies. This fundamental limitation allows the phase to be estimated modulo- 2π with no loss of range information.

Signal Model. The signal of interest will be observed in additive white gaussian noise with a two sided power spectral density of $N_0/2$ watts per Hertz. The task is to estimate a realization, $\phi(t), t_s \leq t \leq t_f$, of the phase process based on a real measurement

$$S(t) = A(t)\cos(\phi(t)+2\pi f_m t) + N(t) \quad t_s \leq t \leq t_f + \tau \quad (9)$$

where $S(t)$ is the real measurement, $A(t)$ is the amplitude of the signal, $N(t)$ is white gaussian noise and the " \sim " denotes a random variable. The interval of the estimate is from t_s to t_f . The interval of the measurement is allowed to extend past t_f by τ seconds. By allowing the measurement interval to be longer than the interval of the estimate, the estimator can operate with a fixed lag and use smoothing to improve the estimate.

For the scanning system described in chapter I, t_s represents the start time of a scan and $t_f + \tau$ is the time at which the scan ends. In practice, an estimate of $\phi(t)$ can be made for the entire measurement interval $t_s \leq t \leq t_f + \tau$; however, the estimate of $\phi(t)$ for $t_f \leq t \leq t_f + \tau$ will not have the benefit of the full lag τ .

The continuous time model of equation (9) can be represented by the complex discrete time measurement

$$Z_k = A_k e^{j\phi_k} + N_k \quad k=1, 2, \dots, K+k_0 \quad (10)$$

where $\phi_k = \phi(t=kT)$ on the interval $(k-1)T \leq t \leq kT$, and T is the sampling interval.

The noise term in equation (11), $N_{\mathcal{U}_k}$, is a white Gaussian process which is discrete in time. It is assumed that $A(t)$ is constant over the interval $(k-1)T \leq t \leq kT$ and $A(t) = A_{\mathcal{U}_k}$ on this interval. The amplitude, $A_{\mathcal{U}_k}$, is assumed to be a random variable with Rayleigh statistics and independent from sample to sample. The effects of a correlation between adjacent amplitude samples is investigated in Chapter IV. The estimator will be developed with the assumption that the sequence of values A_k , $k=1,2,\dots,K+K_0$, is known. The question of sensitivity of the estimator to imperfect knowledge of A_k is investigated in Chapter IV.

As in the continuous case, an estimate of the sequence $\{\phi_k\}_1^K$ will be made based on the measurement sequence $\{Z_k\}_1^{K+K_0}$, where K_0 is the fixed lag. In the discussion of the Viterbi algorithm later in this chapter, the fixed lag K_0 will be referred to as the decision depth, or merely depth.

Phase Statistics. (Ref 9:8-11) In order to obtain a stationary distribution on the process $\phi(t)$, and to calculate conditional transition probabilities, let $\phi(t)$ be a random walk on the unit circle, where $\phi(t)$ can take on values from the interval $(-\pi, \pi)$. The conditional probability of a transition to $\phi(t) = \phi_t$ given that $\phi(s) = \phi_s$, $t > s$, is denoted by $p(\phi_t | \phi_s)$. This conditional density satisfies the partial differential equation (Ref 9:8)

$$\frac{\partial}{\partial t} p(\phi_t | \phi_s) = \frac{1}{2} \sigma_0^2 \frac{\partial^2}{\partial \phi_t^2} p(\phi_t | \phi_s) \quad (11)$$

where σ_0^2 is the infinitesimal variance (random walk diffusion parameter) and $-\pi \leq \phi_t, \phi_s \leq \pi, t > s$. The boundary conditions are

$$\lim_{t \rightarrow s} p(\phi_t | \phi_s) = \delta(\phi_t - \phi_s)$$

$$p(\phi_t = -\pi | \phi_s) = p(\phi_t = \pi | \phi_s) \quad (12)$$

$$\frac{\partial}{\partial \phi_t} p(\phi_t = -\pi | \phi_s) = \frac{\partial}{\partial \phi_t} p(\phi_t = \pi | \phi_s)$$

The solution for equation (11) is (Ref 9:9)

$$p(\phi_t | \phi_s) = \frac{1}{\sqrt{2\pi\sigma_0^2(t-s)}} \sum_{n=-\infty}^{\infty} \exp\left\{-\frac{(\phi_t - \phi_s - n2\pi)^2}{2\sigma_0^2(t-s)}\right\} \quad (13)$$

The process $\phi(t)$ is thus conditionally approximately gaussian with mean $\phi(s)$ and variance $\sigma_0^2(t-s)$ when $\sigma_0^2(t-s)$ is small ($E\{(\phi_t - \phi_s)^2 | \phi_s\} = \sigma_0^2(t-s)$).

The discrete time version of equation (14) can be obtained by considering the sequence $\{\phi_k\}$ arrived at by sampling $\phi(t)$ at intervals $t=kT$, $k=0,1,2,\dots,K$. The transition density from ϕ_{k-1} to ϕ_k is

$$p(\phi_k | \phi_{k-1}) = \frac{1}{\sqrt{2\pi\sigma_0^2T}} \sum_{n=-\infty}^{\infty} \exp\left\{-\frac{(\phi_k - \phi_{k-1} - 2\pi n)^2}{2\sigma_0^2T}\right\} \quad (14)$$

Since $\phi(t)$ is Markov, $\{\phi_k\}$ is a Markov sequence with a probability distribution for $\{\phi_k\}_1^K$ of

$$P_K(\{\phi_k\}_1^K) = \prod_{k=1}^K p(\phi_k | \phi_{k-1}) \quad (15)$$

The initial condition, $p(\phi_1 | \phi_0)$, may be uniform or preset to known initial condition.

In the application of the Viterbi algorithm to this estimation problem, the phase space $(-\pi, \pi)$ will be discretized into values ξ_m , $m=0, 1, \dots, M-1$. The discrete values of phase, ξ_m , will be selected with equal spacing from the interval $(-\pi, \pi)$ and M will be restricted to an odd integer. This allows the possibility of no change in the phase from the current time to the next, and the number of possible levels of phase steps in the positive and negative directions is equal.

It is necessary to calculate the transition probabilities for all M^2 pairs (ξ_j, ξ_m) , j and $m=0, 1, \dots, M-1$.

From equation (14) let

$$\bar{p}(\phi_k = \xi_m | \phi_{k-1} = \xi_j) = b p(\phi_k = \xi_m | \phi_{k-1} = \xi_j) \quad (16)$$

where b is chosen so that

$$\sum_{m=0}^{M-1} \bar{p}(\phi_k = \xi_m | \phi_{k-1} = \xi_j) = 1, \quad j=0, 1, 2, \dots, M-1 \quad (17)$$

The sum in equation (14) must be truncated at some level which

gives sufficient accuracy. If the discrete phase values are equally spaced over $(-\pi, \pi)$, then the value \bar{p} depends only on the distance between phase values $|\xi_j - \xi_m|$ modulo 2π on $(-\pi, \pi)$. Therefore, only $(M+1)/2$ values of \bar{p} need to be stored for transition probability lookup, as opposed to the M^2 number of possible transition pairs.

Scharf (Ref 9:12-13) develops the relationship between a realization, $\phi(t)$, of the continuous phase process and the discrete time realization of the process by a zero order hold (ZOH) approximation, $\phi_k = \phi(t=kT)$, $(k-1)T \leq t \leq kT$. He shows that triples $(P\{\cdot\}, \delta, T)$ can be selected so that the ZOH approximation to $\phi(t)$ is close to $\phi(t)$ where $P\{\cdot\}$ is the probability that ϕ_k differs in value from $\phi(t)$ by more than δ over the interval T . Scharf has shown that this probability is given by

$$P\{\cdot\} = 4Q\left[\frac{\delta}{\sqrt{\sigma_0^2 T}}\right] \quad (\text{Ref 9:12}) \quad (18)$$

where $Q[x]$ is the Q-function

$$Q[x] = \int_x^\infty \frac{1}{\sqrt{2\pi}} \exp(-\delta^2) d\delta \quad (19)$$

The value selected for T depends on the sampling representation of Z_k and the speed of the estimator in computing a MAP estimate. In any event, it is desired that T be less than or equal to the dwell time.

Phase Sequence Estimation. The real and imaginary parts of $Z_k = U_k + jV_k$ can be obtained from $S(t)$ by a quadrature demodulator of the form shown in Figure 4.

This is equivalent to

$$Z_k = \frac{2}{T} \int_{(k-1)T}^{kT} S(t) e^{-j2\pi f_m t} dt \quad (20)$$

As in equation (10), Z_k is the sum of the signal $A_k e^{j\phi_k}$ and white gaussian noise with a power spectral density of $N_0/2$ watts per Hertz. If A_k and ϕ_k are given and constant over the interval $(k-1)T \leq t \leq kT$, then U_k and V_k are each conditionally gaussian with zero mean and variance N_0/T (Ref 9:15). The real and imaginary parts respectively are given by

$$U_k = A_k \cos \phi_k + n_{ck} \quad (21)$$

$$V_k = A_k \sin \phi_k + n_{sk}$$

where n_{ck} and n_{sk} are the discrete time narrowband representations of the noise process $n(t)$ (Ref 14:502-504).

A likelihood function, D_K , can now be developed in order to make a MAP estimate of the phase sequence $\{\phi_k\}_1^K$. The following results are similar to those obtained by Scharf (Ref 9:14-15) but have been expanded to include the case where the amplitude of the signal, A_k , is a random variable, constant over each interval T . A different amplitude value is allowed

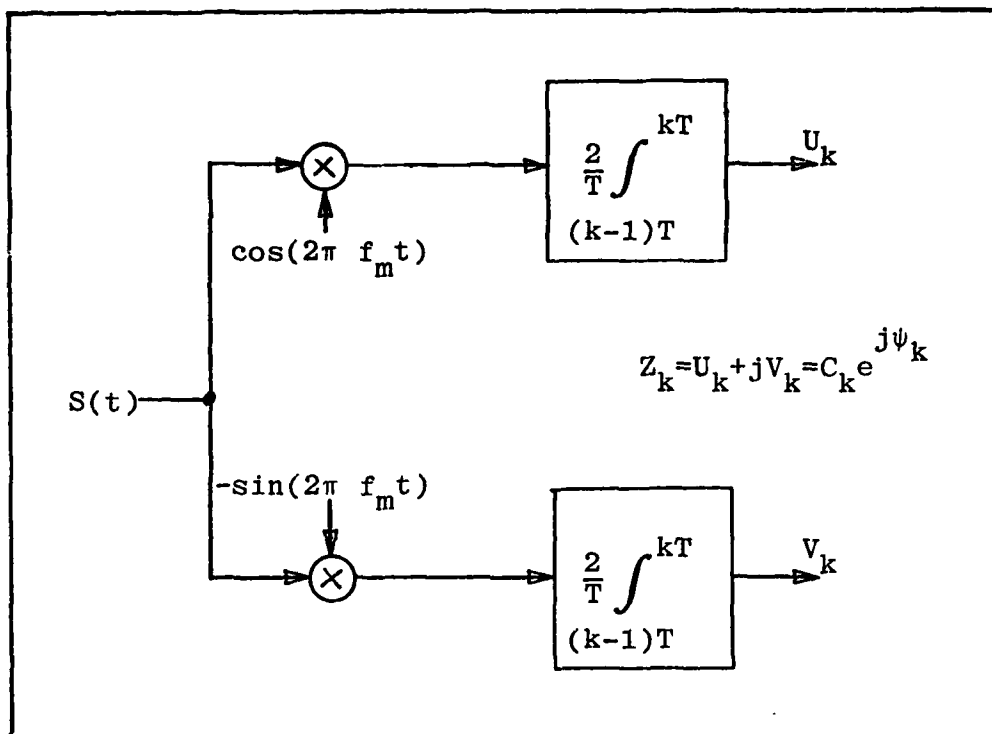


Fig. 4. Quadrature Demodulator

for each T second interval.

The likelihood function can be constructed

$$D_K = \frac{f_1(\{z_k\}_1^K | \{\phi_k\}_1^K) \prod_{k=1}^K p(\phi_k | \phi_{k-1})}{f_0(\{z_k\}_1^K)} \quad (22)$$

in which $f_1(\cdot | \cdot)$ is the joint conditional probability density of $\{z_k\}_1^K$ given the phase sequence $\{\phi_k\}_1^K$ and $f_0(\cdot | \cdot)$ is the joint conditional density of $\{z_k\}_1^K$ given only noise in the measurement.

At time kT , the conditional density of z_k given ϕ_k and A_k is

$$f(z_k | \phi_k, A_k) = \frac{1}{\sqrt{2\pi \frac{N_0}{T}}} \exp \left\{ - \frac{|z_k - A_k e^{j\phi_k}|^2}{\frac{2N_0}{T}} \right\} \quad (23)$$

and the conditional density of z_k given only noise is

$$f(z_k | \text{noise}) = \frac{1}{\sqrt{2\pi \frac{N_0}{T}}} \exp \left\{ - \frac{|z_k|^2}{\frac{2N_0}{T}} \right\} \quad (24)$$

Because the noise is white, the joint conditional densities f_1 and f_0 can be obtained by appropriate products of equations (23) and (24). The likelihood ratio (Refs 9:14 and 11:26-27) portion of equation (22) (neglecting the priors on ϕ) can be written

$$L_K = \frac{f_1}{f_0} = \frac{\left(\frac{T}{2\pi N_0} \right)^K \exp \left\{ - \frac{T}{2N_0} \sum_{i=1}^K |z_k - A_i e^{j\phi_i}|^2 \right\}}{\left(\frac{T}{2\pi N_0} \right)^K \exp \left\{ - \frac{T}{2N_0} \sum_{i=1}^K |z_i|^2 \right\}} \quad (25)$$

This may be simplified to

$$L_K = \exp \left\{ - \frac{T}{2N_0} \sum_{i=1}^K |z_i - A_i e^{j\phi_i}|^2 + \frac{T}{2N_0} \sum_{i=1}^K |z_i|^2 \right\} \quad (26)$$

or

$$L_K = \exp \left\{ - \frac{T}{2N_0} \sum_{i=1}^K \left[-2C_i A_i \cos(\psi_i - \phi_i) + A_i^2 \right] \right\} \quad (27)$$

or

$$L_K = \exp \left\{ \frac{T}{N_0} \sum_{i=1}^K C_i A_i \cos(\psi_i - \phi_i) - \frac{T}{2N_0} \sum_{i=1}^K A_i^2 \right\} \quad (28)$$

Because the $\sum A_i^2$ term in equation (28) is independent of the data of interest, it will be neglected. The likelihood function can now be obtained by multiplying L_K by the priors on $\{\phi_k\}$.

$$D_K = \exp \left\{ \frac{T}{N_0} \sum_{i=1}^K C_i A_i \cos(\psi_i - \phi_i) \right\} \prod_{i=1}^K P(\phi_i | \phi_{i-1}) \quad (29)$$

The expression for D_K gives a measure of the likelihood that a sequence $\{\phi_k\}_1^K$ is the correct sequence given the measurement sequence $\{Z_k\}_1^K$ and the amplitudes $\{A_i\}_1^K$. The phase sequence which maximizes D_K is the MAP estimate of $\{\phi_k\}_1^K$.

By taking the natural logarithm of D_K , this result can be simplified further to

$$\Gamma_K = \ln(D_K) = \frac{T}{N_0} \sum_{i=1}^K A_i C_i \cos(\psi_i - \phi_i) + \sum_{i=1}^K \ln[p(\phi_i | \phi_{i-1})] \quad (30)$$

where C_i is the magnitude of the measurement Z_i and ψ_i is the argument of Z_i , as shown in Figure 4. The subscript K on the likelihood measure Γ_K indicates that Γ_K has been calculated for the sequence of measurements $\{Z_i\}_1^K$. In

general, a Γ_i may be calculated for measurements from Z_1 to Z_i .

A more useful expression can be obtained by noting that Γ_i can be computed recursively and that the phase process is first order Markov.

$$\Gamma_i = \Gamma_{i-1} + \frac{T}{N_0} A_i C_i \cos(\psi_i - \phi_i) + \ln \left[p(\phi_i | \phi_{i-1}) \right] \quad (31)$$

The recursive expression for Γ_i leads very nicely to the application of the Viterbi algorithm for phase sequence estimation.

Viterbi Algorithm

As previously stated, the desired result is selection of the sequence $\{\hat{\phi}_k\}_1^K$ out of all possible sequences which maximizes Γ_K given the measurement sequence $\{Z_k\}_1^K$. This is the MAP estimate of the phase sequence. If, at each time k , the phase ϕ_k can take on one of M values, then there are M^K possible sequences to search through in order to find the one that maximizes Γ_K . The complexity of this calculation quickly becomes too large to be useful as M and K become large.

Because Γ_K can be computed recursively, as in equation (31), this exponential increase in complexity can be avoided. It will be convenient to define γ_k as the path metric

$$\gamma_k(j, m) = \frac{T}{N_0} A_k C_k \cos(\psi_k - \phi_k = \xi_j) + \ln p(\phi_k = \xi_j | \phi_{k-1} = \xi_m) \quad (32)$$

therefore

$$\Gamma_K = \Gamma_{K-1} + \gamma_K(j, m) \quad (33)$$

The sequence $\{\hat{\phi}_k\}_1^K$ which maximizes Γ_K while passing through $\hat{\phi}_{K-1}$ on its way to $\hat{\phi}_K$ must do so by following sequence $\{\hat{\phi}_k\}_1^{K-2}$ which maximizes Γ_{K-1} . If it did not, a better sequence $\{\hat{\phi}_k\}_1^{K-2}$ could be chosen. Therefore, at time K , it is only necessary to store M sequences $\{\hat{\phi}_k\}_1^K$, one ending in each of the M phase values at time K ; M values of Γ_K corresponding to the M sequences; the current time counter, K ; and the transition probability values (Ref 9:24-27).

To extend the MAP estimate of phase to time $K+1$, the estimator algorithm must take the new measurement Z_{K+1} and, for each phase value $\phi_{K+1} = \xi_j$, $j=0, 1, \dots, M-1$, calculate Γ_{K+1} for each sequence $\{\hat{\phi}\}_1^K$ plus $\phi_{K+1} = \xi_j$. For each value of j , the maximum Γ_{K+1} is selected and the value of $\hat{\phi}_{K+1} = \xi_j$ is concatenated with the sequence $\{\hat{\phi}_k\}_1^K$ which ends in $\hat{\phi}_K = \xi_m$. At the end of the calculation, Z_{K+1} will no longer be required and it can be discarded. There will be M phase sequences stored, one ending in each of the M possible discrete values of phase. The sequences can be extended another step in time by taking measurement, Z_{K+2} , and repeating the calculations.

This maximization algorithm can be stated

$$\text{Max}_{\{\hat{\phi}\}_{K-1}^K} \left[\text{Max}_{\{\hat{\phi}\}_1^{K-2}} \left[\Gamma_{K-1} + \gamma_K(j,m) \right] \right] \quad (\text{Ref5:24}) \quad (34)$$

or in algorithm form

For each time $k=1, \dots, K$

Begin

Obtain the current measurement Z_k

For each phase value ξ_j , $j=0, 1, \dots, M-1$

Begin

For each phase value ξ_m , $m=0, 1, \dots, M-1$

Begin

Calculate $\Gamma_{k_m} = \Gamma_{k-1} + \gamma_k(j,m)$

End

Pick the biggest Γ_{k_m}

Concatenate $\hat{\phi}_k = \xi_j$ with the sequence ending

in $\phi_{k-1} = \xi_m$

Set $\Gamma_k = \Gamma_{k_m}$ for the sequence $\{\hat{\phi}_k\}_1^K$ ending

in ξ_j

End

End

At each time k , there will be a sequence of phase values ending in each of the M possible phase values. These are called survivor sequences. In general, there will be survivor sequences from the previous time $(k-1)$ which are not

concatenated with a phase value to form a current survivor sequence. These unused sequences need not be retained.

The phase values stored in the M sequences tend to converge to a single value if the sequences are inspected far enough back in time. Because of this convergence, at time K it is possible to determine the MAP estimate of the phase, $\hat{\phi}_{K-K_0}$, by selecting the sequence $\{\hat{\phi}_k\}_1^K$ with the largest Γ_K and outputting the $\hat{\phi}_{K-K_0}$ value from that sequence. If all the M sequences have not converged to a single value of $\hat{\phi}_{K-K_0}$, then the ambiguity can be resolved by making K_0 larger. It should be noted that this does not guarantee that $\hat{\phi}_{K-K_0}$ is the closest neighbor to the actual phase ϕ_{K-K_0} , only that $\hat{\phi}_{K-K_0}$ is the MAP estimate of the true value.

The number K_0 is the fixed lag of the system and is referred to as depth, or decision depth.

The complexity of the estimator can be seen from the algorithm listing. If the times required for concatenation, picking the biggest Γ_K , and updating the new values of Γ are ignored, then the majority of time is spent in calculation of the values of Γ_{k_m} (Γ_{k_m} is the m th Γ_k value computed in the Viterbi Algorithm). They must be calculated M times for each of the M values of phase, at each time $k=1,2,\dots,K$. Therefore the complexity of computation is proportional to KM^2 . This is better than the M^K complexity required by

the brute force global search method mentioned at the beginning of this section. In addition, the Viterbi algorithm estimator outputs phase value estimates with a fixed lag in time, as opposed to the global search method which must store the entire measurement sequence and then calculate the entire MAP estimate of the phase sequence.

A signal model has been developed which describes the received signal of the laser line scan system. The phase of the received signal can be represented by a sequence of values over time. Using the Viterbi algorithm, it is possible to make a maximum a posteriori estimate of this phase sequence. The question of how well this estimator performs is addressed in Chapter III.

III Performance Analysis

An analysis and prediction of the performance of an estimation scheme is necessary in order to determine if the estimator is worth building and to compare its performance with competitive estimators. In this chapter, the mean-squared error (MSE) of the estimate is presented as the measure of quality for the MAP phase sequence estimator. By using the concept of error events and minimum free distance, approximate values of MSE are predicted for various signal energy to noise power density ratios and number of levels of phase discretization. Also, a strict lower bound on the MSE is calculated. The question of bias in the estimate is discussed and the limitations of the predicted MSE are presented.

Mean-Squared Error

The sequence of phase values $\{\hat{\phi}_k\}_1^K$ which approximates the true phase $\phi(t)$, $0 < t \leq KT$, can be viewed as a path through a trellis. Figure 5 shows one such path through a trellis in which there are five equally spaced discrete phase values. The value of $\phi(t)$, $(K-1)T < t \leq KT$, is represented by the node at K through which the path passes. The lines connecting nodes represent transitions from one phase value to another.

In this example, the phase is shown changing linearly from each point in time to the next. The linear phase

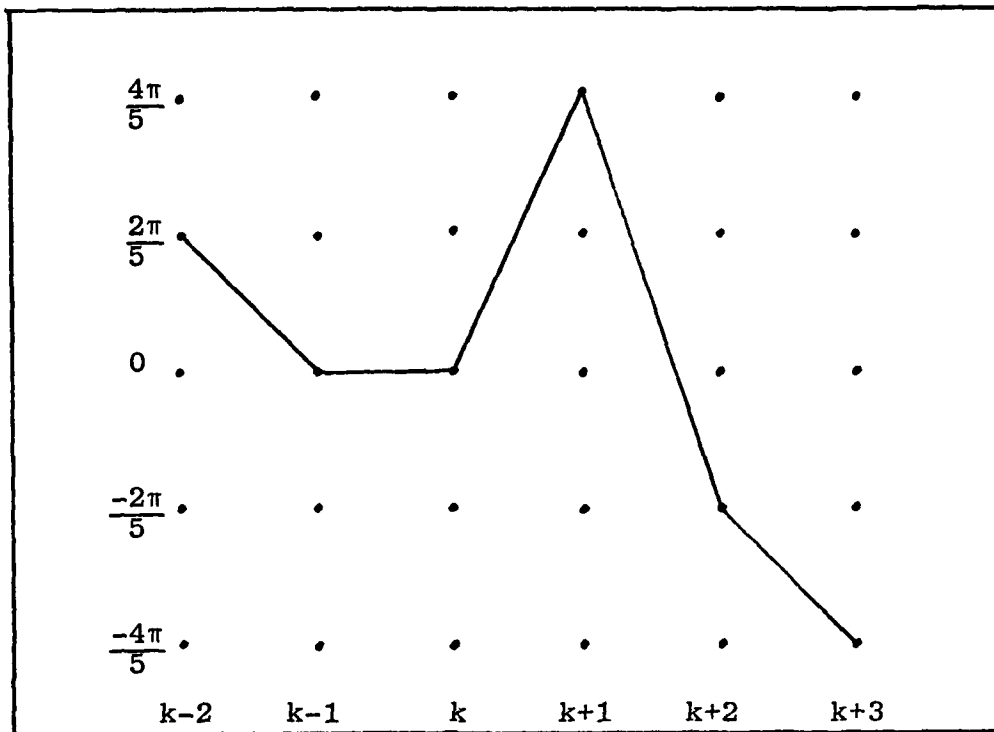


Fig. 5. Phase Trellis, $M=5$

transition case and a step phase transition case will both be used in calculating the predicted mean-square error of the estimator.

The first case can be viewed as a piecewise linearization of the continuous phase (range). This is a reasonable (although simplified) model for the modulo- 2π phase which is proportional to the slant range to the terrain being scanned. This linear transition case will be useful in providing a prediction of the mean-squared error (MSE) of the system when the input phase is a result of a physical process, such as scanning of terrain.

The second case, step phase transition, is included because this case matches the model for the Monte Carlo simulation performed in Chapter IV. In the simulation, the input phase sequence is generated as discrete values which are constant over a T second interval. This corresponds to a step change in phase in each interval.

The free distance (to be defined later) between two signals in signal space is smaller for the linear transition case than for the step transition case. It will be seen, in the following sections, that this results in a higher probability of making an error in phase estimation for the linear transition case.

In this report, the correct path is defined as the sequence of phase values, which is closest in absolute value at each discrete time kT to the actual phase value. Conversely, an error path, e_i , is the i 'th path which is not identical to the correct path at all $k \in (1, 2, \dots, K)$. For a sequence of length K which can take on one of M discrete values at each time k , there will be one correct path and $M^K - 1$ error paths. The entire collection of error paths is denoted as E . It will also be useful to define P_c as the probability that the estimator has chosen the correct path, that is, the sequence of values output from the estimator is the same as the sequence of values of the correct path. In a similar manner, P_{e_i} is defined as the probability that the estimator has chosen

error path e_i and P_E is defined as the probability that the estimator is on any error path.

It follows that

$$P_C = 1 - P_E \quad (35)$$

and

$$\sum_{e_i \in E} P_{e_i} = P_E \quad (36)$$

The estimator chooses either the correct path or an error path. These two events are mutually exclusive and exhaustive, therefore the mean-squared error (MSE) at any point in time on the trellis can be defined as

$$\begin{aligned} \text{MSE} &= (\text{MSE}|C)P_C + (\text{MSE}|E)P_E \\ &= (\text{MSE}|C)(1 - P_E) + (\text{MSE}|E)P_E \\ &= (\text{MSE}|C)(1 - P_E) + \sum_{e_i \in E} (\text{MSE}|e_i)P_{e_i} \end{aligned} \quad (37)$$

where $(\text{MSE}|C)$ is the mean-squared error given the estimator is on the correct path.

The $(\text{MSE}|C)$ term is due to the quantization noise of the approximation of $\phi(t)$ by one of a set of M discrete levels on the interval $(-\pi, \pi)$. If it is assumed that $\phi(t)$ is distributed uniformly over each quantization interval, then

$$(\text{MSE}|C) = \frac{\pi^2}{3M^2} \quad (38)$$

The assumption of uniformity over a quantization interval is reasonable if M is sufficiently large and the probability density function (pdf) of the phase is "smooth" so that the pdf of $\phi(t)$ is essentially constant over each quantization interval.

The $(\text{MSE}|E)$ is similarly defined as the mean-squared error given that the estimator has chosen any path other than the correct path. The average mean-squared error at a point in time (given that the estimator has chosen error path e_i) is denoted $(\text{MSE}|e_i)$. The $(\text{MSE}|e_i)$ is averaged over the length of the error event. It will be seen in the following development that, for many cases of interest, $(\text{MSE}|E)$ is dominated by one $(\text{MSE}|e_i)$ term in equation (37). The dominant term has a length of one and the MSE defined in equation (37) becomes a point MSE for these cases.

For the calculation of $(\text{MSE}|e_i)$ it will be useful to use the following definitions for the signal of interest and its phase (Ref 1:42.4.1)

$$s(t, \underline{\alpha}) = A \cos(2\pi f_m t + \phi(\underline{\alpha})) \quad (39)$$

$$\phi(\underline{\alpha}) = \frac{2\pi}{M} \int_{-\infty}^{\infty} \sum_{i=-\infty}^n \alpha_i g(\sigma - iT) d\sigma \quad -\infty < t \leq (n+1)T \quad (40)$$

where M is the number of discrete phase quantization levels, and $\underline{\alpha}$ is a sequence of integers α_i selected from the alphabet $(0, \pm 1, \pm 2, \dots, \pm(\frac{M-1}{2}))$.

For convenience in the development of the free distance later in this section, the amplitude is defined

$$A = \sqrt{\frac{2E}{T}} \quad (41)$$

where E is the energy in the signal $s(t, \underline{\alpha})$ over a T second interval.

The function $g(t)$ is selected so that

$$\int_{-\infty}^{\infty} g(t) dt = 1 \quad (42)$$

The shape of $g(t)$ determines how the phase of $s(t, \underline{\alpha})$ progresses from one node on the trellis to the next. If $g(t) = \frac{1}{T}$, $0 < t \leq T$ and $g(t) = 0$ elsewhere, then the phase changes linearly with time. If $g(t) = \delta(t)$, then the phase makes a step jump of height $\frac{2\pi\alpha_i}{M}$ in each T second interval. The elements α_i of $\underline{\alpha}$ specify the number of $\frac{2\pi}{M}$ radian steps in phase the signal changes on the interval $iT < t \leq (i+1)T$. The α_i are limited in magnitude to $\frac{M-1}{2}$ to reflect the modulo- 2π nature of the estimator.

Selection of a function for $g(t)$ which gives a linear phase change (or similar smooth change in phase versus time) is useful for modeling a physical system such as the laser line scanner described in the Introduction. This is due to the bandwidth constraints which limit the dynamics of the phase change. The simulation results presented in Chapter IV

are based on an estimator model in which the measurements are discrete in time and quantized in value. Thus, the Dirac delta function more closely describes the phase transitions for the estimator simulation.

For the rest of this section, $\underline{\alpha}$ is a sequence of integers which describes the correct path of the estimator and the sequence $\underline{\beta}$ will represent one of the error paths which differs from $\underline{\alpha}$ at L nodes. The value L is defined as the length of the error event. An example of a correct path $\underline{\alpha}$ and an error event $\underline{\beta}$ with $L=2$ is shown in Figure 6.

In this example of an error event the error path diverges from and merges with the correct path only once. In general, $\underline{\beta}$ could diverge from the correct path several times and it need not merge; however, it will be seen in the following development that it is the $L=1$ "minimum error path" which is of primary interest.

The averaged MSE given error path e_i (described by $\underline{\beta}$) and correct path $\underline{\alpha}$ can be defined as

$$(\text{MSE}|e_i) = \frac{\Delta}{L} \sum_j [\phi(\alpha_j) - \phi(\beta_j)]^2 \quad (43)$$

where the sum is taken over the L nodes at which $\underline{\alpha}$ differs from $\underline{\beta}$.

Forney has shown (Ref 2:273) that error events are recurrent, or statistically independent of each other. The averaged MSE

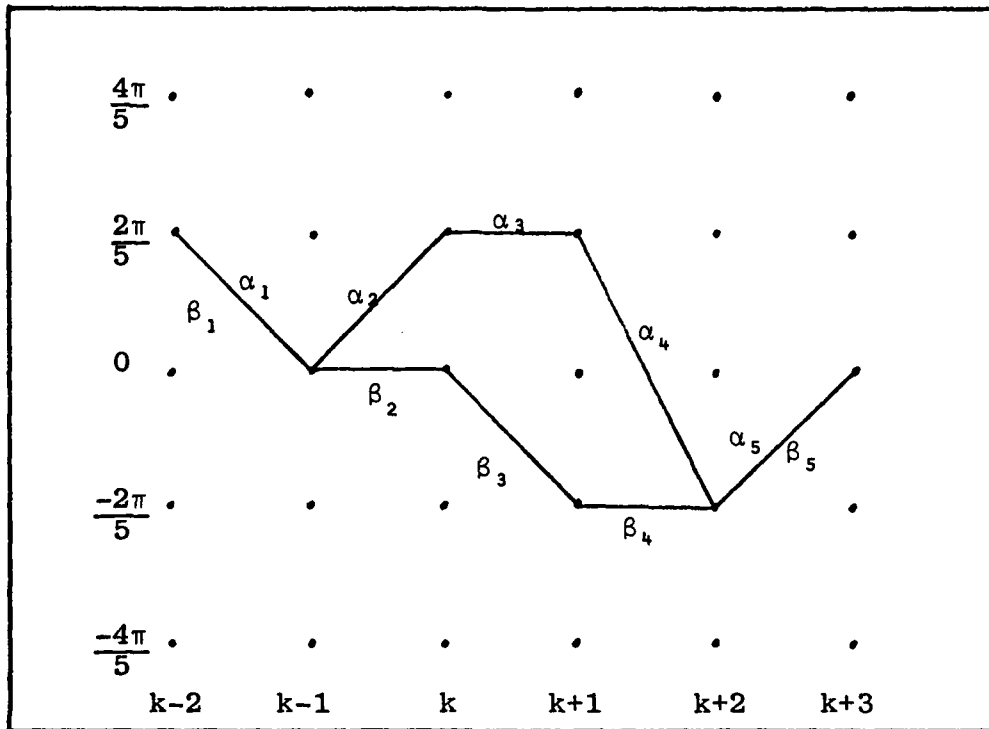


Fig. 6. Error Event

for a particular error event is defined as the average of the point mean-square errors over the length, L , of the error event. It will be seen that the most probable error path has length $L=1$, and that $(\text{MSE}|e_i)$ for this most probable error path collapses to a point mean-square error.

If the error path diverges once at time $(n-L-1)T$ and merges once at time nT , then

$$(\text{MSE}|e_i) = \left(\frac{2\pi}{M}\right)^2 \frac{1}{L} \sum_{j=n-L}^{n-1} \left[\sum_{i=n-L}^j \alpha_i - \sum_{i=n-L}^j \beta_i \right]^2 \quad (44)$$

Further development of the total mean-squared error requires an expression for the probability of an error path.

Probability of Error Path

The desired error measure is the probability per unit time that the estimator will select a particular incorrect node in the phase trellis. From this, the MSE per unit time could be calculated using an equation of the same form as equation (37). This probability measure is not directly available; however, useful approximations and bounds to the mean-squared error can be obtained by calculating the probability that an error event starts at time nT given that the estimator was on the correct path at time $(n-1)T$ (Ref 4: 273-274).

The probability that the estimator selects a particular error path instead of the correct path is a binary hypothesis problem and depends on the euclidean distance between the two signals in signal space. These error events are not mutually exclusive, therefore, the probability that any error event occurs, P_E , can be upper bounded by the sum of all the binary decision error probabilities (union bound). A lower bound on the probability of any error event is the largest of the probabilities of specific error events (Ref 4:273-274). These bounds are summarized as follows (Ref 4:274)

$$\max_i [P_{e_i}] \leq P_E \leq \sum_i P_{e_i} = \max_i [P_{e_i}] + \sum_{i \neq j} P_{e_j} \quad (45)$$

The binary hypothesis probability of an error, P_{e_i} , is
(Ref1:42.4.2)

$$P_{e_i} = Q \left[\frac{D(\underline{\alpha}, \underline{\beta})}{\sqrt{2N_0}} \right] \quad (46)$$

where N_0 is the one sided power spectral density for additive white gaussian noise, D is the euclidean distance between two signals defined by $\underline{\alpha}$ (the correct path) and $\underline{\beta}$ (the i 'th error path), and $Q(\cdot)$ is the error function defined by

$$Q(x) = \frac{1}{\sqrt{2\pi}} \int_x^{\infty} e^{-\frac{y^2}{2}} dy \quad (47)$$

The Q function is monotonically decreasing and rapidly becomes small as D becomes large. As a result, the P_E in equation (45) can often be approximated by

$$P_E \approx P_E' = Q \left[\frac{D_m(\underline{\alpha}, \underline{\beta})}{\sqrt{2N_0}} \right] \quad (48)$$

where D_m is

$$D_m = \text{Min}_{e_i} [D(\underline{\alpha}, \underline{\beta})] \quad (49)$$

Note that $P_E' \leq P_E$ by equation (45). The minimum is taken over all possible error paths e_i .

The total mean-square error can now be approximated by

$$\text{MSE} = \frac{\pi^2}{3M^2} (1 - P_E') + (\text{MSE}|e_m) P_E' \quad (50)$$

In equation (50), e_m is the error path which is the minimum distance from the correct path defined by $\underline{\alpha}$.

Since P'_E is a lower bound on P_E , a lower bound on MSE can be defined as

$$\text{MSE} \geq (\text{MSE}|e_m)P'_E \quad (51)$$

An upper bound on the MSE is desirable; however, this would require evaluation of the union bound sum in equation (45). This would provide an upper bound on P_E and, therefore, an upper bound on MSE by a substitution into equation (50).

The large number of paths over which the sum must be calculated makes evaluation of an upper bound infeasible, so an upper bound on MSE is not evaluated in this report. As will be shown in the following development, a measure of the "tightness" of the approximation of MSE is the value of the argument of the Q function used in equation (48). This will give an indication of the quality of the approximation without actual calculation of an upper bound.

The minimum free distance, D_m , must be calculated before actual values of MSE can be evaluated.

Minimum Free Distance

In this section, the normalized free distance, $d=D/\sqrt{2E}$ (Ref 11:42.3.2), will be developed for two cases of $g(t)$ and then the minimum free distance, D_m , will be evaluated. The signal and phase are modeled as in equations (39) and (40),

respectively. It should be noted that the amplitude of the signal is constant in this development. The case of varying amplitude will be discussed in a following section.

Linear Phase Transition. For the first case of interest, the phase changes linearly from one time interval to the next. This case can be viewed as a piecewise linearization of a continuously changing phase.

The phase $\phi(\underline{\alpha})$ is zero for $t < 0$ and

$$g(t) = \frac{1}{T} \quad 0 \leq t \leq T \quad (52)$$

$$= 0 \quad \text{elsewhere}$$

The element α_i of sequence $\underline{\alpha}$ is defined over the interval $(i-1)T \leq t \leq iT$.

With this $g(t)$, the signal becomes

$$s(t, \underline{\alpha}) = \sqrt{\frac{2E}{T}} \cos \left(2\pi f_m t + \frac{2\pi}{M} \left[\sum_{i=1}^{n-1} \alpha_i + \frac{1}{T} \alpha_n [t - (n-1)T] \right] \right) \quad (53)$$

$$(n-1)T \leq t \leq nT$$

The normalized squared distance is defined as

$$d^2 = \frac{D^2}{2E} = \frac{1}{2E} \sum_{j=n-N+1}^n \int_{jT}^{(j+1)T} [s(t, \underline{\alpha}) - s(t, \underline{\beta})]^2 dt \quad (54)$$

(Ref 1:42.4.2)

where N is the number of intervals of length T over which

the phases differ. If $\omega_m T \gg 1$, then

$$d^2 = N - \frac{1}{T} \sum_{j=n-N+1}^n \int_{jT}^{(j+1)T} \cos \left[\frac{2\pi}{M} \left(\sum_{i=1}^j (\alpha_i - \beta_i) + \frac{t}{T} (\alpha_{j+1} - \beta_{j+1}) \right) \right] dt \quad (55)$$

The integral in equation (55) must be evaluated in two cases. When $\alpha_{j+1} = \beta_{j+1}$

$$\int \cdot dt = T \cos \left[\frac{2\pi}{M} \sum_{i=1}^j (\alpha_i - \beta_i) \right] \quad (56)$$

When $\alpha_{j+1} \neq \beta_{j+1}$

$$\int \cdot dt = \frac{TM}{2\pi(\alpha_{j+1} - \beta_{j+1})} \left[\sin \left[\frac{2\pi}{M} \left(\sum_{i=1}^j (\alpha_i - \beta_i) + (\alpha_{j+1} - \beta_{j+1}) \right) \right] - \sin \left[\frac{2\pi}{M} \sum_{i=1}^j (\alpha_i - \beta_i) \right] \right] \quad (57)$$

The term $\int \cdot dt$ represents the entire integral in equation (55).

From equations (55), (56) and (57), it can be seen that an error path defined by $\underline{\beta}$ will have a minimum distance from the correct sequence when its phase differs from $\underline{\alpha}$ for only two T second intervals. This is illustrated in Figure 7, with $N=2$

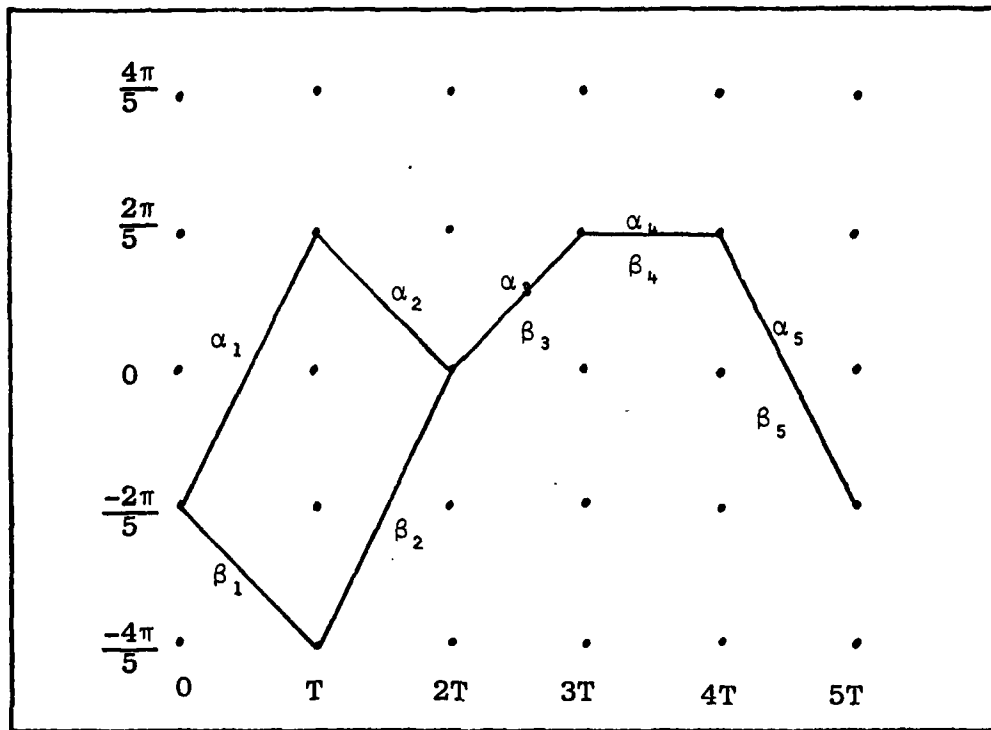


Fig. 7. Minimal Error Path β

and the phase difference occurring at the beginning of the sequence. The location of the phase difference in time does not affect the value of d^2 .

For this error event,

$$\alpha_1 + \alpha_2 = \beta_1 + \beta_2 \quad (58)$$

therefore

$$\alpha_1 - \beta_1 = -(\alpha_2 - \beta_2) \quad (59)$$

so the resulting normalized squared distance is

$$d^2 = 2 \left[1 - \text{sinc} \frac{2\pi}{M} (\alpha_1 - \beta_1) \right] \quad (60)$$

where

$$\text{sinc}(x) = \frac{\sin x}{x} \quad (61)$$

To minimize d^2 in equation (60), the argument of the sinc function must be made as small as possible. For a fixed value of M , this can be done by selecting $\beta_1 = \alpha_1 \pm 1$. (They cannot be equal because that would imply that $\underline{\alpha} = \underline{\beta}$, and no phase difference existed.)

The minimum free distance squared can now be stated as

$$D_m^2 = 2Ed_m^2 = 4E(1 - \text{sinc} \frac{2\pi}{M}) \quad (62)$$

It should be noted that for each correct path defined by $\underline{\alpha}$, there are two error paths which have the same minimum distance, D_m , from the correct path. Equation (48) is modified to include both of these minimum distance paths.

$$P'_E = 2Q \left[\frac{D_m(\underline{\alpha}, \underline{\beta})}{\sqrt{2N_0}} \right] \quad (63)$$

This result can be combined with equations (44), (50), (51) and (62) to calculate the approximate MSE and a lower bound on the MSE as shown in Figures (8) and (9). The MSE values in all figures have been divided by $\frac{\pi^2}{3}$ to normalize them with respect to a uniform phase distribution over $(-\pi, \pi)$: $\text{MSEN} = (\text{MSE}) \frac{3}{\pi^2}$.

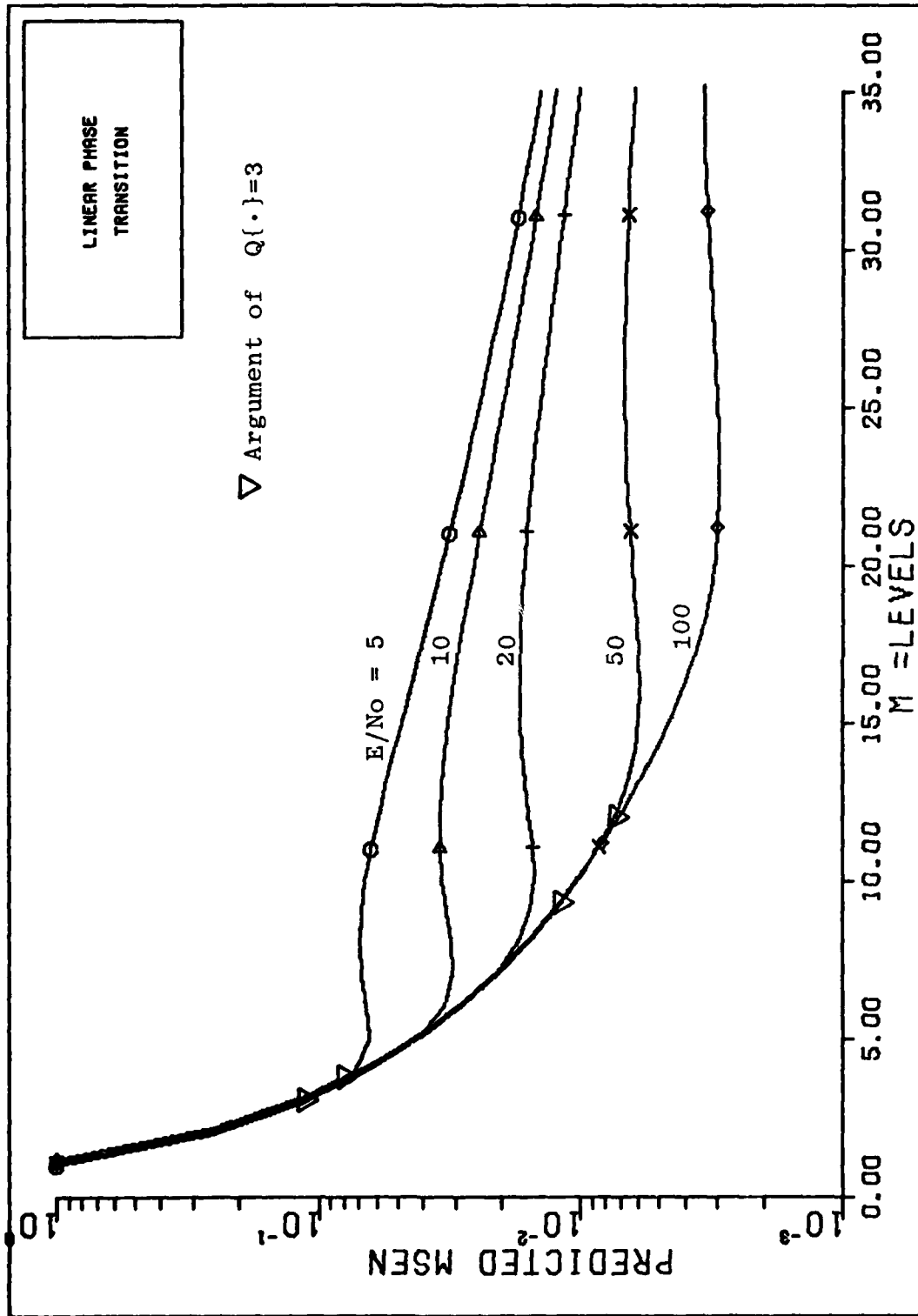


Figure 8 Predicted MSEN, Linear Transition, Constant A

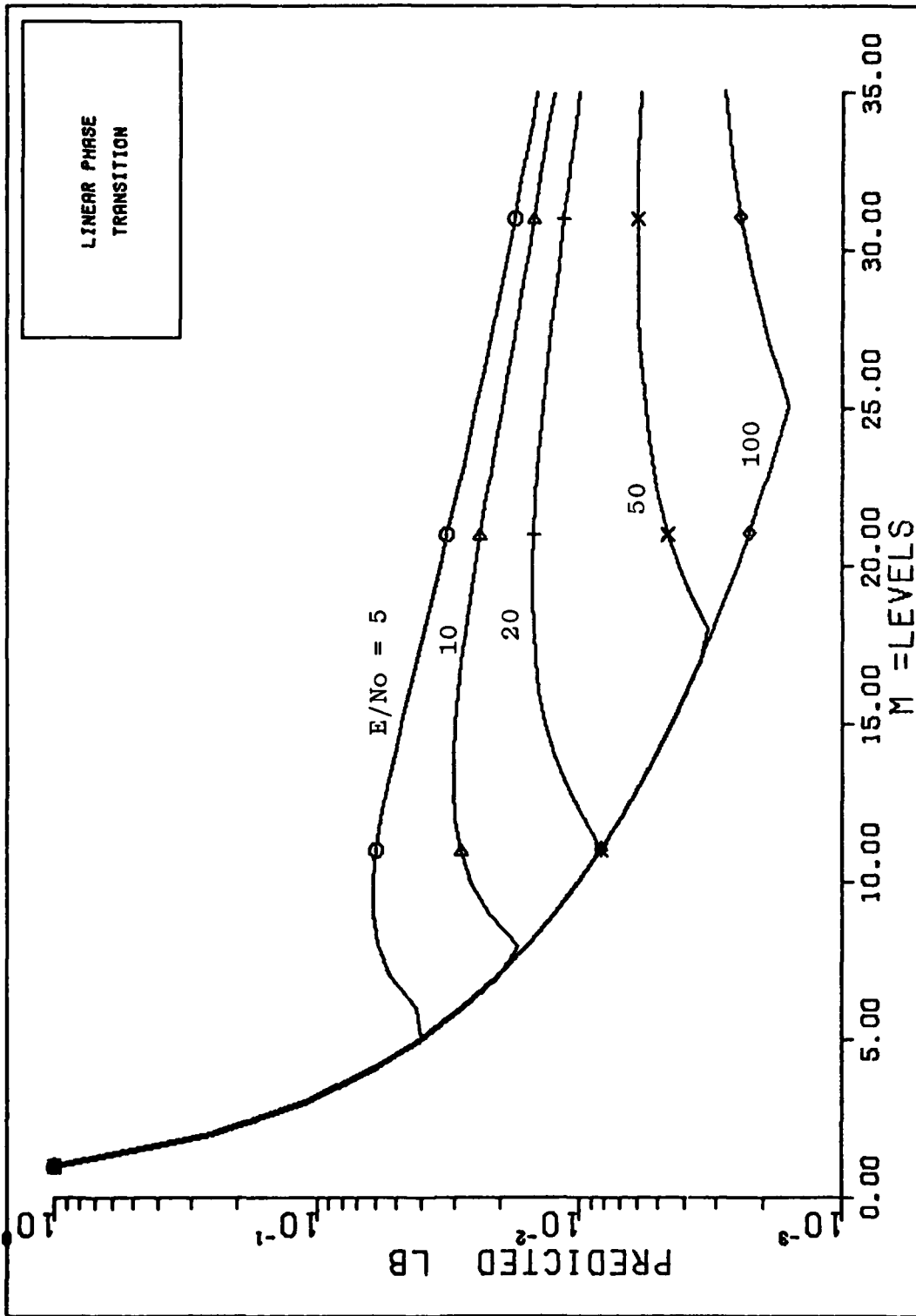


Figure 9 Lower Bound on MSE, Linear Transition, Constant A

The equation for approximate MSEN is

$$\text{MSEN} \approx \frac{1}{M^2} + \frac{3}{M^2} \left(8 - \frac{2}{3}\right) Q \left[\sqrt{2 \left(\frac{E}{N_0}\right) \left(1 - \text{sinc} \frac{2\pi}{M}\right)} \right] \quad (64)$$

The lower bound is initially calculated by

$$\text{MSEN} \geq \frac{24}{M^2} Q \left[\sqrt{2 \left(\frac{E}{N_0}\right) \left(1 - \text{sinc} \frac{2\pi}{M}\right)} \right] \quad (65)$$

Since the MSEN cannot be less than the quantization noise due to M levels, the lower bound depicted in Figure(9) is actually calculated by

$$\text{MSE} \geq \text{Max} \left[\frac{1}{M^2}, \text{ or, } \frac{24}{M^2} Q \left(\sqrt{2 \frac{E}{N_0} \left(1 - \text{sinc} \frac{2\pi}{M}\right)} \right) \right] \quad (66)$$

Figures (10) and (11) display the predicted MSEN and lower bound on MSEN versus an abscissa of E/N_0 . As shown, the performance of the estimator is limited by the quantization noise caused by representing a continuous phase by one of M discrete values. The flat portions of these curves denote the domain of E/N_0 over which quantization noise is the limiting factor.

Step Phase Transition. The second case of interest is that in which the phase is allowed to make a step change at time $t=kT$, for $k=0,1,2,\dots,K$. In this case, $g(t)=\delta(t)$, the Dirac delta function. As previously described, this case models the Monte Carlo simulation described in Chapter IV.

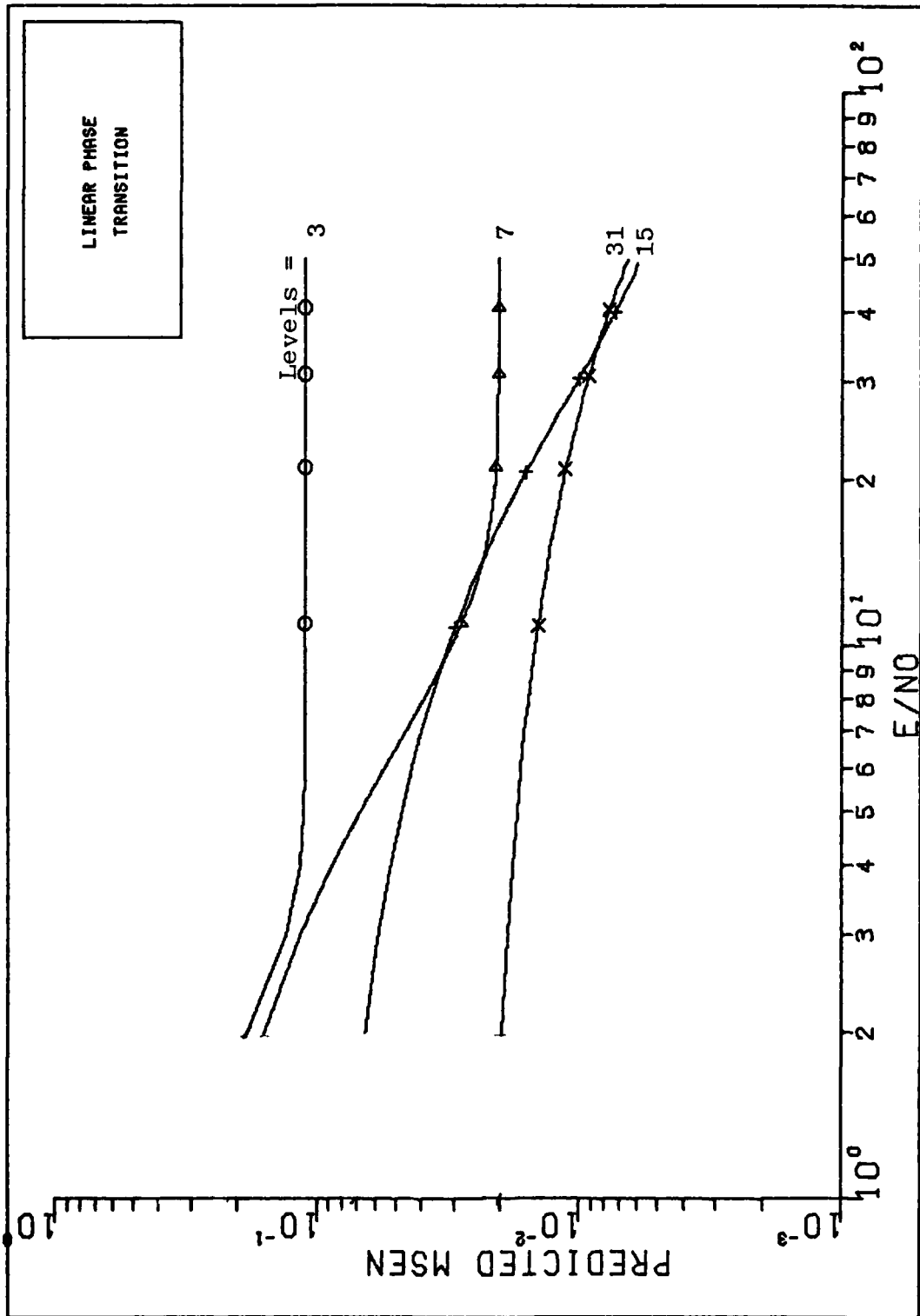


Figure 10 Predicted MSEN, Linear Transition, Constant A

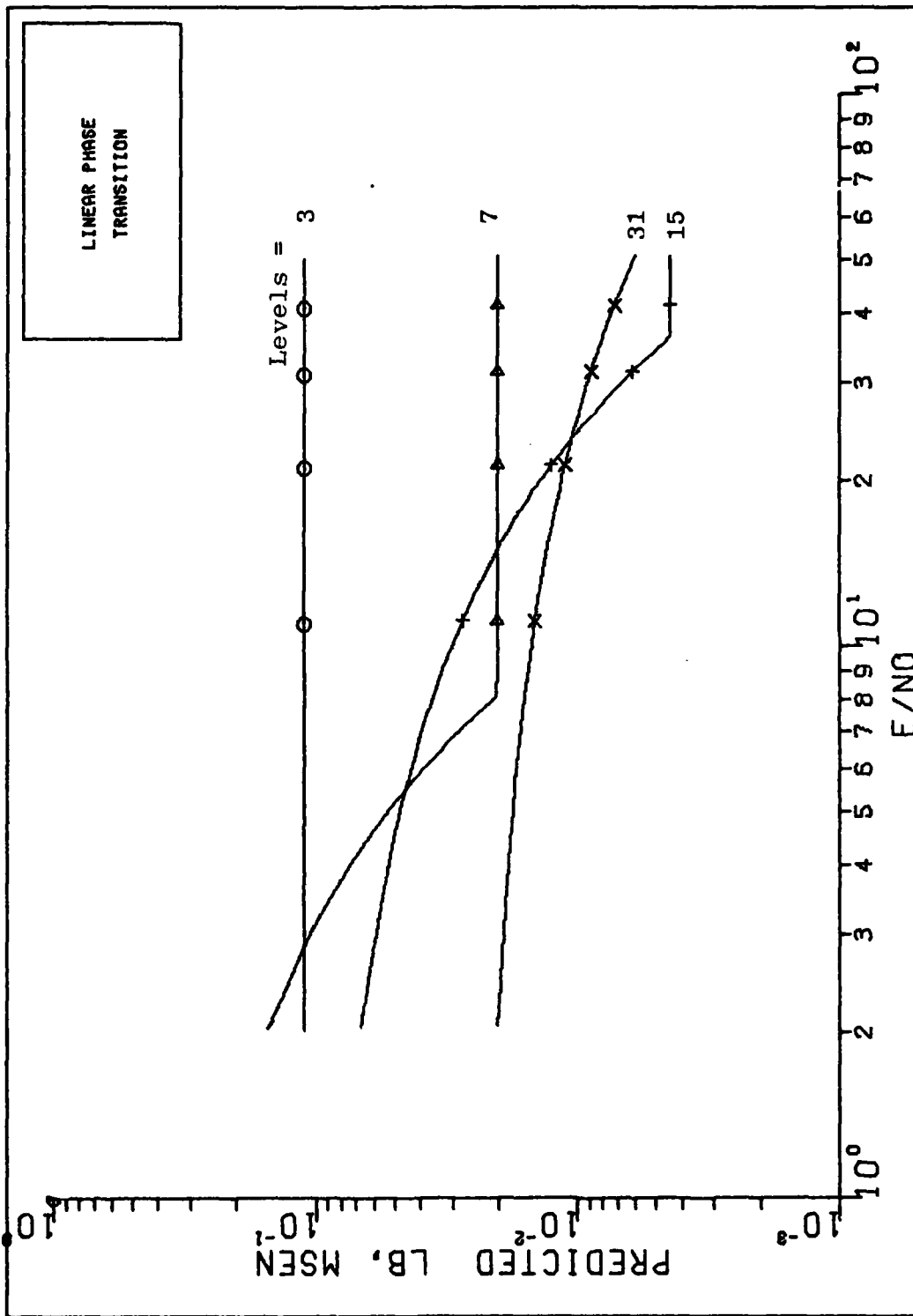


Figure 11 Lower Bound on MSEN, Linear Transition, Constant A

The phase function is

$$\phi(\underline{\alpha}) = \frac{2\pi}{M} \sum_{i=1}^n \alpha_i \quad (67)$$

and the normalized distance squared is

$$d^2 = N - \sum_{j=n-N+1}^n \cos \left(\frac{2\pi}{M} \sum_{i=1}^j (\alpha_i - \beta_i) \right) \quad (68)$$

where the inner sum in equation (68) is zero for $j=0$. The same conditions for minimization of d apply for this case as in the linear case: $N=2$ and $\alpha_1 + \alpha_2 = \beta_1 + \beta_2$. Therefore

$$D_m^2 = 2Ed_m^2 = 4E(1 - \cos(\frac{2\pi}{M})) \quad (69)$$

There are also two minimum distance error paths for the step transition case so the $(MSE|e_m)$ term is multiplied by two to calculate the approximate MSE and the lower bound on MSE.

By combining equations (44), (50), (51) and (69), the approximate MSEN can be calculated as

$$MSEN \approx \frac{1}{M^2} + \frac{3}{M^2} \left(8 - \frac{2}{3}\right) Q \left[\sqrt{\frac{E}{N_0} \left(1 - \cos \frac{2\pi}{M}\right)} \right] \quad (70)$$

and the lower bound is given by

$$MSEN \geq \frac{24}{M^2} Q \left[\sqrt{\frac{E}{N_0} \left(1 - \cos \frac{2\pi}{M}\right)} \right] \quad (71)$$

The lower bound cannot be less than the quantization noise, therefore

$$\text{MSE} \geq \text{Max} \left[\frac{1}{M^2}, \text{ or, } \frac{24}{M^2} Q \left[\sqrt{\frac{E}{N_0} \left(1 - \cos \frac{2\pi}{M} \right)} \right] \right] \quad (72)$$

Figures (12) and (13) show the results of the Normalized MSE calculations versus M(quantization levels) for the step transition case. The predicted MSEN results for this case are slightly better than those predicted for the linear phase transition case. Equations (70) and (72) are also used to calculate MSEN and a lower bound on MSEN versus E/N_0 as displayed in Figures (14) and (15).

As in the linear transition case, the flat portions of the curves in Figures (14) and (15) indicate regions where the quantization noise dominates the MSE performance of the estimator.

Random Variable Amplitude

The predicted mean-square error shown in Figures (8) through (15) are all based on a constant amplitude signal. If the amplitude, $A = \frac{2E}{T}$, is a random variable then the signal can be defined as

$$s(t, \alpha) = \sqrt{\frac{2E}{T}} \cos(2\pi f_m t + \phi(t, \alpha)) \quad (73)$$

It is assumed that E is constant over each T second

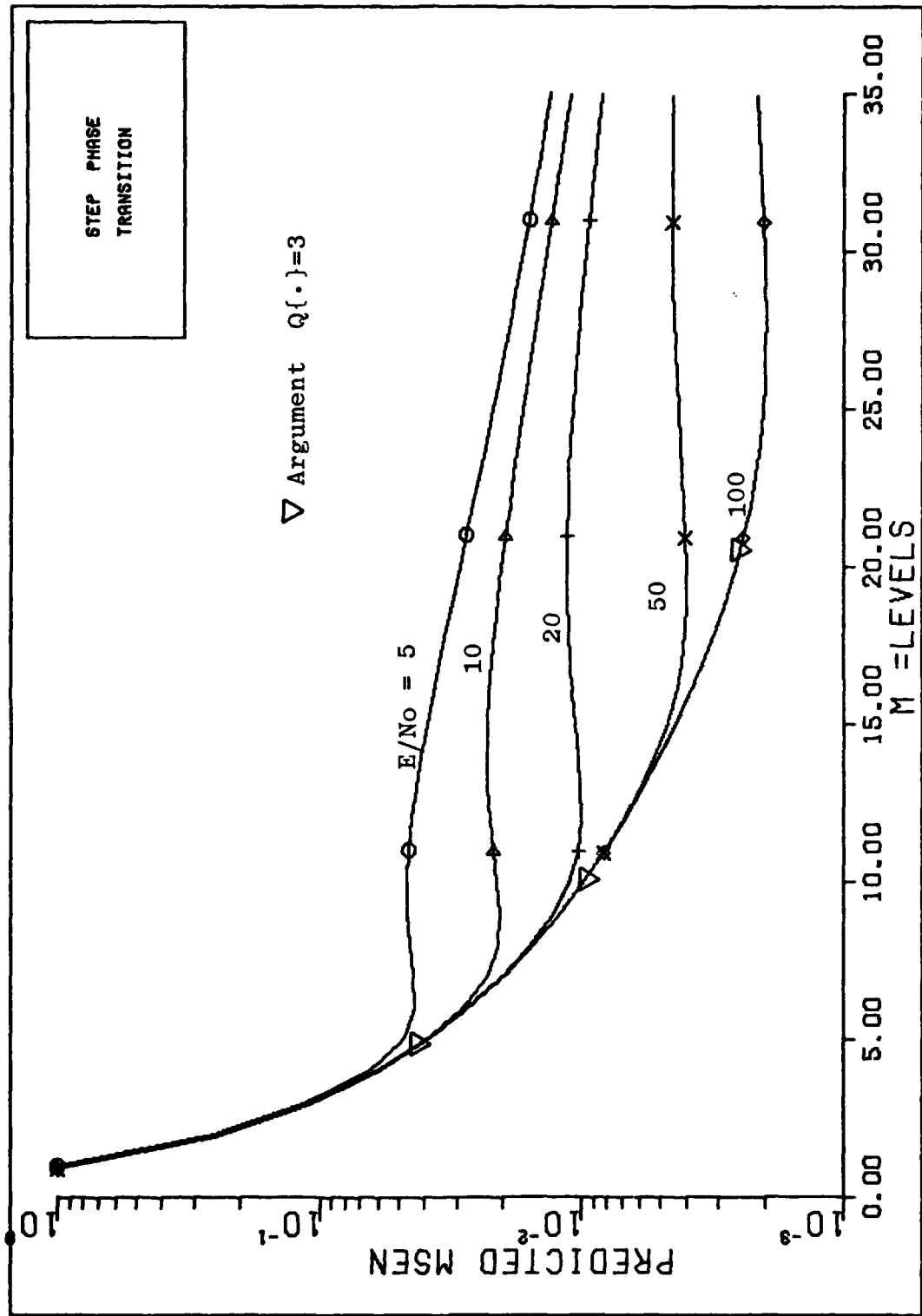


Figure 12 Predicted MSEN, Step Transition, Constant A

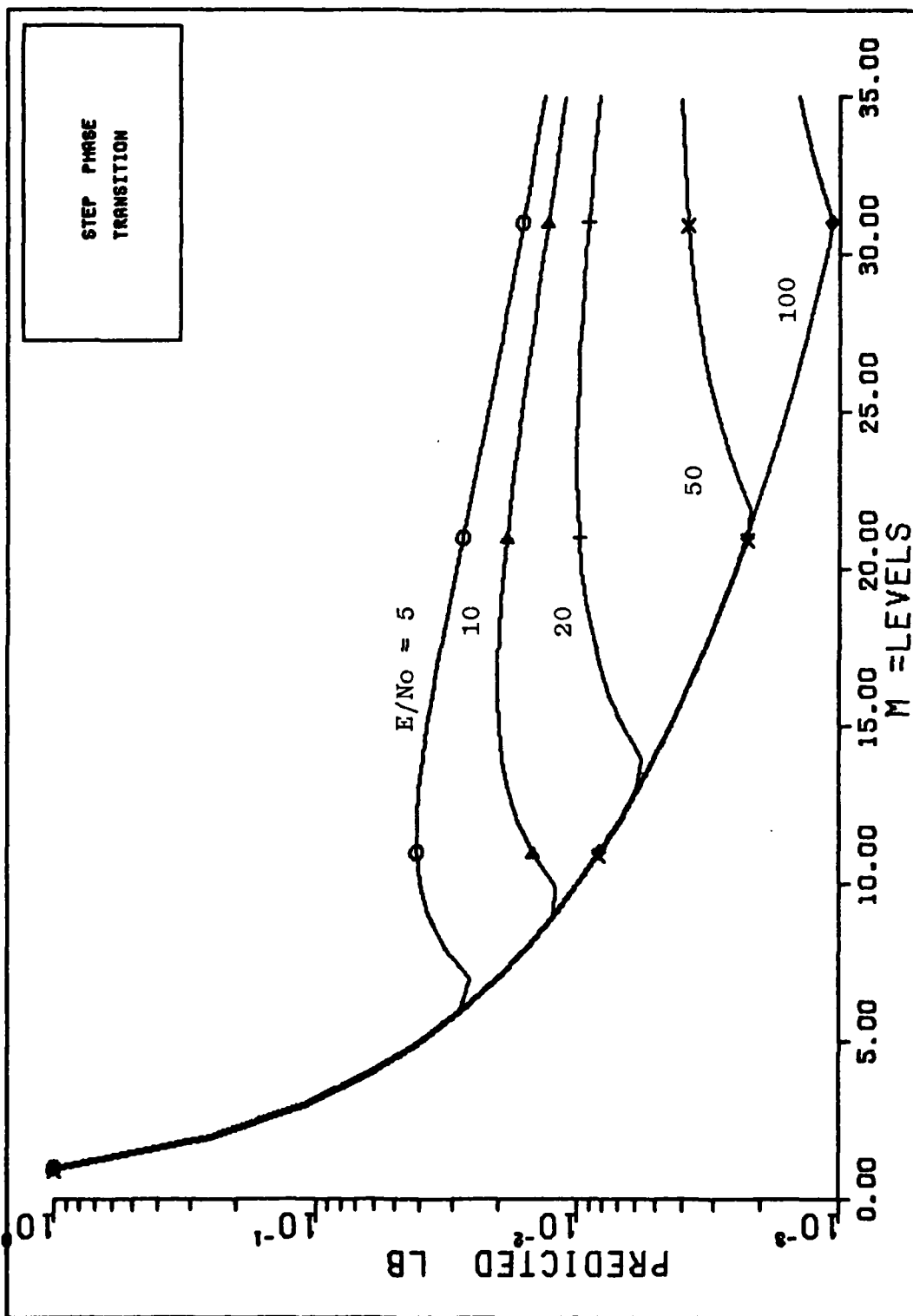


Figure 13 Lower Bound on MSEN, Step Transition, Constant A

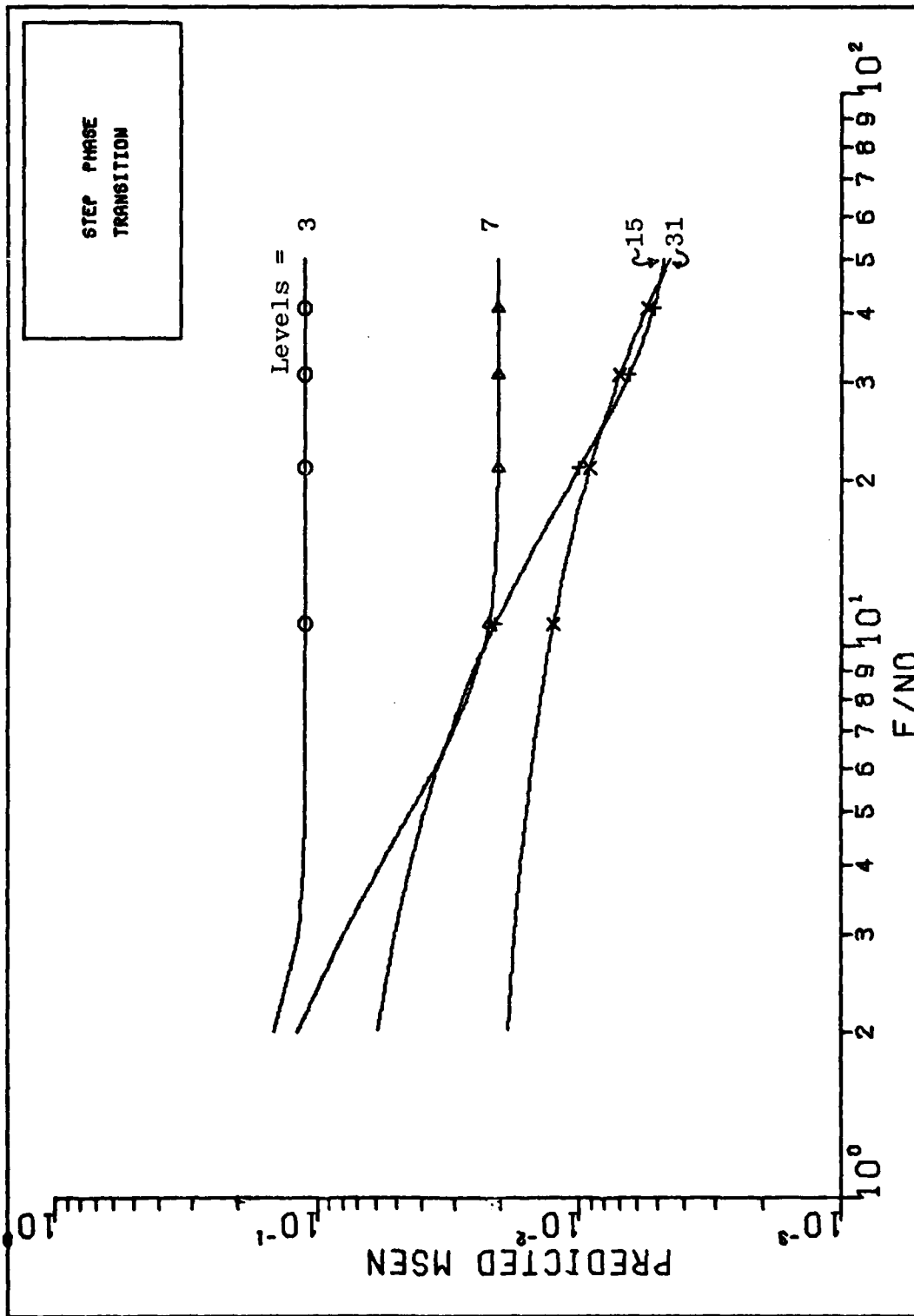


Figure 14 Predicted MSEN, Step Transition, Constant A

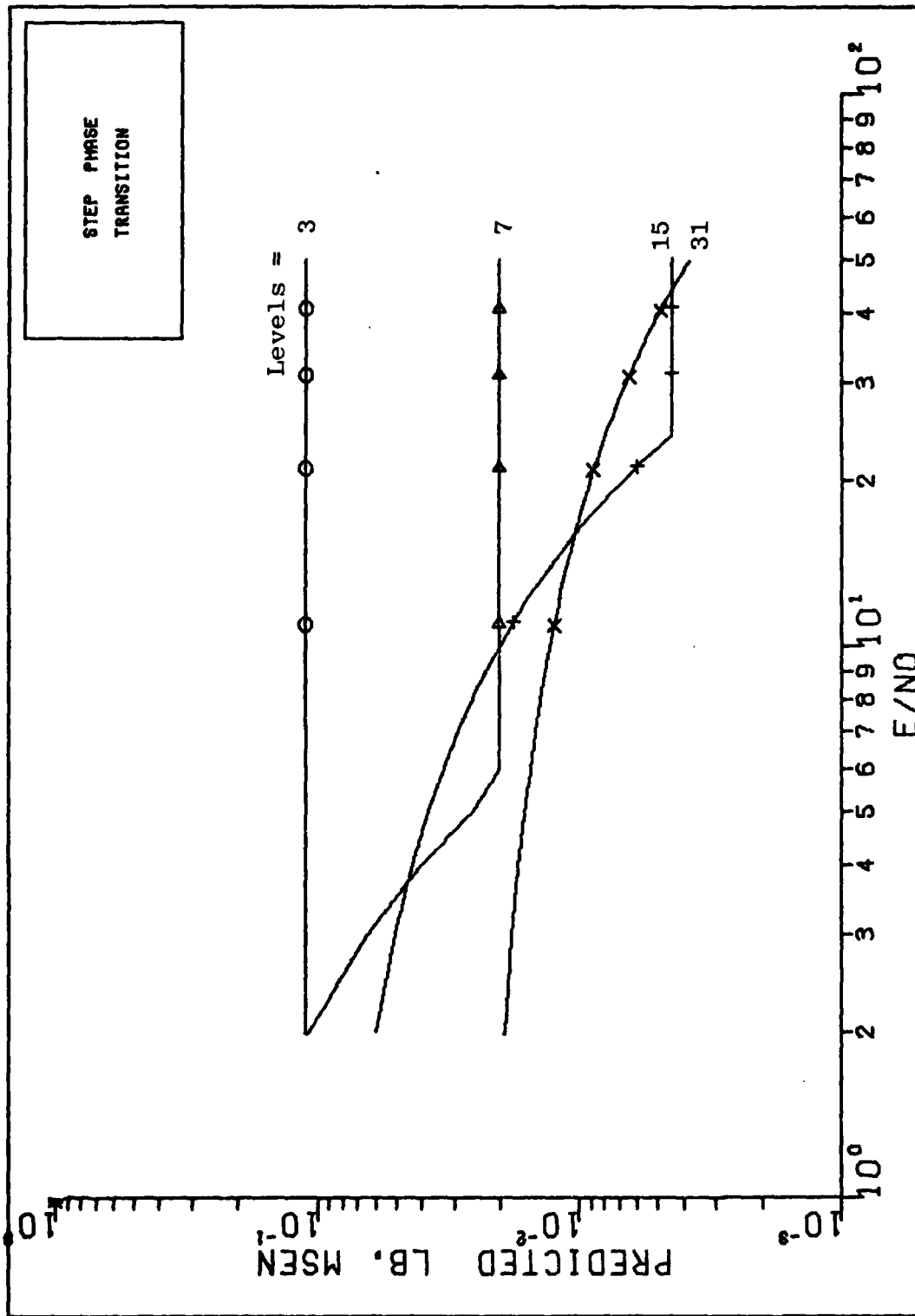


Figure 15 Lower Bound on MSEN, Step Transition, Constant A

interval and $E_i = E(t)$ for $(i-1)T < t \leq iT$. Perfect knowledge of the E_i 's by the estimator is assumed and the E_i 's are assumed identically independently distributed. The signal can now be represented by.

$$s(t, \alpha_i, E_i) = \sqrt{\frac{2E_i}{T}} \cos(2\pi f_m t + \phi(t, \alpha_i)) \quad (74)$$

$$(i-1)T \leq t \leq iT$$

A signal with phase sequence β is defined to have amplitude values B_i .

Calculation of a predicted MSE for the varying amplitude case requires evaluation of the minimum euclidean distance D_m for the phase transition being considered and

$$P_E = E \left\{ Q \left(\frac{D_m(E)}{\sqrt{2N_0}} \right) \right\} \quad (75)$$

The notation $E\{\cdot\}$ is the expected value operator on the random variable E and D_m is a function of the random variable E . Due to the complexity of calculating $E \left\{ Q \left(\frac{D_m(E)}{\sqrt{2N_0}} \right) \right\}$ in closed form, the $Q[\cdot]$ function is approximated by

$$Q[x] \leq \frac{1}{2} e^{-\frac{x^2}{2}} \quad (\text{Ref 11:40}) \quad (76)$$

This allows calculation of the expected value of P_E which is now defined as

$$E\{P_E\} = E \left\{ \frac{1}{2} \exp \left[\frac{-D_m^2}{4N_0} \right] \right\} \quad (77)$$

The predicted mean-squared error can now be calculated for the two phase transition cases previously described.

Linear Phase Transition. The normalized squared distance is defined as in equation (54); and $g(t)$ is $\frac{1}{T}$ for $0 \leq t \leq T$, and zero otherwise.

For the error event when $N=2$, $\alpha_1 + \alpha_2 = \beta_1 + \beta_2$ and $E_1 = E_2$; it can be shown that

$$D^2 = 2(E_1 + E_2) - 2E_1 \operatorname{sinc} \left(\frac{2\pi}{M}(\alpha_1 - \beta_1) \right) - 2E_2 \operatorname{sinc} \left(\frac{2\pi}{M}(\alpha_1 - \beta_1) \right) \quad (78)$$

The minimum free distance occurs when $|\alpha_i - \beta_i| = 1$, as in the previous examples.

The amplitude of the signal, A , is assumed to have a Rayleigh probability distribution function. A transformation of variables (Ref 7:129-131) gives the probability density function for E :

$$f_E(E) = \frac{2\alpha}{T} e^{-\frac{2\alpha E}{T}}, \quad E \geq 0 \quad (79)$$

= 0, otherwise

where

$$E\{A^2\} = \frac{1}{\alpha} \quad (80)$$

The expected value of P'_E over E_1 and E_2 is

$$E\{P'_E\} = \frac{1}{2 \left[1 + \frac{\frac{E}{N_0} (1 - \text{sinc} \frac{2\pi}{M})}{2} \right]^2} \quad (81)$$

\bar{E}/N_0 is the expected value of signal energy to noise power density ratio. The predicted normalized mean-squared error for linear phase transition and Rayleigh amplitude is

$$\text{MSEN} = \frac{1}{M^2} + \frac{3}{M^2} \left(8 - \frac{2}{3} \right) \frac{1}{2 \left[1 + \frac{\frac{E}{N_0} (1 - \text{sinc} \frac{2\pi}{M})}{2} \right]^2} \quad (82)$$

The results of equation (82) are shown for various values of M and \bar{E}/N_0 in Figures (16) and (17). In general, the predicted MSE for the Rayleigh amplitude case is higher than the MSE for the corresponding constant amplitude case. As in the constant amplitude cases, the MSEN becomes smaller as the signal to noise (\bar{E}/N_0) is increased and as the number of quantization levels is increased.

Step Phase Transition. For the step transition case $g(t)=\delta(t)$. When the error event is minimum length ($N=2$) and $E_i = E_1$, the euclidean distance squared is

$$D^2 = 2E_1 - 2E_1 \cos\left(\frac{2\pi}{M}(\alpha_1 - \beta_1)\right) \quad (83)$$

The minimum D^2 occurs when $|\alpha_1 - \beta_1| = 1$.

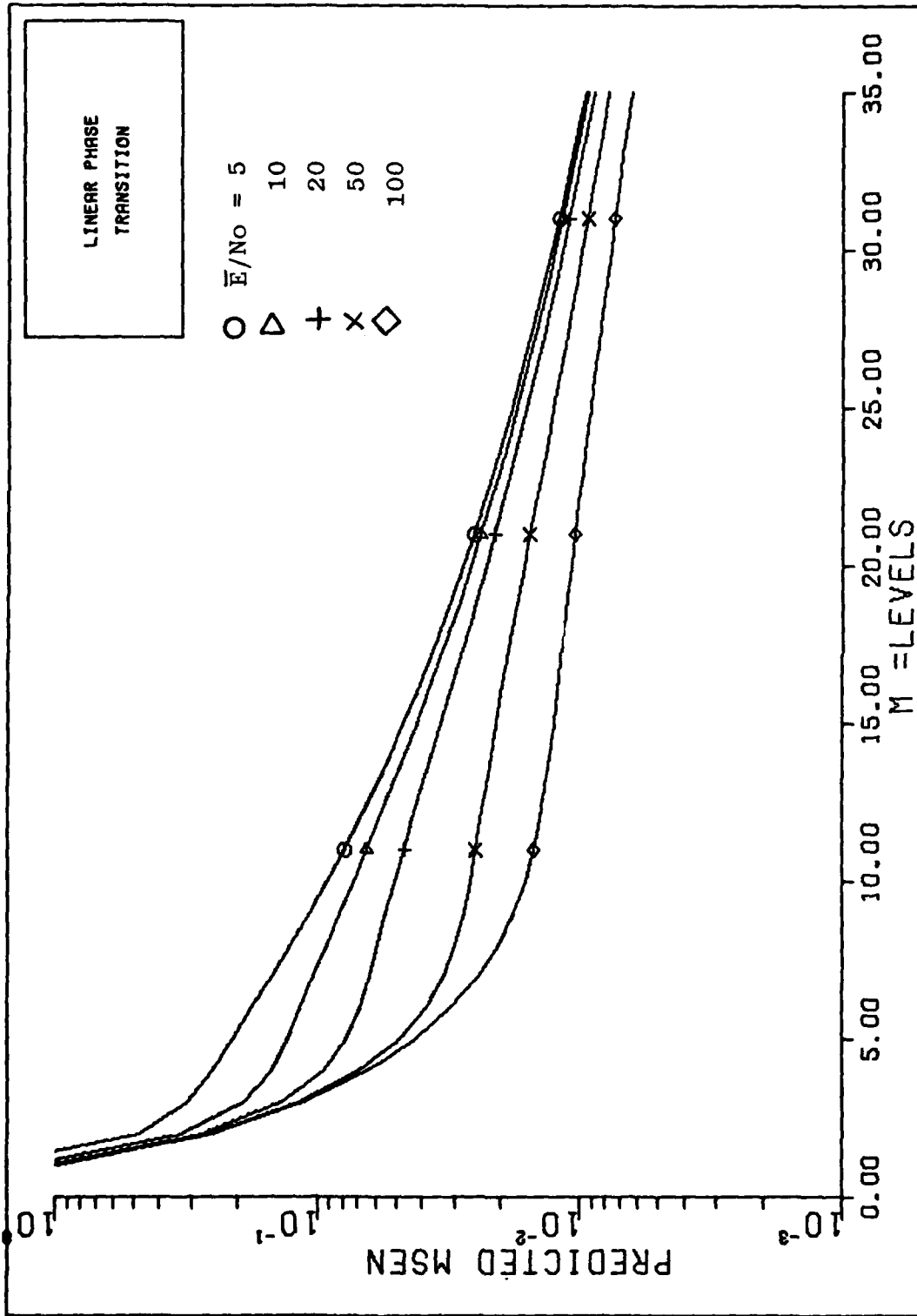


Figure 16 Predicted MSN versus M , Linear Transition, Random Variable A

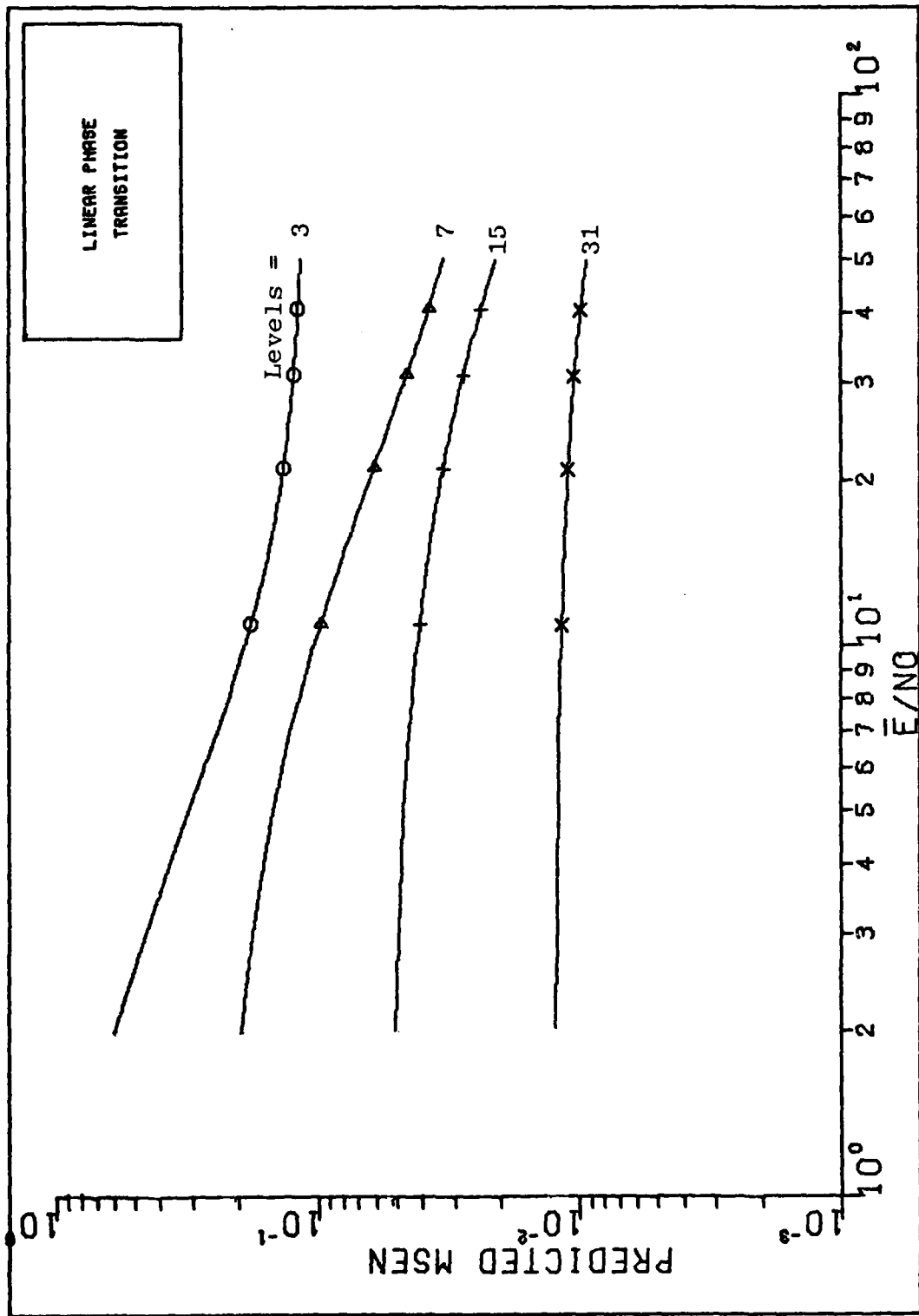


Figure 17 Predicted MSN versus \bar{E}/N_0 , Linear Transition, Random Variable A

The expected value of probability of any error, $E\{P_E\}$, is given by

$$E\{P_E\} \approx E\{P'_E\} = E \left\{ \frac{1}{2} e^{-\frac{D_m^2}{4N_0}} \right\} \quad (84)$$

$$E\{P'_E\} = \frac{1}{2 + 2 \frac{\bar{E}}{N_0} (1 - \cos \frac{2\pi}{M})} \quad (85)$$

The predicted normalized MSE for the step transition case is given by

$$\text{MSEN} = \frac{1}{M^2} + \frac{3}{M^2} \left(8 - \frac{2}{3}\right) \frac{1}{2 + 2 \frac{\bar{E}}{N_0} (1 - \cos \frac{2\pi}{M})} \quad (86)$$

The results for this case are shown for various values of M and \bar{E}/N_0 in Figures (18) and (19). The familiar trend towards smaller MSEN with increasing \bar{E}/N_0 and M is evident in these figures. Overall, the predicted MSEN is better for this case than for the linear phase transition case. The reason for this is that there is a larger euclidean distance between two signals which make step transitions than two signals which make linear transitions (over the same sequence of phase values).

Bias

It has been shown by Scharf (Ref 9:21-23) that the maximum likelihood (ML) estimator is modulo- 2π unbiased for the complex normal model when the phase is constant. As pointed

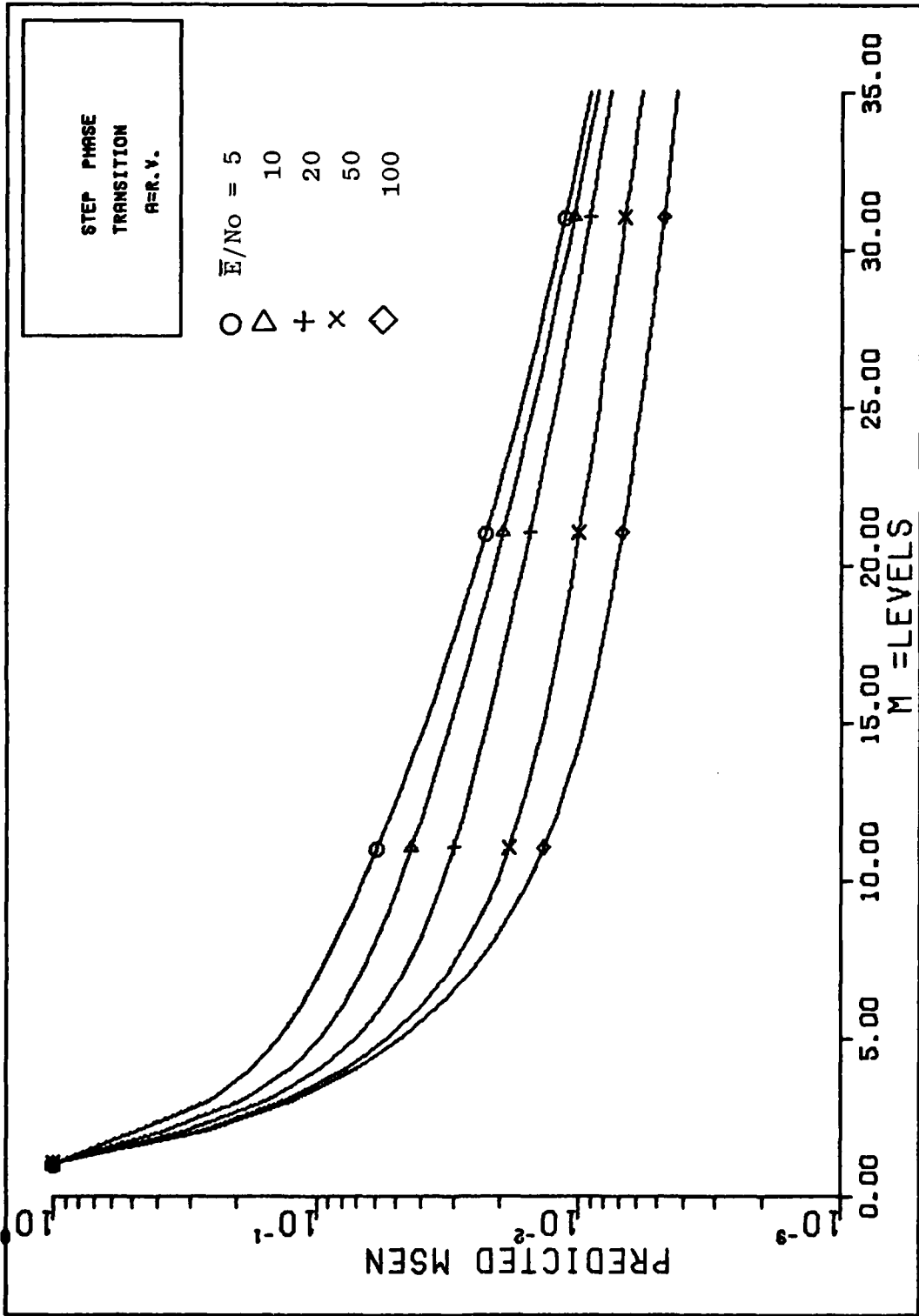


Figure 18 Predicted MSEN versus M, Step Transition, Random Variable A

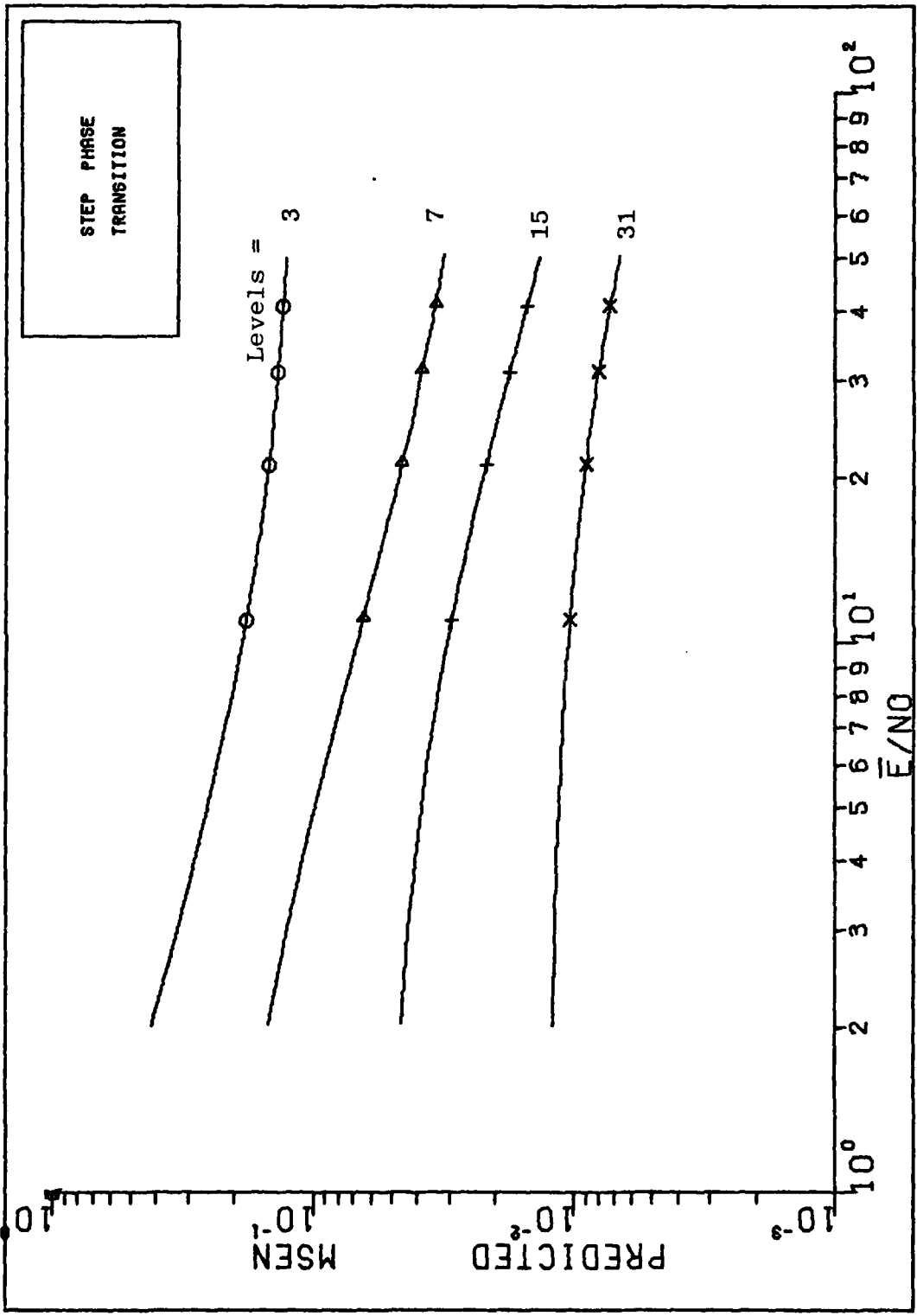


Figure 19 Predicted MSEN versus \bar{E}/NO , Step Transition, Random Variable A

out in the reference, this is identical to the MAP case with uniform prior statistics on the phase process.

Performance Analysis Comments

The lower bounds in figures (9), (11), (13) and (15) are strict; however, the tightness of the bounds and the accuracy of the predicted MSEN depends on the argument of the Q function in the prediction equation. Constant argument lines are plotted on these graphs. There is a high degree of confidence in the predicted values whenever the argument is larger than about three because equation (48) is a good approximation to P_E in this region.

As can be seen from the figures, many of the predicted points are outside of the high confidence region. Although the predictions may be good, there is no way to estimate how good they are with these methods. In addition, these performance predictions give no indication of the sensitivity of the estimator to decision depth, phase variance, or various correlation times.

Because of these limitations in the performance analysis, a simulation of the estimator is useful.

IV. Estimator Simulation

A Monte Carlo simulation of the Viterbi algorithm modulo- 2π phase sequence estimator is useful to obtain performance data for an entire range of input data and estimator parameters.

Simulation Setup

The simulation program was written in FORTRAN and run on the Cyber 175/Cyber 74 systems available for use at The Air Force Institute of Technology. After the parameters for the simulation have been input, the program generates a true phase sequence, constructs the signal model in quadrature form, adds white gaussian noise to the signal, and then estimates the phase based on the noise corrupted measurement. The phase sequence is estimated over one scan (100 measurements) and the error and mean-square error are calculated for each time interval. The value of 100 measurements per scan was selected to be much larger than the largest decision depth (10) so that any transient effects due to startup could be observed. Estimations can be repeated for many runs (scans) in order to calculate ensemble averages of error and mean-square error at each time interval.

Two cases of true phase of the signal are used in the simulation. In the first, the phase is constant over the length of the scan and the value for each run is selected randomly from a uniform distribution on $(-\pi, \pi)$. This allows

exercising of the estimator's parameters without any masking effects due to changing phase. The random choice of phase is made with the use of the intrinsic and subroutine functions for selecting uniform random deviates.

The second sample phase function, a tactical phase, is used to approximate what could occur in actual use. It is assumed that the dwell time T is $0.5 \mu s$, the illuminated area is a circle one foot in diameter, and the range ambiguity distance is 20 feet. The phase of a signal received from scanning over the length of a vehicle (an interesting tactical target) on flat ground can be approximated by the phase function shown in Figure 20.

The phase in Figure 20 is shown beginning at $-\pi/2$ radians for clarity, but the phase is allowed to start at any value selected from a uniform distribution on $(-\pi, \pi)$. The sample phase in Figure 20 is modified by adding zero mean white gaussian noise with a variance that corresponds to one foot squared. This is done to depict the roughness of a typical surface which would be found under real conditions. Instead of white noise, the phase can be varied by adding correlated noise in order to match the phase statistics of a random walk on a unit circle. A simple way to do this is by filtering white gaussian samples with a one stage infinite impulse response (IIR) digital filter and then adding the correlated phase noise to the phase function of Figure 20.

After the true phase sequence has been constructed for

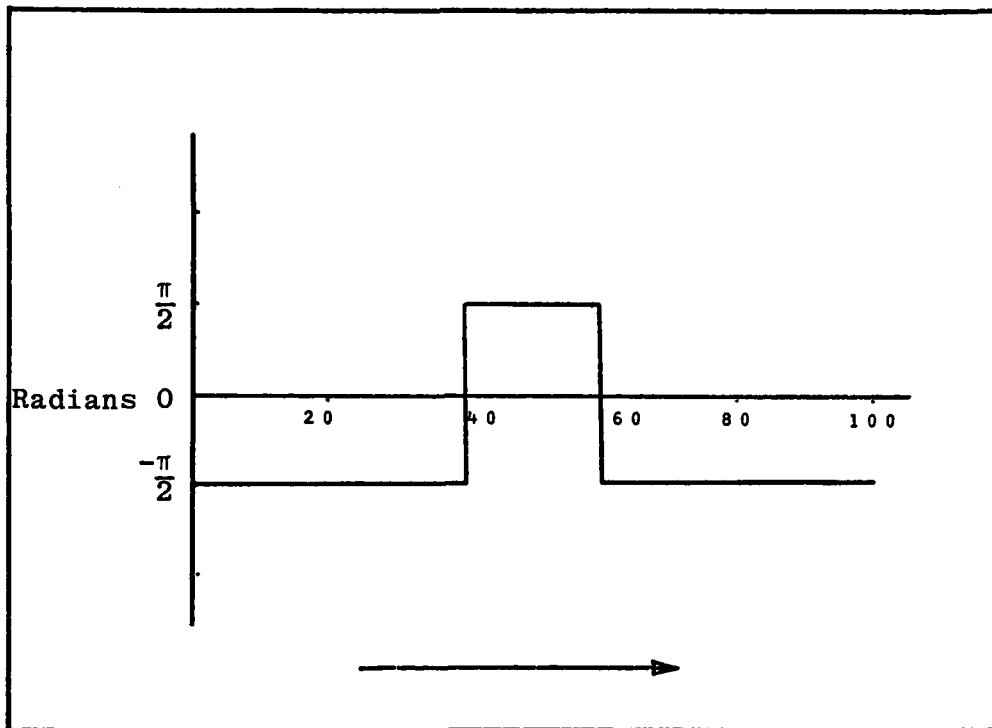


Fig. 20. Tactical Phase Signal

the whole scan, individual measurements Z_k are calculated using equation (10). Two cases of amplitude values are used in the results that follow. In the first case, the amplitude is constant over the entire scan and the value of A_k is calculated by

$$A_k = \sqrt{\frac{E}{N_0} \frac{2N_0}{T}} \quad (87)$$

In the second case, the discrete time amplitude values, A_k , are selected from a Rayleigh distribution to simulate a fading signal. The second moment of A_k is determined by

$$E\{A^2\} = \frac{\bar{E}}{N_0} 2N_0 T \quad (88)$$

where \bar{E}/N_0 is the expected value of the signal to noise ratio. The second moment specifies the Rayleigh distribution. Sample values are calculated by generating a random uniform sample and then converting it to a Rayleigh distribution sample. The coherence time of the fading amplitude can be varied by letting each Rayleigh sample be valid for n measurement samples; the "coherence time" for amplitude is then approximately $t_c = nT$.

In the following results, the word depth refers to the decision depth of the algorithm. This is identical to K_0 , the fixed lag described in Chapter II. At time k , an estimate of the phase at time $k-K_0$ is produced by the algorithm. The number of discrete phase values the estimate can attain is labelled LEVELS= M in the figures that follow, where M is odd. The term $\sigma_0^2 T$ from equation(14) is labelled VARPH in the graphical results. This is a measure of the variance of the phase process which the algorithm "assumes" it is tracking. As $\sigma_0^2 T$ becomes small, the transition density of equation (14) becomes gaussian and the distribution on ϕ_k becomes $N(\phi_{k-1}, \sigma_0^2 T)$. If $\sigma_0^2 T$ is too small, the estimator will not follow rapid fluctuations in the true phase. Conversely, if $\sigma_0^2 T$ is too large, the estimator will be susceptible to tracking isolated noise bursts even when the phase is constant.

The number of ambiguous decisions for a scan is labelled AMBIG in the figures. This is a figure of merit which gives the number of possible values of $\hat{\phi}_{k-K_0}$ when the value of $\hat{\phi}_{k-K_0}$ for each of the M sequences is not identical. In general, the values stored in the M sequences will converge to a single sequence as time progresses. The decision rule implemented in this simulation selects the sequence with the largest Γ_k and then outputs the $k-K_0$ value of $\hat{\phi}$ from that sequence. The ambiguity counter is incremented once for each sequence which does not have the same value for $\hat{\phi}_{k-K_0}$ as the MAP sequence. An ambiguous decision count of zero does not guarantee that the correct sequence $\{\phi_k\}_1^K$ was estimated, only that the MAP sequence given the measurement sequence was estimated.

Simulation Results

The results of the estimator simulations are discussed in this section and shown in the figures that follow. The parameter values and conditions are shown on the figures.

Confidence of Sample Statistics. The data presented in the following figures is a result of taking ensemble averages of the mean-squared error over 50 Monte Carlo runs. This value was selected by observing how the ensemble mean square error changes with increased number of runs, shown in Figure(21). As the number of runs increases, the ensemble average mean-square error tends to settle down to a specific value. The number 50 was

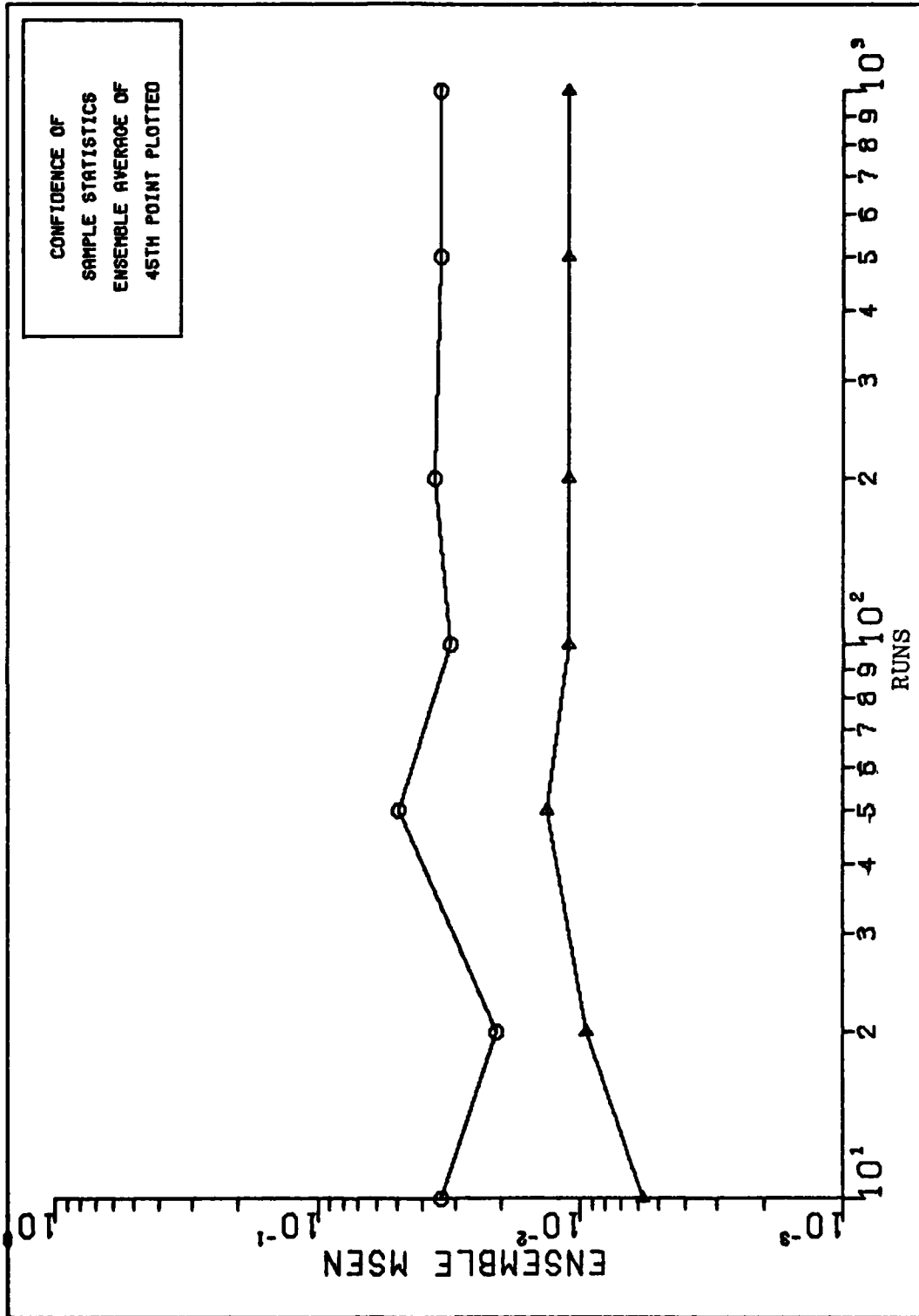


Figure 21 Number of Runs

selected to provide good results at a reasonable expenditure of computer time. Similar results can be obtained by observing the ensemble average of the phase errors as the number of runs is increased.

The weak law of large numbers can be used to calculate the probability that the ensemble average of the phase estimates is more than 0.1 radians away from the ensemble average of the true phase. For a probability of 0.1 that the phase difference is larger than 0.1 radians, 3290 runs are necessary. A similar argument using the central limit theorem gives a result that 809 runs are required.

The data calculated from these two limit theorems fit the data collected from simulations. Since MSE is the prime measure of performance and it settles quickly for number of runs greater than 50, the value of 50 was selected for use in the generation of the following data.

Sample Estimation. A sample phase estimation for one scan is shown in Figure (22). The normalized ensemble mean-squared error for 50 simulation runs with these parameters is shown in Figure (23). The true phase plot is marked with a " ϕ " every ten points. As can be seen, the estimator tracks the true phase very well.

Because the estimator is modulo- 2π , estimates may be obtained which appear poor, but which are actually good. An example of this is shown in Figures (24) and (25). In this example, the true phase crosses over the $+\pi$ boundary several

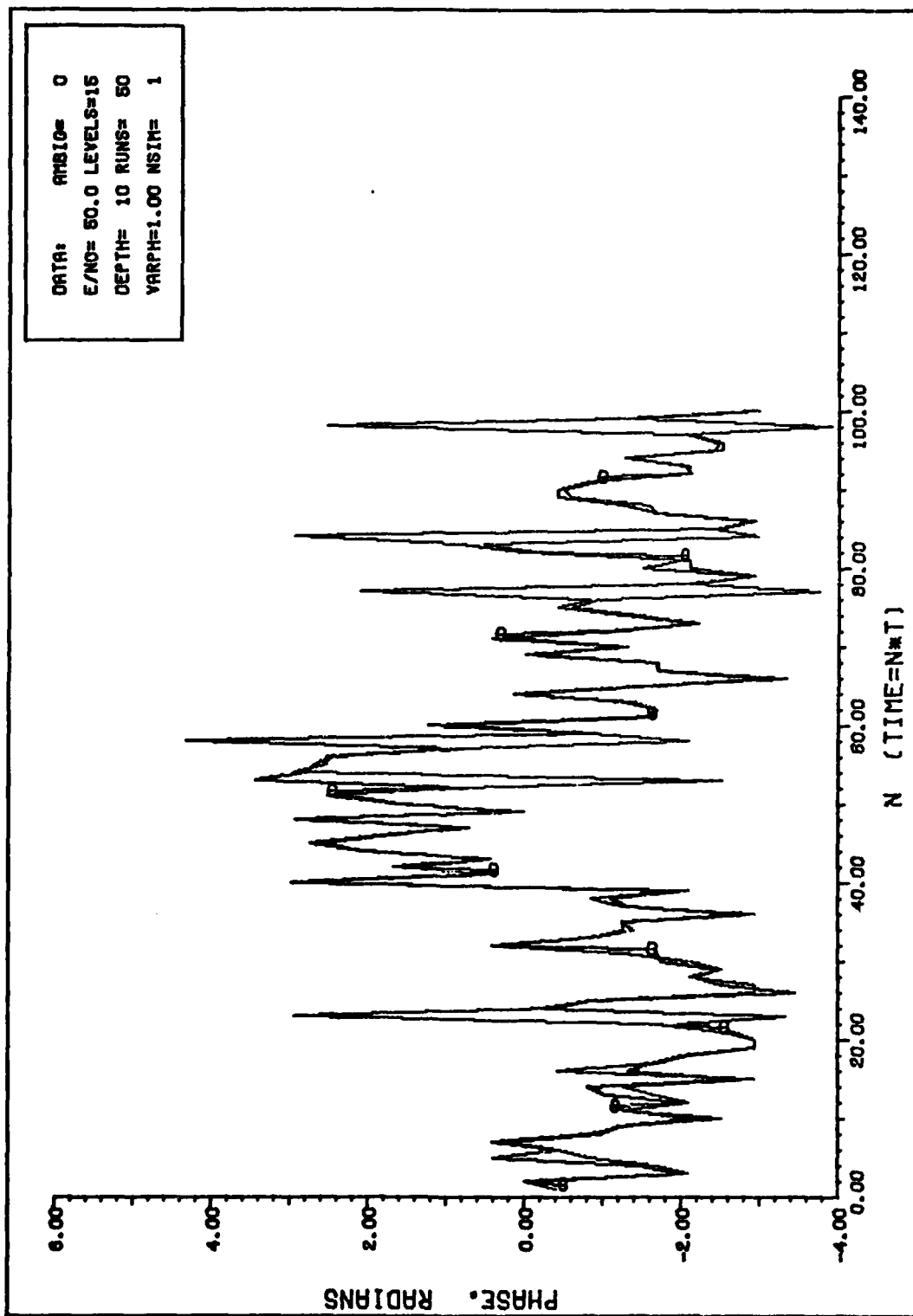


Figure 22 Sample Estimation

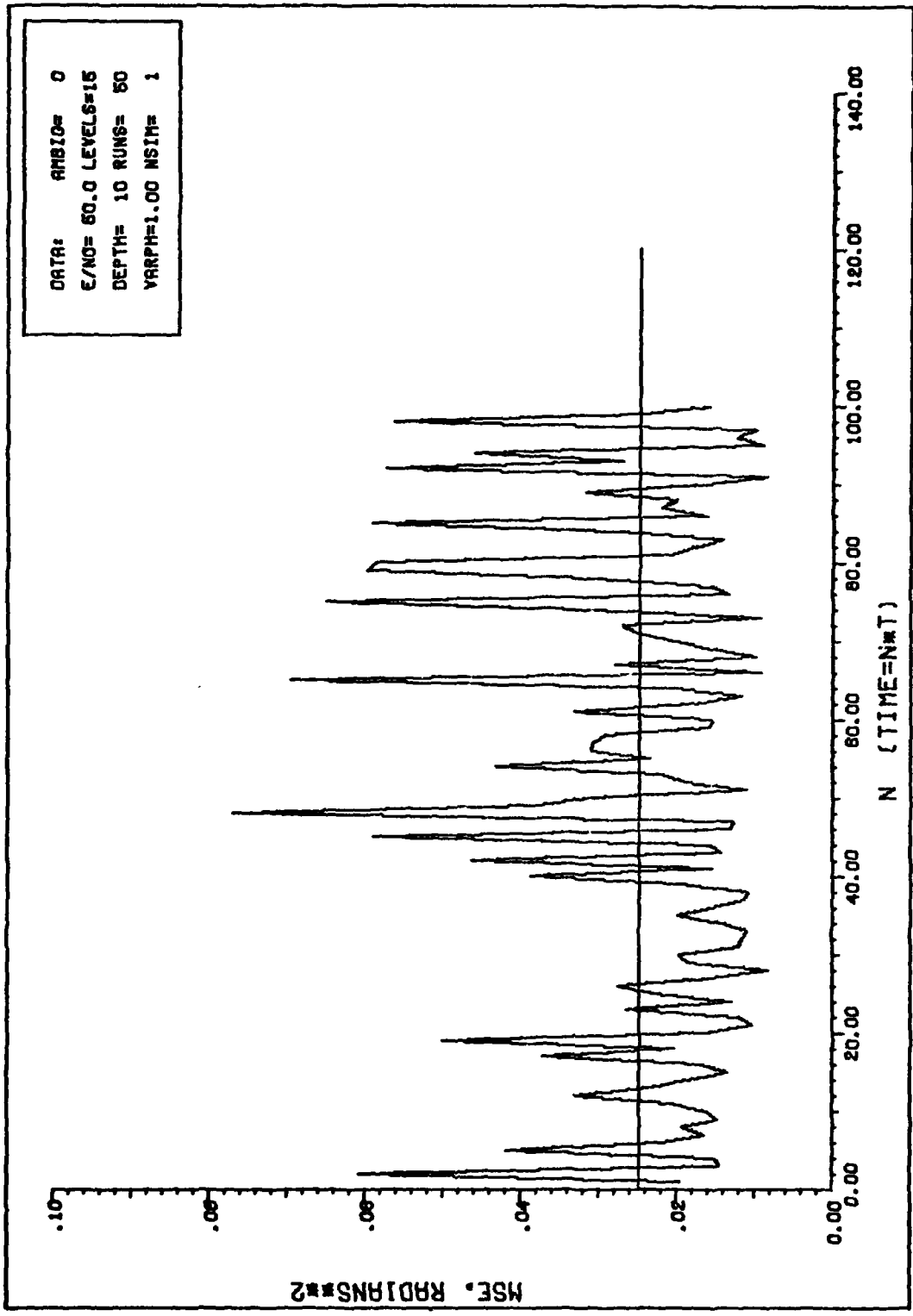


Figure 23 Ensemble Mean-Squared Error

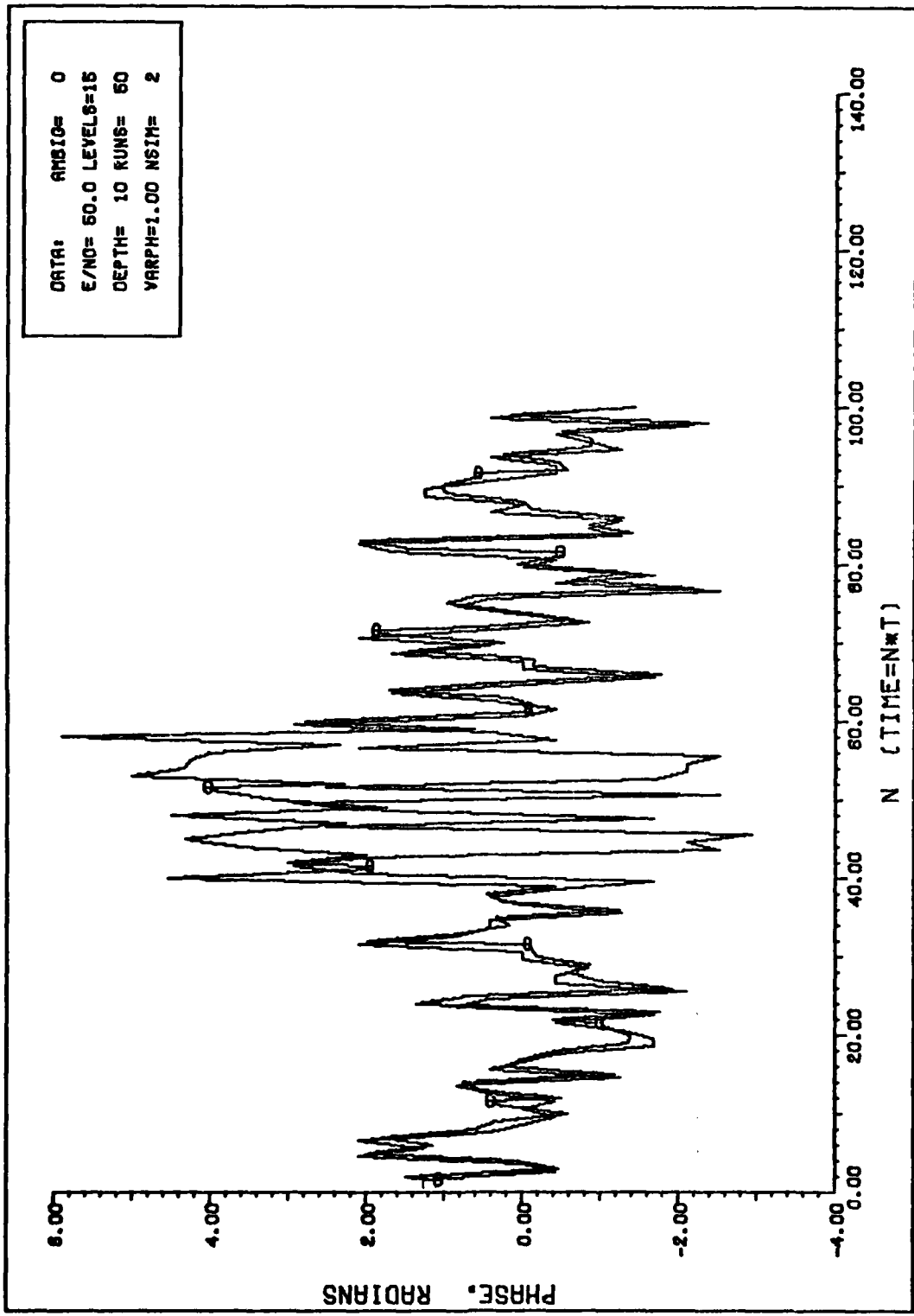


Figure 24 Sample Estimation

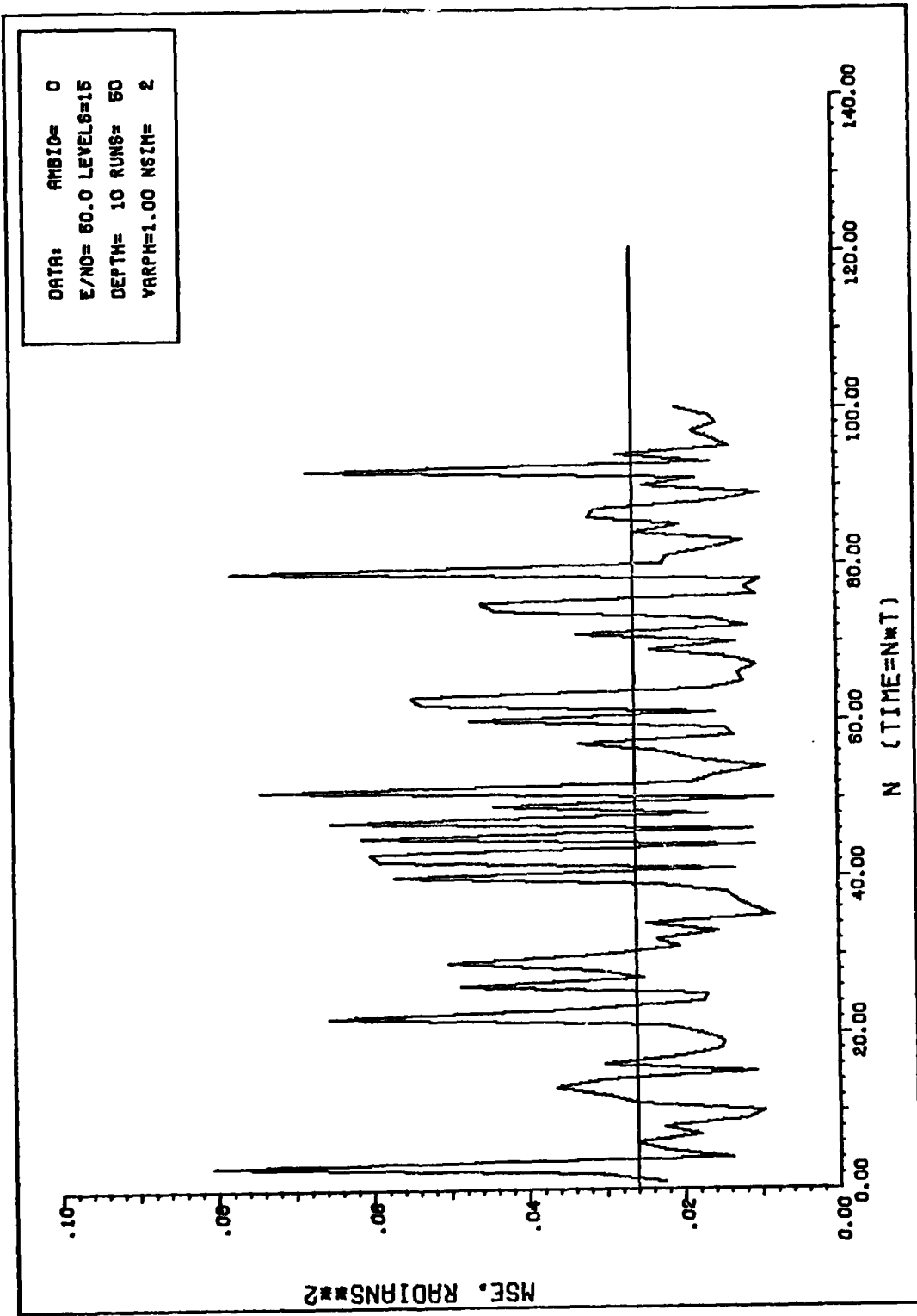


Figure 25 Ensemble Mean-Squared Error

times between $N=40$ and 60 . The estimator produces a value "close modulo- 2π " to the true value, but because the true phase is out of the estimator's output range, the phase estimate appears to vary wildly. If the estimated values near $-\pi$ on Figure(24) are adjusted up by 2π , the figure appears very much like Figure (22). This is also shown by comparing the ensemble mean-squared error plots corresponding to the two examples. The mean-squared errors for both are nearly identical despite the fluctuations in the estimated phase. This is analogous to cycle slipping in a phase locked loop (PLL). This characteristic of a modulo- 2π estimator must be considered when designing the equipment which will use the phase estimate.

Ambiguous Decisions. The number of ambiguous decisions varied from 1400 for depth=0, to 700-800 when depth=5, and zero when depth=10. The number of ambiguities drops quickly to zero as depth is increased. Very little variation in the number of ambiguities was found as other parameters such as $M, \bar{E}/N_0$, or $\sigma_0^2 T$ were changed. With a depth of 10, $\bar{E}/N_0 > 2$, and either fixed or varying amplitude; there were no ambiguous decisions observed.

Parameter Variations. The performance of the estimator as the key parameters are varied is displayed in Figures (26) through (42). Analysis of the individual figures is given in the following paragraphs. Performance is graphed as normalized mean-squared error versus \bar{E}/N_0 and families of curves are plotted for varying levels, $\sigma_0^2 T$, depth, amplitude coherence time, and errors in the estimation of the amplitude.

Curves are plotted for the four combinations of constant phase, constant amplitude; constant phase, Rayleigh amplitude; tactical phase, constant amplitude; and tactical phase, Rayleigh amplitude. The figures are labeled with the parameters of interest and the performance of the estimator is evident.

Figures (26) through (29) are of particular interest because they correspond to the parameters used in predicting the performance of the estimator. In these figures, change in performance is displayed as the number of quantization levels is varied. Values of predicted MSEN and the lower bound on MSEN (from Chapter III) are plotted on Figures (26) through (29) for the case of $M=15$. A comparison of the predicted values with the measured results shows that the prediction is good in areas of the curve where the argument of the $Q(\cdot)$ function is larger than three. Also, the lower bound is fairly tight. This is as expected for the step phase transition case since the Viterbi algorithm estimator implemented in this simulation has as its input discrete phase values which are equivalent to a continuous phase input with step changes in value. As predicted, the mean-squared error decreases as the number of quantization levels is increased. The match between predicted MSEN and the simulation results is least good for high values of M and low values of E/N_0 . This is not unexpected, since the argument of the Q function is small for low E/N_0 and large M .

As predicted, the performance of the estimator degraded

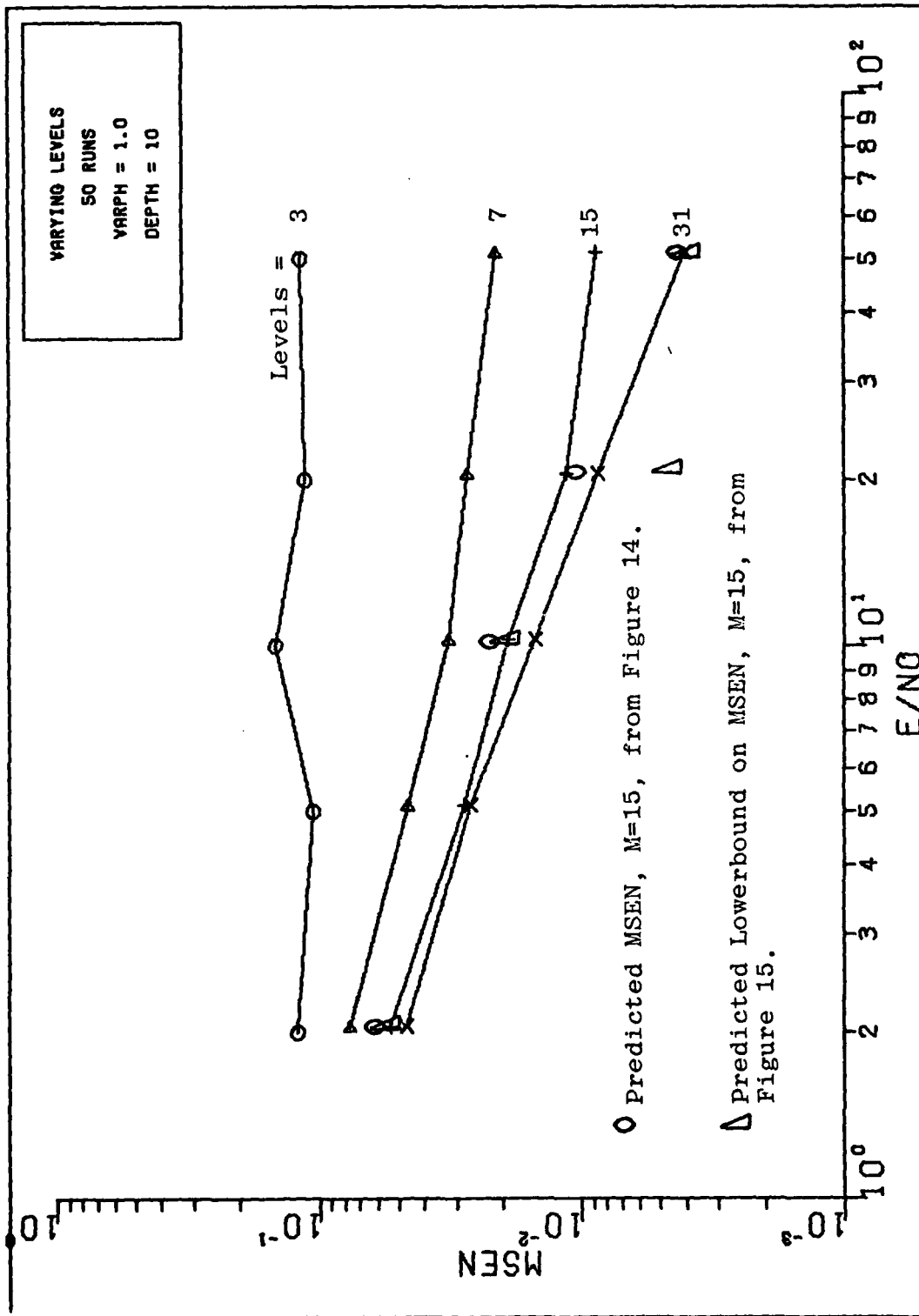


Figure 26 MSEN, Varying Levels, A, ϕ

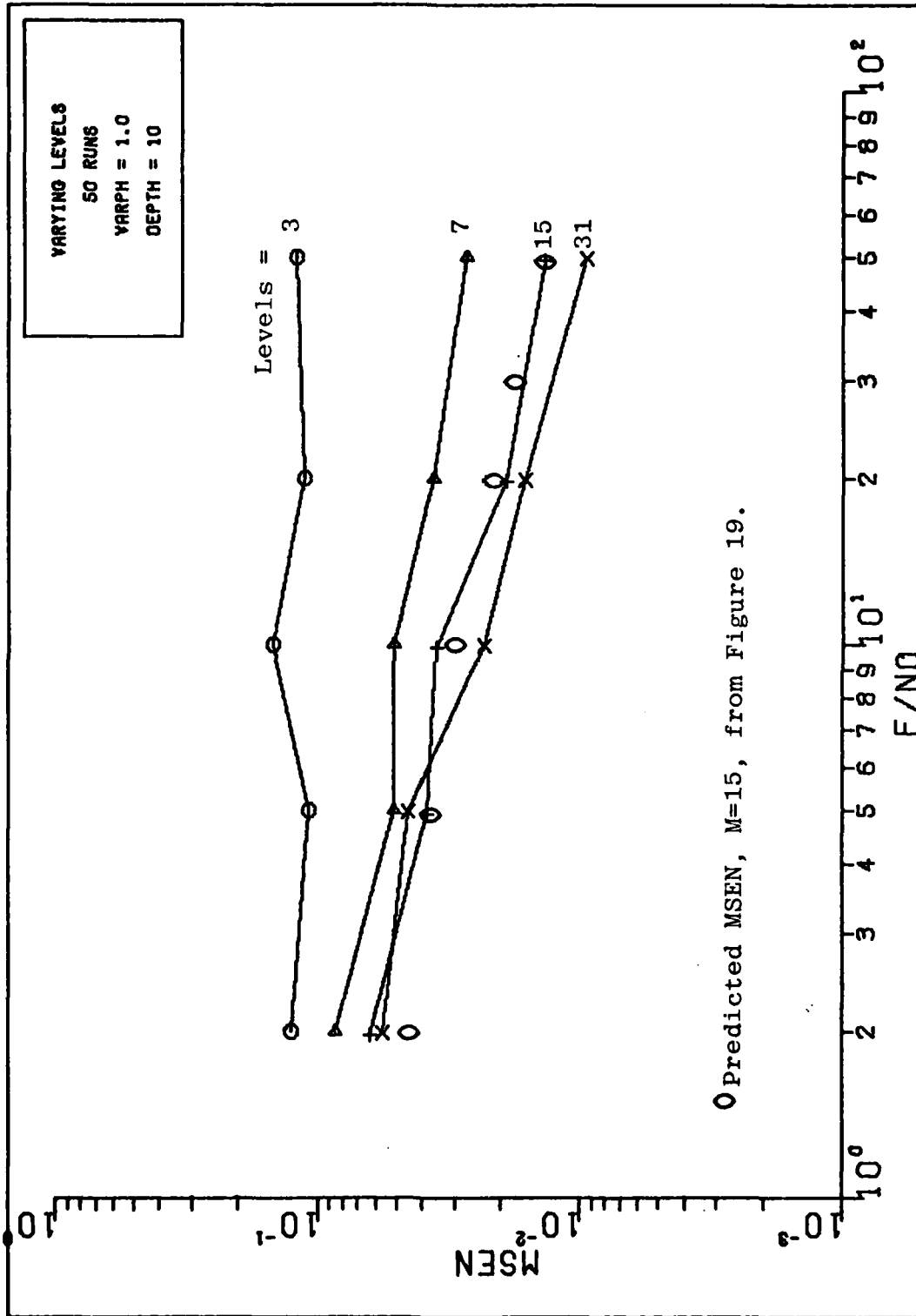


Figure 27 MSEN, Varying Levels, ϕ, A

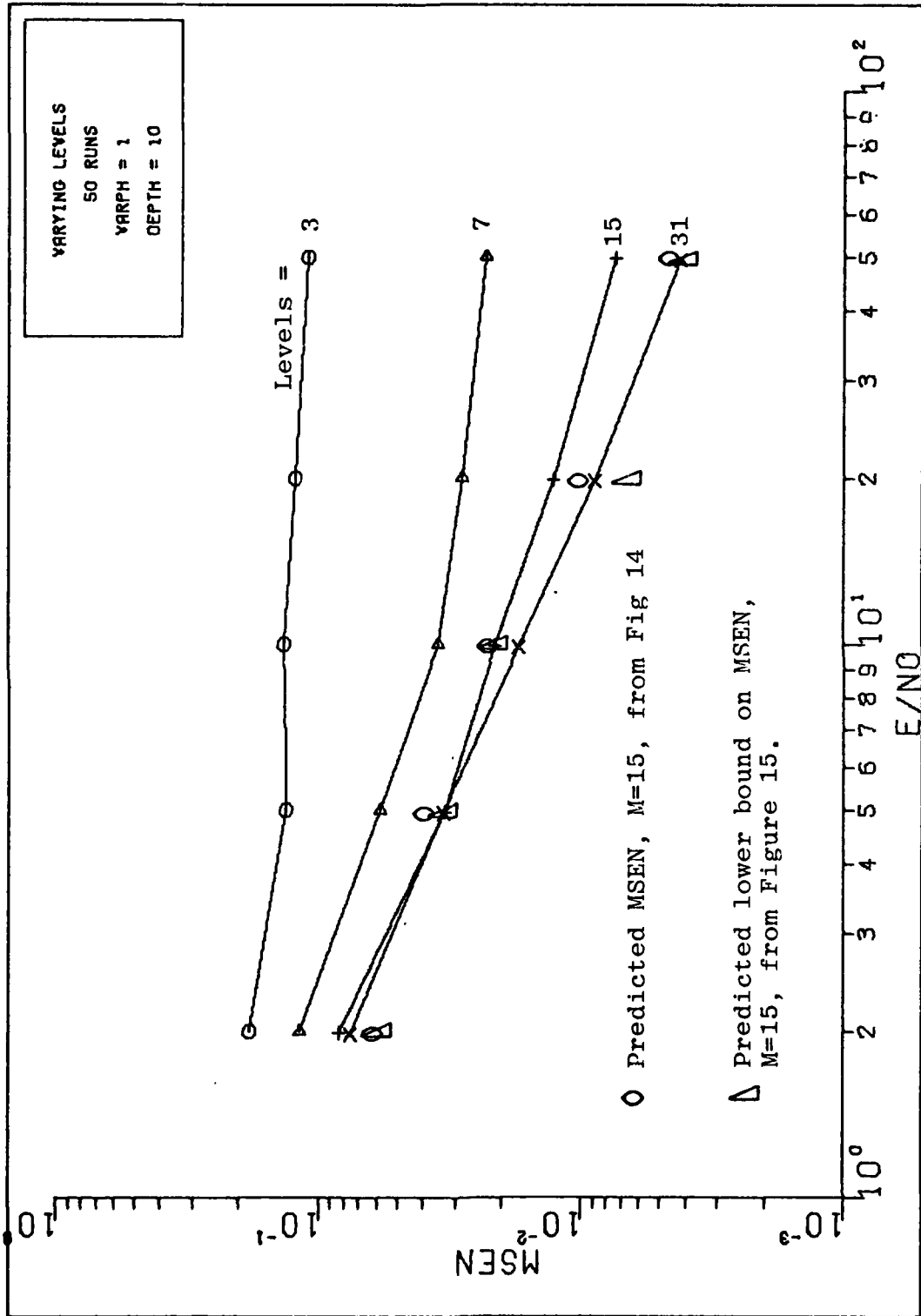


Figure 28 MSEN versus E/No, Varying Levels, Tactical ϕ , A

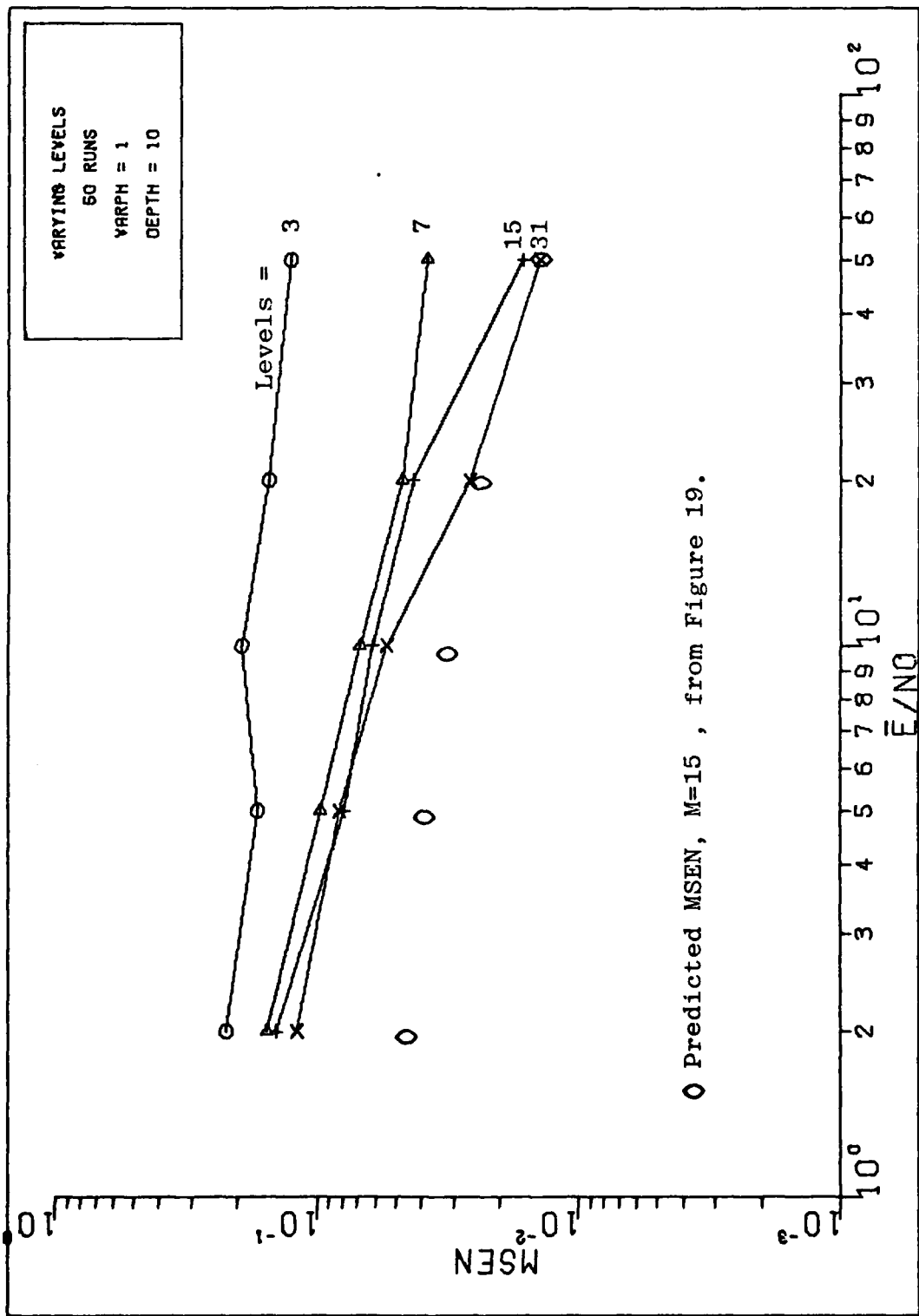


Figure 29 MSEN versus \bar{E}/N_0 , Varying levels, tactical ϕ , A

when the amplitude was allowed to vary. Simulation results for the Rayleigh fading amplitude case for various values of M are shown in Figures (27) and (29). Results of several simulations indicate that the crossover of the $M=15$ and $M=31$ lines is a result of the randomness of the Monte Carlo simulation for a sampling of 50 runs and not an inherent trait of the estimator. These results also correspond closely with the predicted MSEN shown in Figure (19) for the random amplitude case.

Figures (30) through (33) reflect the variation of mean-squared error performance for several values of $\sigma_0^2 T$ with $M=15$. As described previously, $\sigma_0^2 T$ is the variance the estimator "assumes" for the transition probabilities of the phase process. Figures (30) and (31) reflect the performance when the phase is constant but unknown over the whole scan. The best performance is achieved when $\sigma_0^2 T$ is small ($\sigma_0^2 T=0.1$ for the values displayed). This is an intuitively pleasing result since a constant phase has a conditional transition variance of zero and this MAP estimator will tend to select constant values of $\hat{\phi}_k$ when $\sigma_0^2 T$ is very small. It should be noticed that performance varies more at low values of E/N_0 than at high values. This, too, is as expected because when the signal amplitude is very small, the estimator "relies" more heavily on the transition probabilities than the signal measurement for calculation of the Γ_k 's.

The performance is reversed for cases in which the phase

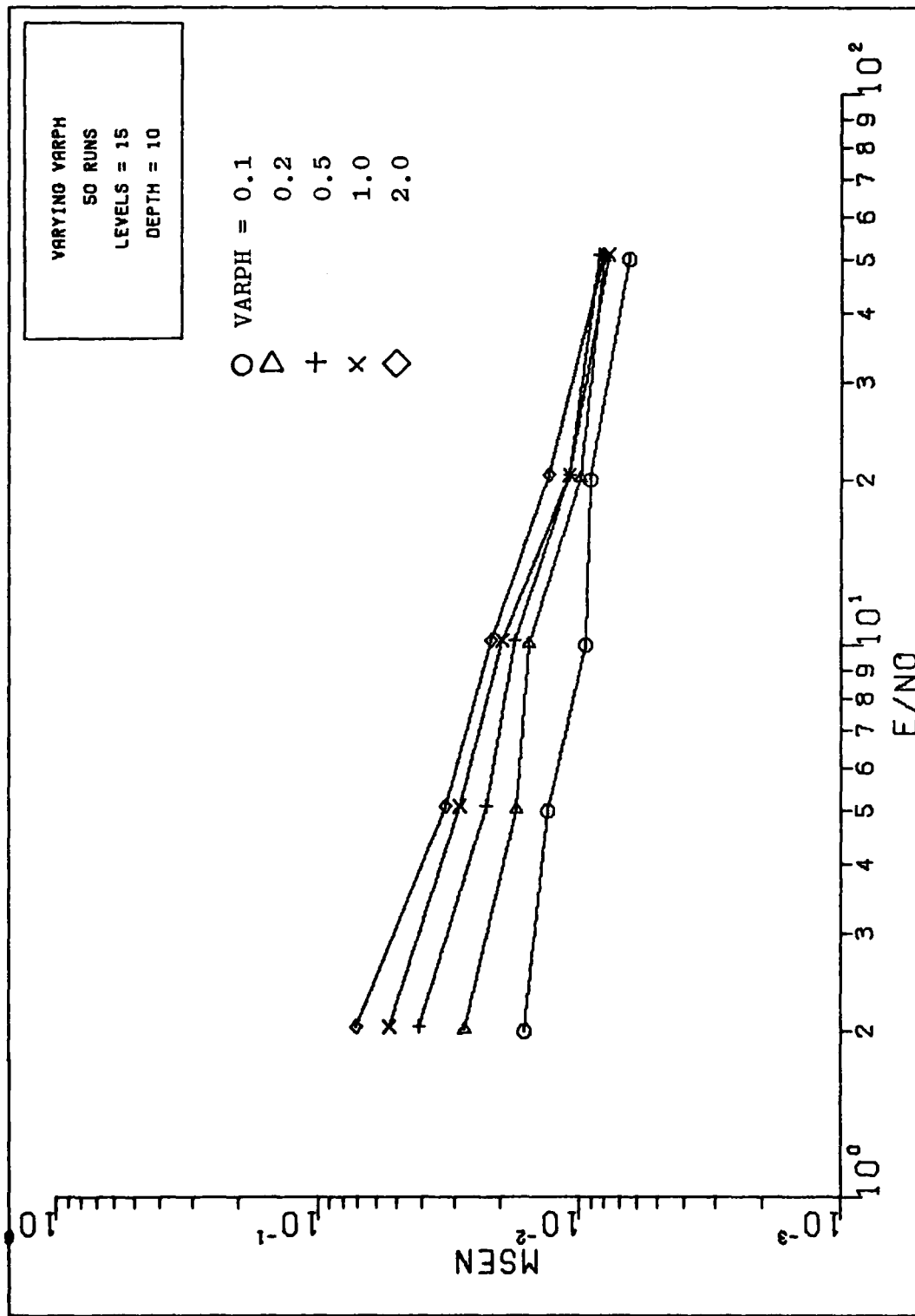


Figure 30 MSEN, Varying VARPH, ϕ , A

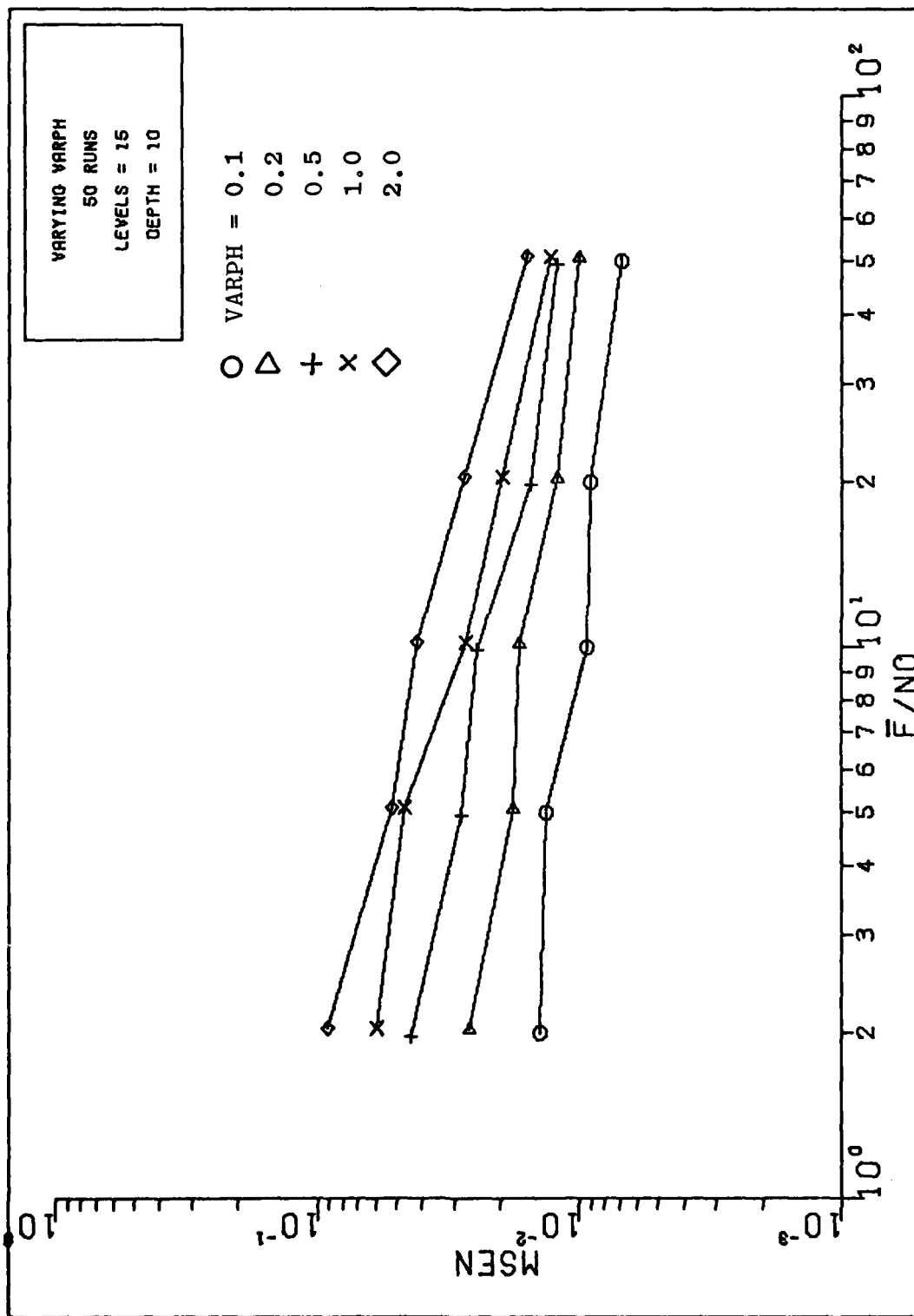


Figure 31 MSEN, Varying VARPH, ϕ , λ

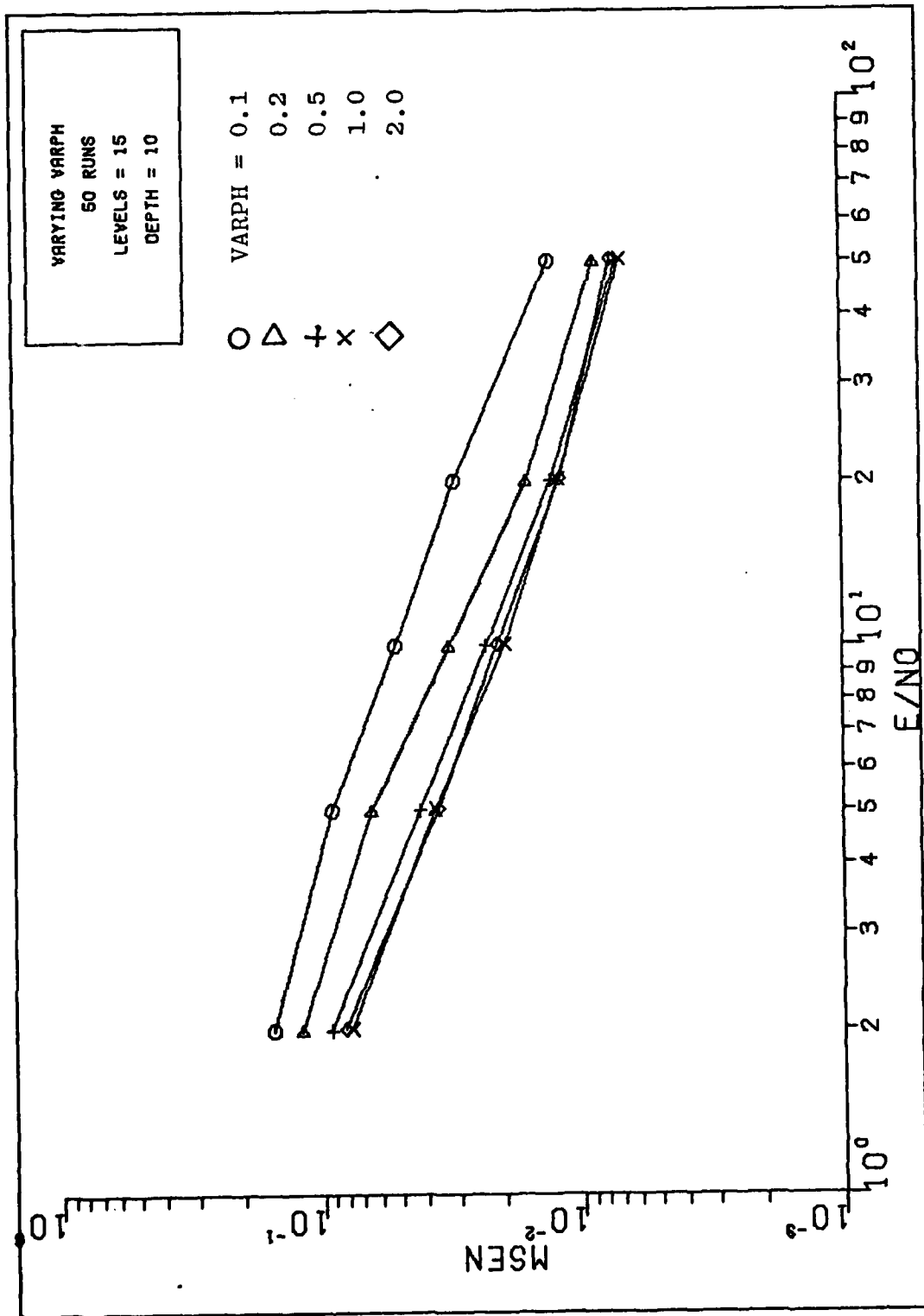


Figure 32 MSEN, Varying VARPH, Tactical ϕ , A

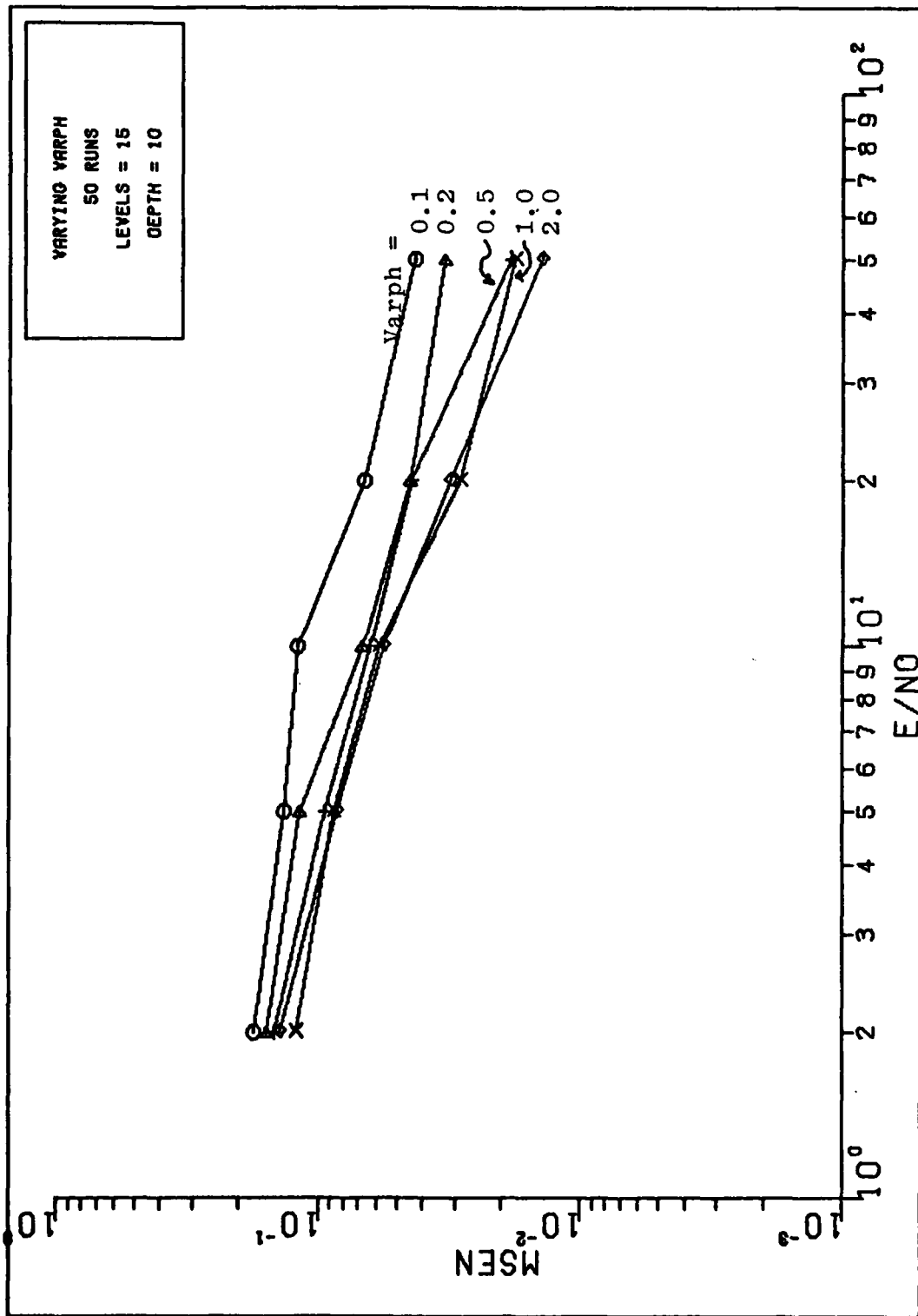


Figure 33 MSEN, Varying VARPH, Tactical ϕ , A

is allowed to vary as shown in Figures (32) and (33). In these simulations, white noise samples with a variance of 0.31 radians squared were added to the underlying tactical phase shape. As can be seen from these figures, as $\sigma_0^2 T$ was increased from 0.1 to 0.5 radians squared, the MSEN performance improved. Further increase in $\sigma_0^2 T$ produced no significant improvement in performance. A large value of $\sigma_0^2 T$ may allow the estimator to track the phase of a noise burst instead of the true phase of the signal for a specific realization of the random measurement process; however, this degradation in performance as $\sigma_0^2 T$ becomes too large is not evident in the figures because they show results of 50 scans and the data are averaged over the 50 scans.

Figures (34) through (37) display the performance of the estimator as the decision depth is varied. In all of these simulations, the number of quantization levels is 15. The results closely correspond to the results predicted in Chapter III. There is little variation in performance due to a change in depth over the domain of signal to noise ratios displayed. Figure (35) does show a tendency of lower MSEN for larger values of depth.

Figures (38) and (39) show the effect of varying the coherence time of the random amplitudes. As defined previously, "coherence time" is $t_c = nT$, where T is the sampling time and n is the number of time intervals for which a specific realization of the random amplitude is valid. There is little change

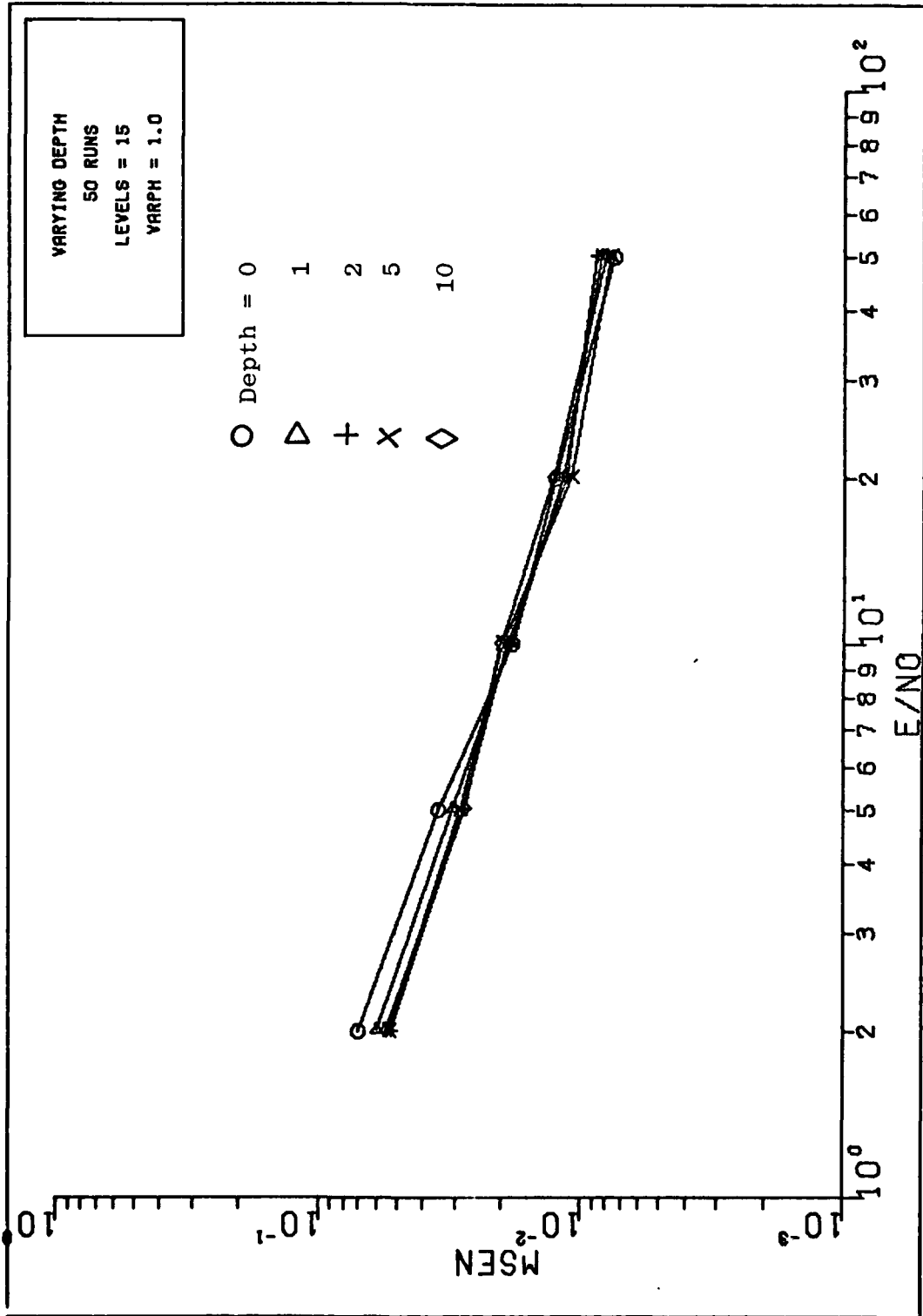


Figure 34 MSEN, Varying Depth, A, ϕ

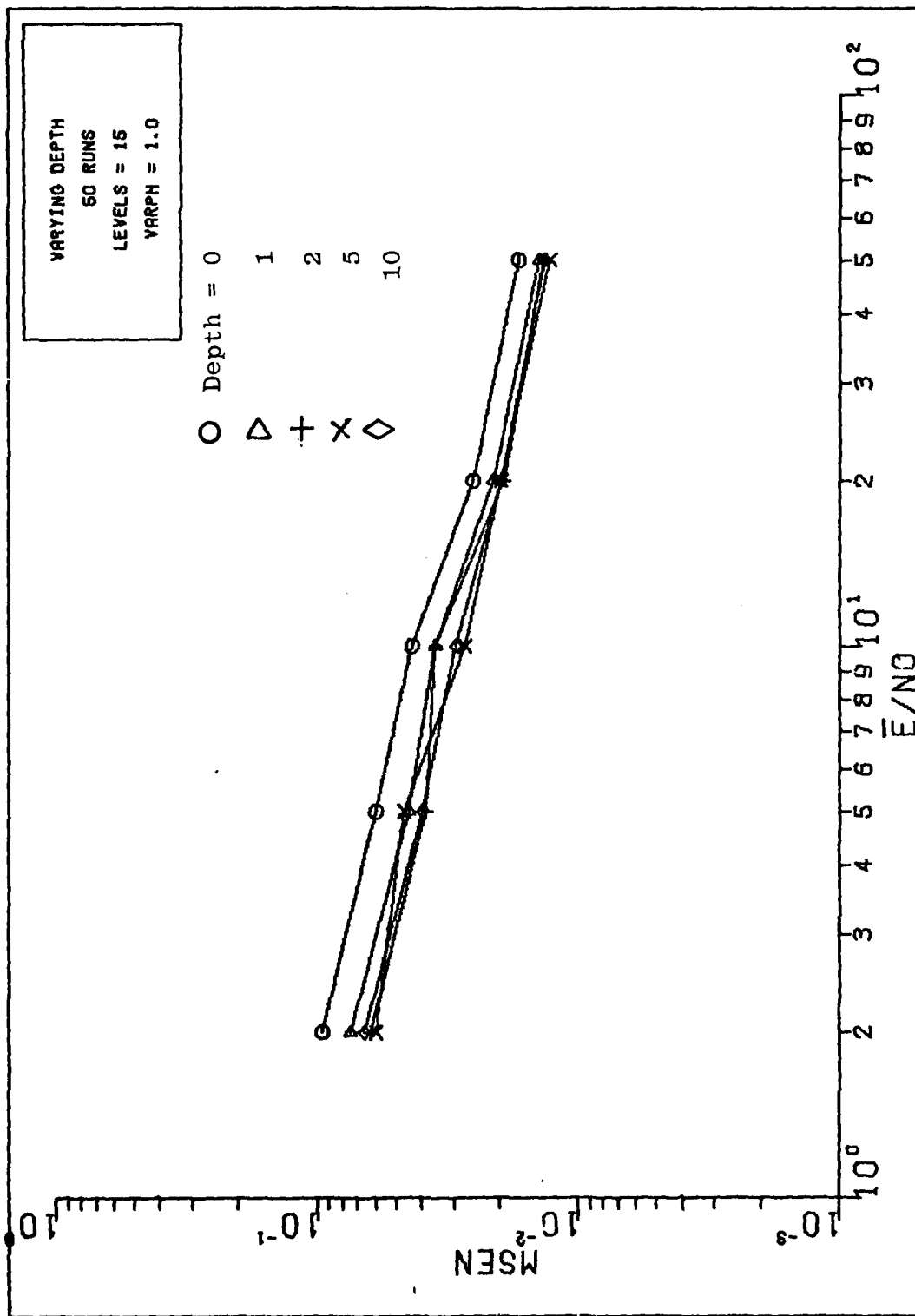


Figure 35 MSEN, Varying Depth, A, ϕ

AD-A080 368

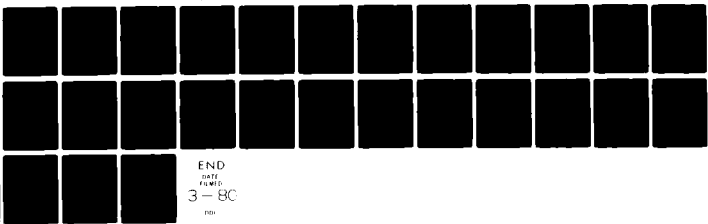
AIR FORCE INST OF TECH WRIGHT-PATTERSON AFB OH SCH00--ETC F/G 17/8
PHASE SEQUENCE ESTIMATION FOR LASER LINE-SCAN IMAGERY IN THE PR--ETC(U)
DEC 79 D E NEER
AFIT/6E/EE/79D-24

UNCLASSIFIED

NL

2 of 2

AD-A080 368



END
DATE
FILMED
3-80

FOUO

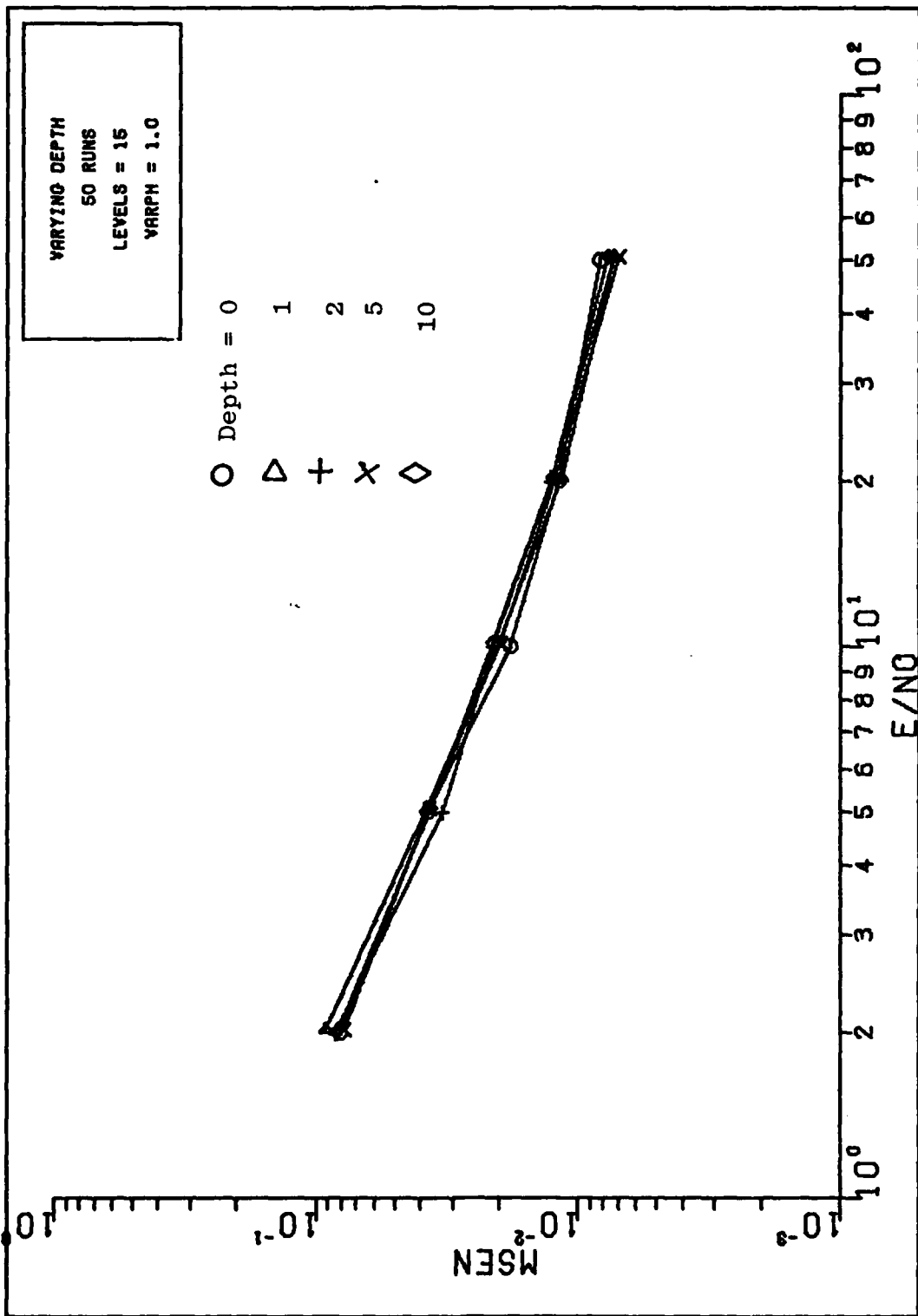


Figure 36 MSEN, Varying Depth, A, Tactical ϕ

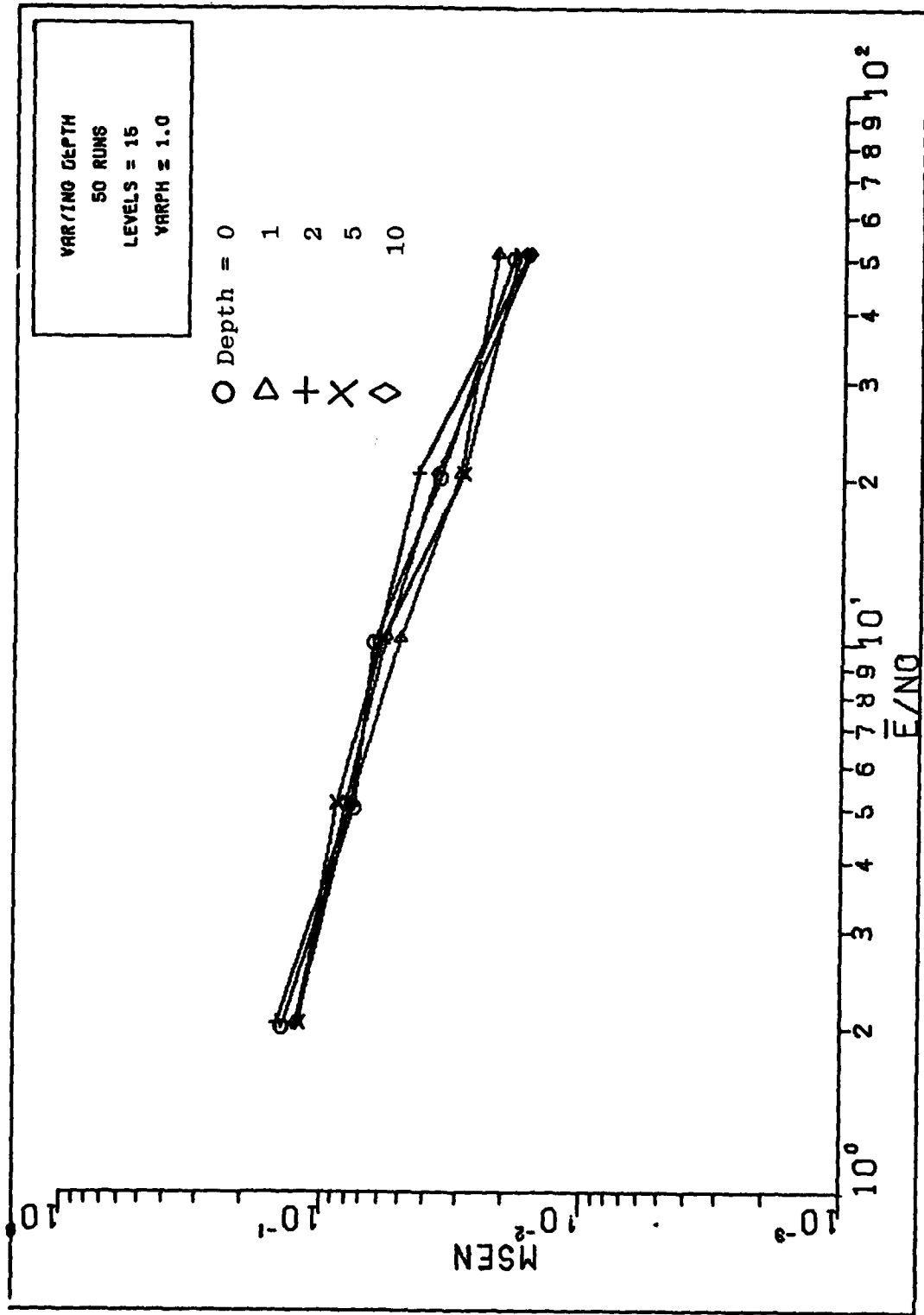


Figure 37 MSEN, Varying Depth, ϕ , Tactical ϕ

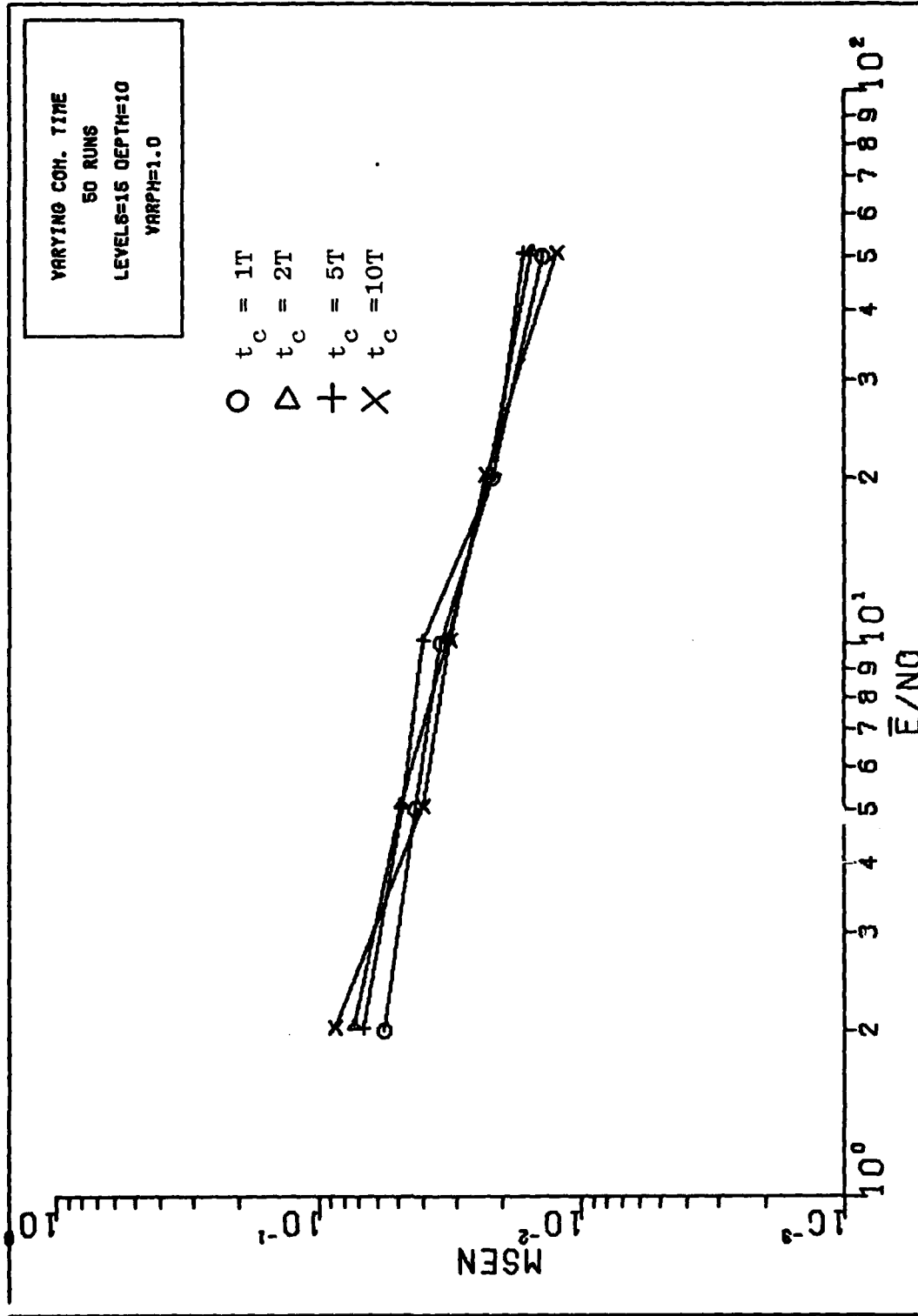


Figure 38 MSEN, Varying Coherence Time, A_c, ϕ

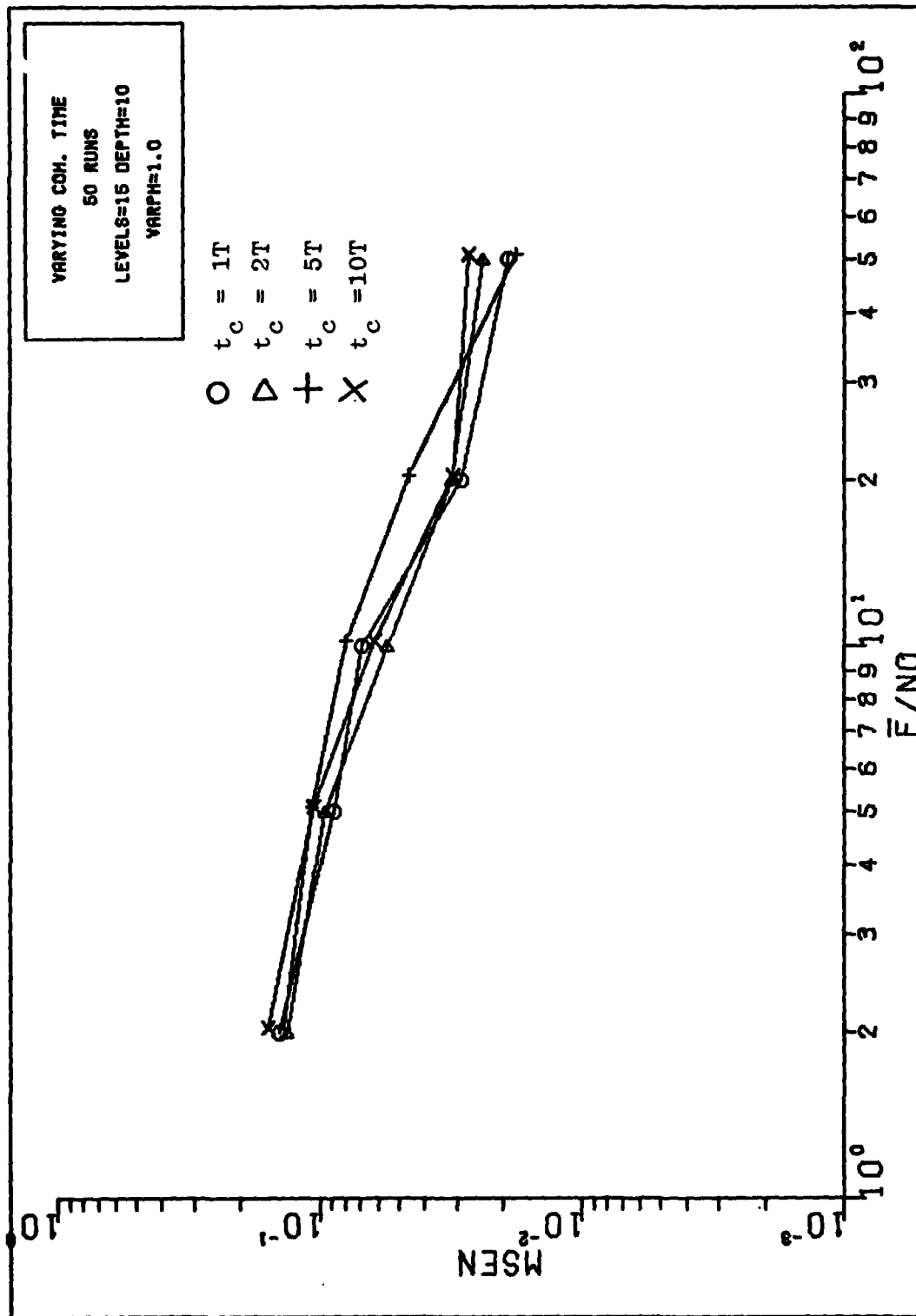


Figure 39 MSEN, Varying Coherence Times, A , Tactical ϕ

in performance as t_c varies from T to $10T$. The performance curves match closely the predicted performance.

Figures (40) and (41) display the effects of perturbations in the estimation of the discrete time signal amplitudes, A_k . The perturbed \hat{A}_k is calculated for the inphase case by

$$\hat{A}_k = A_k + a_I \quad (89)$$

and for the quadrature case by

$$\hat{A}_k = \sqrt{(A_k + a_I)^2 + a_Q^2} \quad (90)$$

where A_k is the Rayleigh amplitude, and a_I and a_Q are Gaussian random variables with zero mean and variance σ_{aI}^2 and σ_{aQ}^2 , respectively. Little change in performance is exhibited by the estimator over the range of disturbed amplitude samples. The estimator MSEN increases by a factor of two as the variance of the disturbance is increased from 0.1 to 2.0 (at $\bar{E}/N_0=2$). The change in MSEN is less at higher values of \bar{E}/N_0 . In general, the estimator is insensitive to disturbances in the amplitude estimation. This is an extremely useful result. Not only is the estimator insensitive to a fast fluctuating signal, it is not greatly sensitive to errors in the amplitude estimate.

Figure (42) shows the results of the estimator performance when the input is as shown in Figure (20) with correlated noise added. The "noise" portion of the input phase was calculated

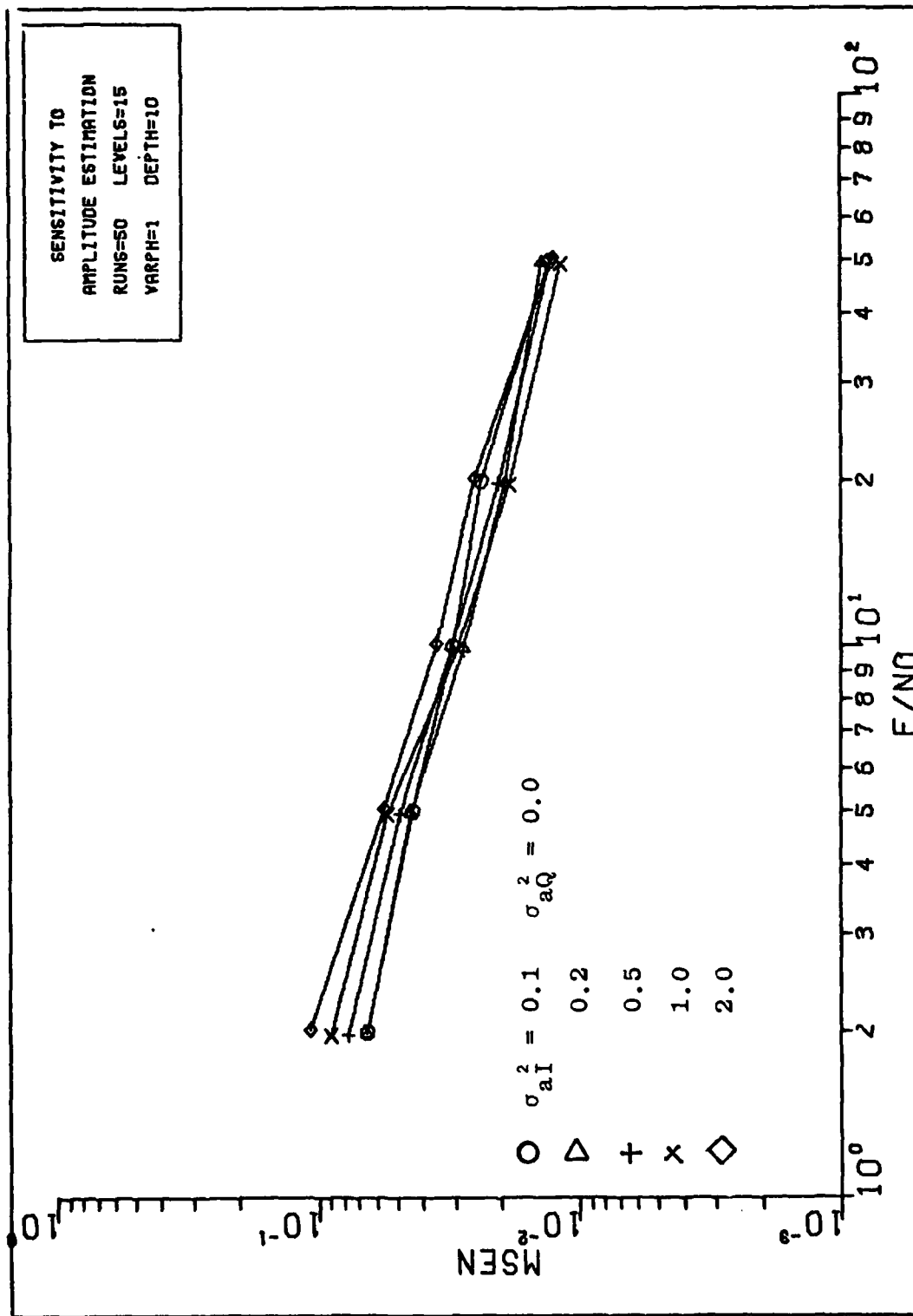


Figure 40 MSEN versus \bar{E}/N_0 , In Phase Amplitude Estimation Disturbance

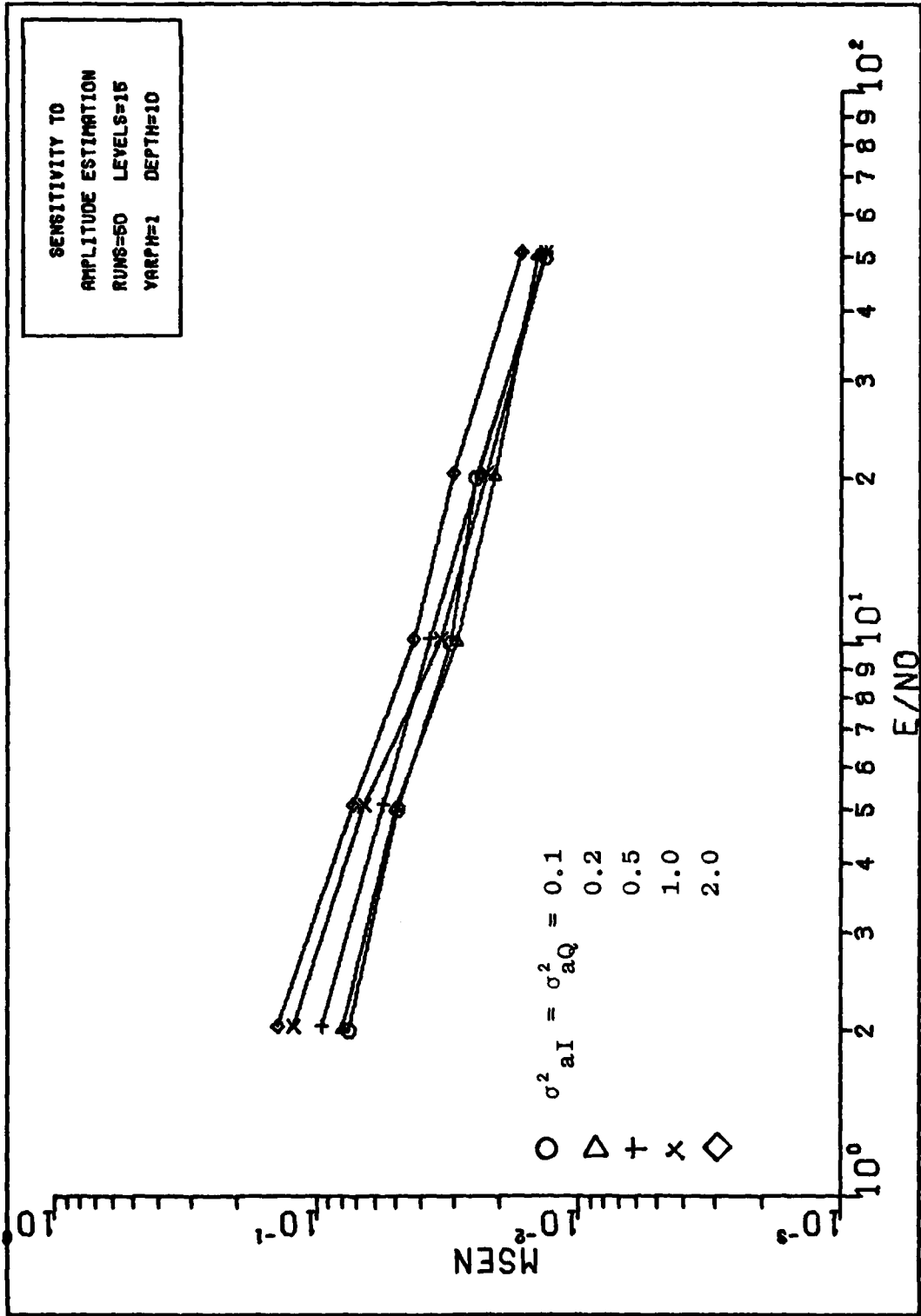


Figure 41 MSEN versus \bar{E}/N_0 , Quadrature Amplitude Estimation Disturbance

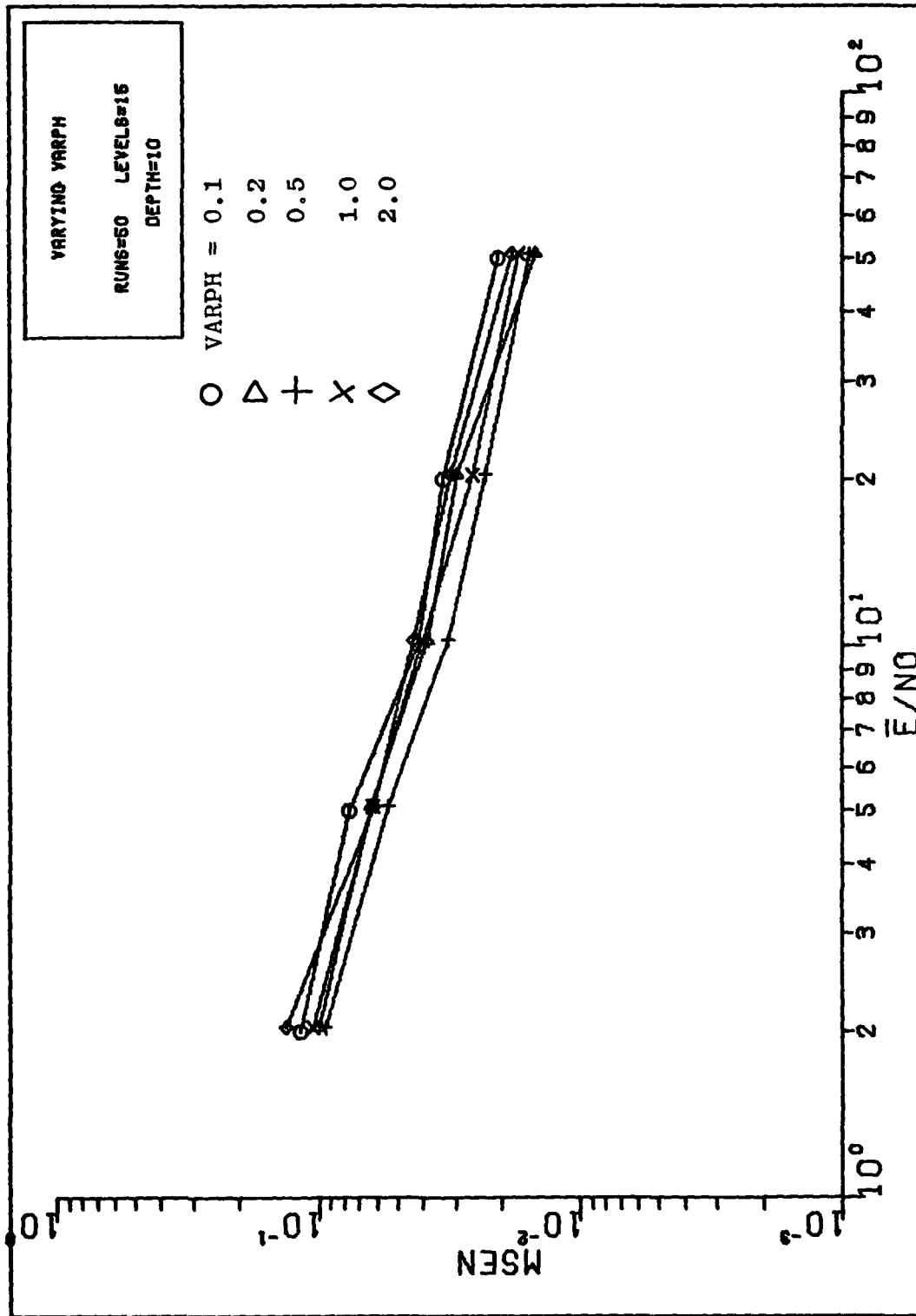


Figure 42 MSE/N versus \bar{E}/NO , Correlated Phase, Varying VARPH, \bar{A}

recursively by

$$\phi_k = \phi_{k-1} + W_k \quad (91)$$

where W_k is a Gaussian random variable with zero mean and variance of 0.5 .

The results shown in Figure (42) are very close to those of Figure (33) (same parameters except the input phase is "roughened" with white noise). The estimator displayed little sensitivity to the match between the $\sigma_0^2 T$ of the transition density and the variance of the input phase process.

The simulation results compare favorably with the performance predictions developed in Chapter III. In addition, the simulation results provide information on the effect of the parameters depth, $\sigma_0^2 T$, coherence time, and amplitude disturbance on performance. The next chapter compares these results with other estimation schemes.

V. Comparison with Other Estimators

A comparison of the performance of this estimator with bounds on estimator performance and predicted results of other methods is necessary in order to judge which scheme is best.

Cramer Rao Lower Bound

Rife and Boorstyn (Ref 8) have shown that the variance of a phase estimate, $\hat{\phi}$, can be lower bounded by the Cramer Rao (CR) bound

$$\text{Var}\{\hat{\phi}\} \geq \frac{\sigma^2}{b_0^2 N} \quad (92)$$

where b_0 is the amplitude of the real signal $b_0 \cos(\omega t + \phi)$, σ^2 is the variance of additive zero mean Gaussian noise, and N is the number of discrete time observations of the same constant phase signal made by the estimator. This CR bound is for a maximum likelihood (ML) estimator and corresponds to the Viterbi algorithm estimator when the a priori statistics on phase are uniform over the range $-\pi$ to π . The amplitude (b_0) and radian frequency (ω) are assumed constant and known.

When $N=1$, one observation is made for each value of $\hat{\phi}$ estimated. This corresponds to a decision depth of zero in the Viterbi algorithm estimator.

For the signal model posed in Chapter II, the signal to

noise ratio of the input signal is

$$\frac{E}{N_0} = \frac{A_K^2 T}{2N_0} \quad (93)$$

and the variance of the additive noise is

$$\sigma^2 = \frac{N_0}{T} \quad (94)$$

The CR bound (normalized by $\pi^2/3$) is

$$\text{Var}\{\hat{\phi}\} \geq \frac{3}{2 \frac{E}{N_0} \pi^2} \quad (95)$$

This CR lower bound is shown in Figure (43) along with simulation results of the ML Viterbi algorithm estimator for constant amplitude and phase with depth equal to zero. This assumes that the estimator is unbiased so that $\text{Var}\{\hat{\phi}\} = \text{MSE}$.

The CR lower bound for a larger N can be easily calculated from equation (87); however, the problem posed by Rife and Boorstyn is that of estimating constant but unknown parameters. The estimation problem investigated in this thesis is that of phase sequence estimation in which the phase can assume different values at each discrete time. Thus, the lower bound given by equation (92) for $N > 1$ is not relatable to results obtained from a simulation of the estimator presented in this report.

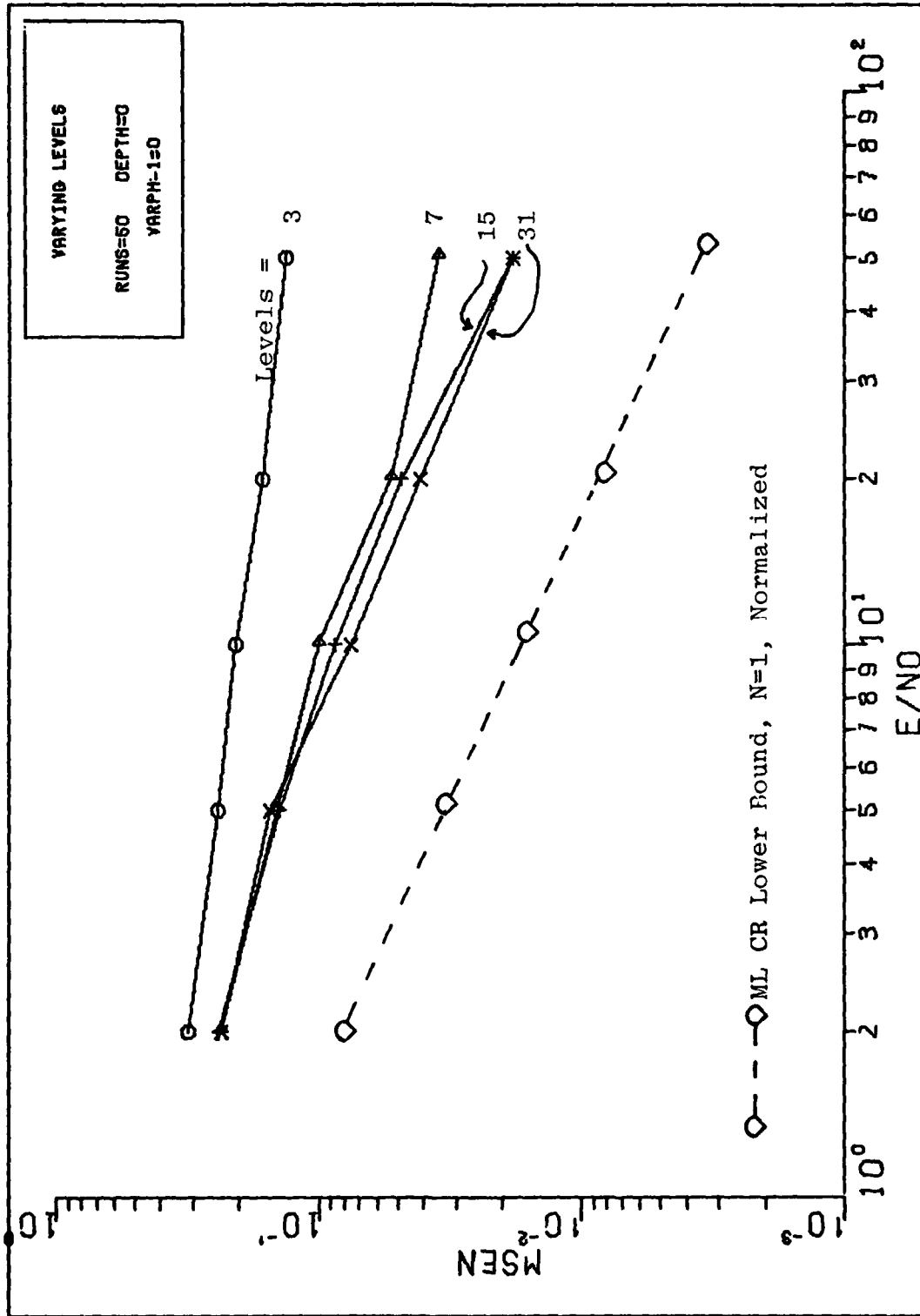


Figure 43 CR Lower Bound and ML Estimator Performance

Phase-Locked-Loop, Constant Amplitude

The performance of a phase-locked-loop for phase demodulation is well modeled and useful for comparison.

The phase-locked-loop (PLL) is assumed to be first order and linearized. The variance of the phase estimate is given by

$$\sigma_{\phi}^2 = \frac{1}{E/N_{0i}} \quad (96)$$

where E/N_{0i} is the input signal to noise ratio above threshold.

Values of σ_{ϕ}^2 , normalized by $\pi^2/3$ are shown in Figure (44) plotted with simulation results for various numbers of quantization levels. The PLL results have been taken from Viterbi (Ref12:94).

When compared with the simulation case of 15 quantization levels, the following results can be observed. The Viterbi estimator outperforms the PLL by almost six db at low signal to noise ratios and by about two db at the higher signal to noise ratios displayed in this figure.

It is also evident from Figure (44) that the PLL outperforms the $M=3$ and $M=7$ Viterbi estimator above a specific "crossover" signal to noise ratio. This is due to the quantization MSE lower bound inherent in the discrete value representation of the phase by the Viterbi estimator. The other two cases ($M=15$ and $M=31$) also have a lower bound on MSE; however, the bound is reached at a higher signal to noise ratio than

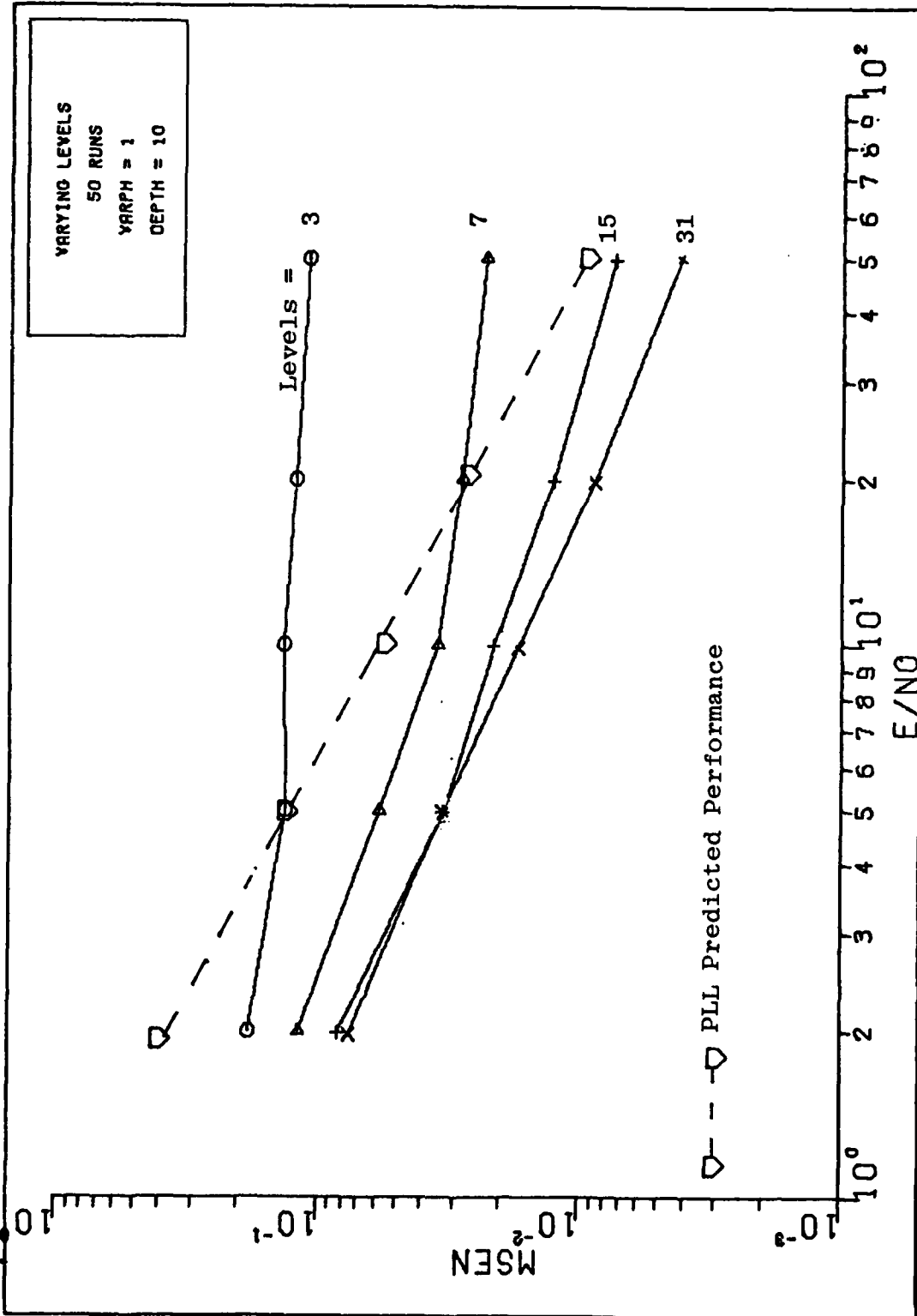


Figure 44 Simulated Estimator Performance versus PLL, Constant A

displayed in this figure.

Phase-Locked-Loop, Rayleigh Amplitude

The predicted results for PLL performance have been extended by Weber (Ref:13) to include the case of phase estimation for a signal with Rayleigh slowly fading amplitude.

Results for the slowly fading amplitude case are shown on Figure (45). All conditions are the same as for the PLL constant amplitude case with the exception that the amplitude is now allowed to fade.

A comparison with the $M=15$ case can again be made showing that the PLL requires an input signal to noise ratio of approximately 20 (13db) to achieve the same mean-squared error the Viterbi estimator attains at a signal to noise ratio of two (three db). This 10 db margin is nearly constant over the domain of signal to noise ratios displayed in Figure (45). Weber also notes that as the fading bandwidth becomes large (or the loop bandwidth bandwidth becomes small) the phase tracking becomes worse until the PLL loses lock (Ref13:497).

Comments

From the foregoing comparisons, it can be seen that in the constant amplitude case with $E/N_0 > 10$, the Viterbi estimator ($M=15$) outperforms the PLL by up to 5 db. This margin decreases with increasing E/N until the Viterbi estimator's performance is limited by quantization noise. Below a signal to noise ratio of 10, the smoothing effect and use of prior in the MAP Viterbi

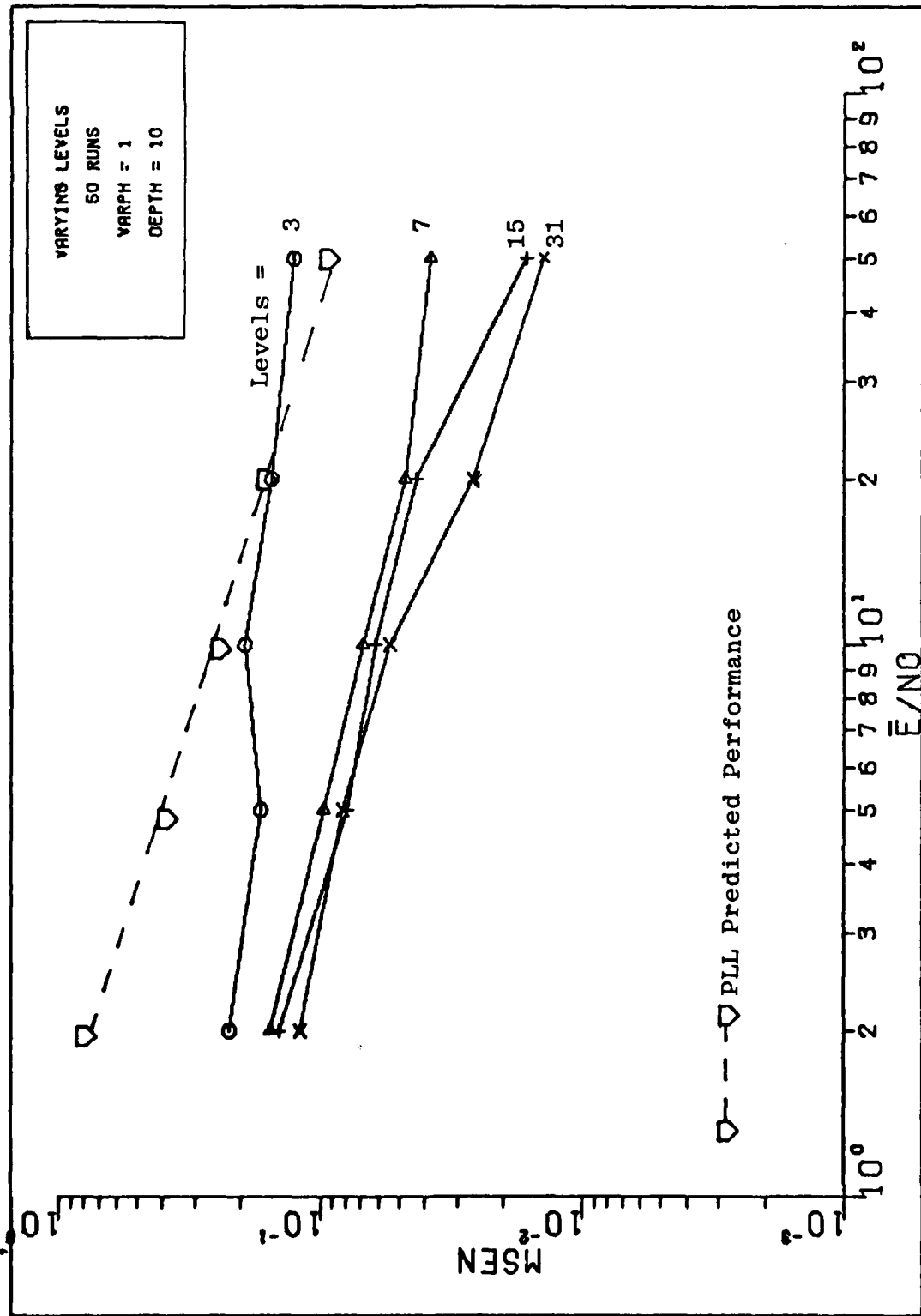


Figure 45 Simulated Estimator Performance versus PLL, Slowly Fading A

estimator provide significant improvements over the PLL.

Similar results are evident for the fading amplitude case when the quantization is over 15 levels. The performance margin of the Viterbi estimator is approximately 10 db better than the PLL. It is important to note that the Viterbi algorithm MAP estimator's performance is achieved under conditions in which the amplitude is allowed to vary from sample to sample. The Rayleigh fading PLL results were limited to a slowly fading signal. It can be expected that the PLL would perform much worse under the rapid fading conditions and eventually lose lock as the fading bandwidth is increased.

VI. Implementation Considerations

This chapter will consider the storage requirements, complexity, and speed requirements for implementation of the Viterbi algorithm for modulo- 2π phase sequence estimation. The problem of correct interpretation of modulo- 2π data will also be discussed.

Storage Requirements

The estimator must store M sequences, $\{\hat{\phi}_k\}_1^K$, one for each of the M phase states. Each sequence contains $K_0 + 1$ floating point numbers representing the estimates of phase over the time interval $(k - K_0)T$ to kT . This is a total of $(M) \cdot (K_0 + 1)$ locations. For each sequence a value of Γ_K must be stored. The current time counter, k , must be stored as well as the $\frac{M+1}{2}$ values of conditional transition probabilities. This gives a total of $Mk_0 + 2M + \frac{M+1}{2}$ permanent storage locations. Temporary storage is necessary for the estimated signal amplitude A_k , the measurement amplitude, C_k , and the measurement argument, ψ_k . Temporary storage will also be required for holding the values of Γ_{k_m} during calculation of the algorithm. This requirement can vary greatly. For example, if all the M values of Γ_{k_m} are computed in parallel, then all M values must be stored until the biggest is picked. On the other hand, if the values of Γ_{k_m} are computed serially, then only the current and "biggest-to-date" values need be

stored. Because of the large time versus storage trade off possible with temporary storage, more definite statements on the requirements are not possible until the specific implementation of the algorithm is selected.

Complexity

This complexity and speed analysis will concern only the serial algorithm stated in Chapter II. It is assumed that a separate processing circuit can select the output value $\hat{\phi}_{k-K_0}$ independent of the algorithm computation. It is also assumed that all possible calculations are made outside of the repetitive algorithm to conserve time.

In order to advance all M sequences one step in time, M values of Γ_k must be computed. For each one, M values of Γ_{k_m} must be computed and $M-1$ magnitude comparisons must be made. The calculation of one value of Γ_{k_m} requires two additions, one subtraction, one cosine calculation, and three multiplies. Memory reference times for fetching values are ignored since dedicated hardware designed for the Viterbi algorithm can greatly optimize these times.

If the times required for the above calculations are defined as follows:

$$\begin{aligned} t_a &= \text{addition or subtraction time} \\ t_m &= \text{multiply time} \\ t_{\text{comp}} &= \text{comparison time} \\ t_{\text{cos}} &= \text{cos}(\cdot) \text{ calculation time} \end{aligned} \tag{97}$$

then the total time to calculate one value of Γ_{k_m} is

$$t_{\Gamma} = 3t_a + t_{\cos} + 3t_m \quad (98)$$

and the total time required to advance all M sequences by one value is

$$\begin{aligned} t_{VA} &= M^2 t_{\Gamma} + M(M-1) t_{\text{comp}} \\ &\approx M^2 (t_{\Gamma} + t_{\text{comp}}) \end{aligned} \quad (99)$$

Therefore, the complexity of the algorithm is KM^2 . This can be computationally unfeasible for large values of M, but is certainly better than the M^K complexity previously described for the global search version of MAP sequence estimation.

Modulo- 2π Data Interpretation

As previously described in the results section of Chapter IV, a phase sequence which is estimated very well modulo- 2π may appear to be quite bad.

One possible solution is to use a mapping function on the estimated phase, $\hat{\phi}$, to produce the display phase ϕ_D . Two example functions are shown in Figure (46).

Both mapping functions will satisfy the requirement that a wraparound of $\hat{\phi}$ from π to $-\pi$ produces very little change in the displayed phase sequence. However, both methods reduce

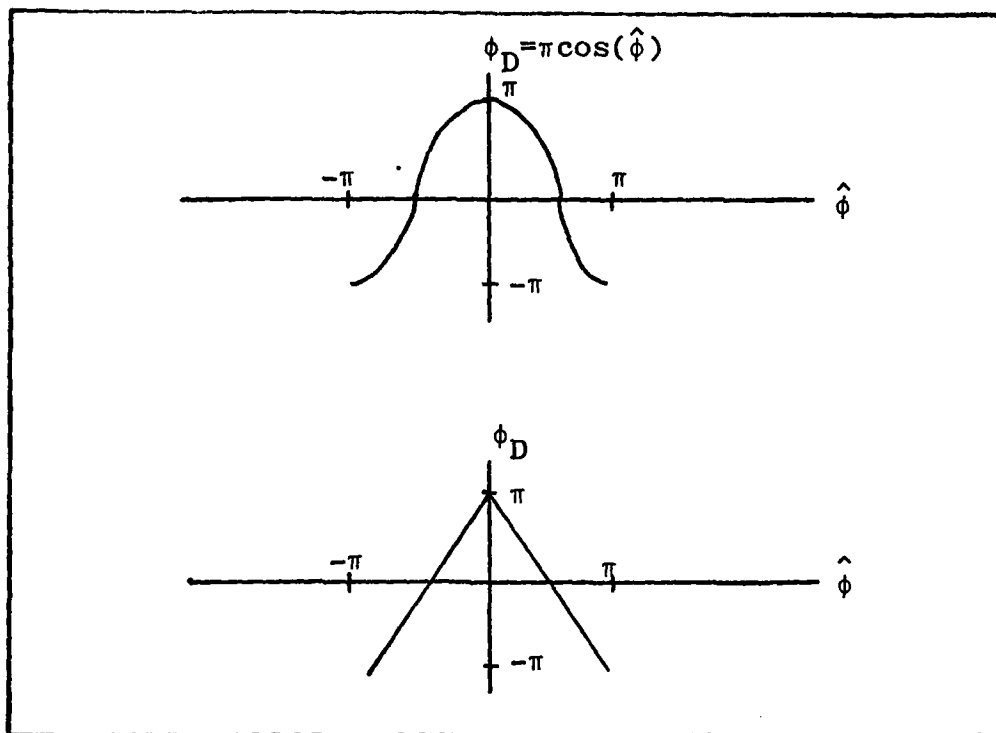


Fig. 46. Display Mapping Functions

the range ambiguity by a factor of two and they tend to accentuate any noise in the phase estimate. In addition, the cosine mapping is nonlinear.

Another possible method to improve the display characteristics is to adjust the phase estimate up or down by 2π radians depending on certain conditions. One method for doing this can be described by the algorithm:

```

For each  $\hat{\phi}_k$ ,  $k=1,2,\dots,k$ 
Begin
  If  $|\hat{\phi}_k| > \text{threshold}$  and  $|\hat{\phi}_{k+1}| > \text{threshold}$ 
  Begin
    If  $|\hat{\phi}_k - \hat{\phi}_{k+1}| > \pi$ 
    Begin
      Adjust  $\hat{\phi}_{k+1}$  up or down by  $2\pi$  to make the
      the sign of  $\hat{\phi}_{k+1}$  equal the sign of  $\hat{\phi}_k$ 
    End
  End
End
End

```

This algorithm simply adjusts the next value of $\hat{\phi}$ up or down by 2π when both the current value and the next value are close to the π or $-\pi$ boundary. As the threshold approaches π , fewer adjustments are made. There will be cases for which the algorithm is "fooled" into making an unwarranted adjustment, but these occurrences can be minimized by proper selection of the threshold.

VII. Conclusions and Recommendations

This report has dealt with the problem of nonlinear phase sequence estimation in the presence of additive white Gaussian noise and Rayleigh fading. Perfect knowledge of each realization of the signal amplitude has been assumed. The problem was motivated by the laser line-scan imagery system developed by the Air Force Avionics Laboratory; however, the estimator and performance indicators derived have a much broader application. This estimator can provide excellent phase sequence estimates for other communications and optics problems in which the phase is dynamically changing and the signal amplitude is rapidly varying.

Conclusions

The modulo- 2π phase sequence Viterbi algorithm estimator with 15 phase quantization levels outperforms a first order PLL operating on a constant amplitude signal by 2-6 dB over the input signal to noise range of 3-17 dB. For each value of the number of quantization levels, there is a value of signal to noise ratio above which the PLL performance is better. This is due to the inherent quantization noise of the Viterbi MAP estimator.

For rapidly fading signals, the Viterbi MAP estimator significantly outperforms a first order PLL. The estimator requires approximately 10 dB less input signal to noise

ratio to equal the performance of a PLL estimating the phase of a signal with slowly fading amplitude. As the fading bandwidth is increased for the PLL estimator, performance rapidly degrades until the PLL loses lock.

Imperfect knowledge of the signal amplitude does degrade the phase estimate by a factor of about two when $E/N_0=2$; however, there is little degradation at higher signal to noise ratios. The fact that the estimator is insensitive to errors in the amplitude estimate is significant because this implies that the assumption of perfect knowledge of the signal amplitude is not critical to the performance predicted in this report.

The performance indicators developed in Chapter IV and extended to the Rayleigh fading case have been validated by the Monte Carlo simulation of the Viterbi estimator. The predicted MSE is accurate when the signal to noise ratio is large or when the number of phase quantization levels is small. As shown by the simulation results, the predicted results are also useful, although not as accurate, for other regions of the data.

The computational complexity of the algorithm is proportional to KM^2 , where M is the number of discrete phase levels and K is the length of the sequence. This compares favorably with the M^K complexity of a global search for the MAP phase sequence.

Recommendations for Further Study

The following areas are recommended for further study.

The statistics on the phase process only assumed a correlation in the direction of the scan. It may be possible to exploit the correlation in two dimensions to improve the phase estimate.

It is recommended that the joint estimation of amplitude and phase be investigated. Solution of the joint problem will eliminate the need for a separate amplitude required by the Viterbi estimator described in this report. In addition, it may be possible to exploit any correlation between amplitude and phase in order to improve the phase estimate.

Filters with sharp cutoffs are often required to reduce the aliasing effects described in Chapter II. These filters often have nonlinear phase responses as a result of the requirement for a sharp cutoff. It is recommended that a model be developed which includes the effects of aliasing. With this model, it can be determined if the filtering requirements can be made less stringent while still maintaining an acceptable level of performance for the phase sequence estimator.

This report considered phase estimation of a signal in white gaussian noise. In optical systems such as this lin-scan imager, quantum noise with point process statistics is a significant part of the overall system noise. It is

recommended that a similar estimator be developed for a signal which includes quantum noise.

The simulation of this estimator has assumed either perfect knowledge of the signal amplitude or perfect knowledge corrupted by gaussian quadrature noise. It is recommended that the actual performance be determined given actual amplitude estimation schemes.

Bibliography

1. Aulin, Tor; Nils Rydbeck; and Carl-Erik Sundberg. "Bandwidth Efficient Digital FM with Coherent Phase Free Demodulation," Proceedings of ICC-79: IEEE, 42.4.1-42.4.6 (1979).
2. Aulin, Tor; and Carl-Erik Sundberg. "M-ary CPFSK Type of Signaling with Input Data Symbol Pulse Shaping-Minimum Distance and Spectrum," Proceedings of ICC-79: IEEE, 42.3.1-42.3.6(1979).
3. Chapuran, Robert C. An Analysis of Modulation Techniques for the Simultaneous Measurement of Range and Reflectance Information by an Airborne Laser Scanner. Master's Thesis Air Force Institute of Technology, Wright-Patterson AFB, Dayton, Ohio, 45433, December 1976, AFIT/GE/EE/76-18, ADA035291.
4. Forney, G. David, Jr. "The Viterbi Algorithm," Proceedings of the IEEE, Vol. 61, No.3: 268-278(March 1973).
5. Gardner, Floyd M. Phaselock Techniques. New York: John Wiley and Sons, Inc., 1966.
6. Lyons, Barry W. A Speckle Noise Model for Optical Heterodyne Line-Scan Imagery. Master's Thesis, Air Force Institute of Technology, Wright-Patterson AFB, Dayton, Ohio, 45433, December 1977, AFIT/GEO/EE/77-4, ADA 053350.
7. Papoulis, Athanasios. Probability, Random Variables, and Stochastic Processes. New York: McGraw-Hill, Inc., 1965.
8. Rife, David C. and Robert R. Boorstyn. "Single-Tone Parameter Estimation from Discrete Time Observations," IEEE Transactions on Information Theory, Vol. IT-20, No.5:591-598(September 1974).
9. Scharf, Louis L., et al. Modulo- 2π Phase Sequence Estimation. ONR Technical Report #27. Colorado State University, Fort Collins, Colorado, February 1978.
10. Strautman, William D. Spatial Filtering Design Considerations for a Laser Line Scanning Sensor. Master's Thesis, Air Force Institute of Technology, Wright-Patterson AFB, Dayton, Ohio, 45433, December 1977, AFIT/GEO/EE/77-6, ADA 056503.

11. Van Trees, Harry L. Detection, Estimation, and Modulation Theory, Part I. New York: John Wiley and Sons, Inc., 1968.
12. Viterbi, Andrew J. Principles of Coherent Communication. New York: McGraw-Hill Book Company, 1966.
13. Weber, William J., III. "Performance of Phase-Locked Loops in the Presence of Fading Communication Channels," IEEE Transactions on Communications, Vol. COM-24, No. 5: 487-499 (May 1976).
14. Wozencraft, John M., and Irwin M. Jacobs. Principles of Communication Engineering. New York: John Wiley and Sons, Inc., 1965.

VITA

David E. Meer was born on 15 April 1949 in Iowa City, Iowa. He attended the University of Iowa in Iowa City and graduated with a B.S.E.E. with honors in June, 1972. Upon graduation, he received a commission in the USAF through AFROTC. Prior to active duty, he worked as an Electronic Engineer for the University of Iowa Physics Department on their Helios, IMP, and Hawkeye satellites. After entering active duty, his first assignment was to the Communications Electronics Engineering School at Keesler AFB, Mississippi. Upon completion, he served as Maintenance Supervisor for the AN/FSS-7 Sea Launched Ballistic Missile Detection and Warning Radar for Det 4, 14 Missile Warning Squadron, Mt. Laguna AFS, California. In May 1975, he was assigned to the 1961st Communications Group, Clark Air Base, Republic of the Philippines. He served as Tactical Communications Engineer and head of the Mobile Communications Division until being assigned to the School of Engineering, Air Force Institute of Technology in June 1978.

Permanent address: 1305 Franklin
Iowa City, Iowa 52240

REPORT DOCUMENTATION PAGE		READ INSTRUCTIONS BEFORE COMPLETING FORM
1. REPORT NUMBER AFIT/GE/EE/79D-24	2. GOVT ACCESSION NO.	3. RECIPIENT'S CATALOG NUMBER
4. TITLE (and Subtitle) PHASE SEQUENCE ESTIMATION FOR LASER LINE- SCAN IMAGERY IN THE PRESENCE OF RAYLEIGH FADING		5. TYPE OF REPORT & PERIOD COVERED MS Thesis
		6. PERFORMING ORG. REPORT NUMBER
7. AUTHOR(s) David E. Meer, Capt, USAF		8. CONTRACT OR GRANT NUMBER(s)
9. PERFORMING ORGANIZATION NAME AND ADDRESS Air Force Institute of Technology AFIT/EN Wright-Patterson AFB, Dayton, OH 45433		10. PROGRAM ELEMENT, PROJECT, TASK AREA & WORK UNIT NUMBERS
11. CONTROLLING OFFICE NAME AND ADDRESS Air Force Avionics Laboratory/RWI Wright-Patterson AFB, Dayton, OH 45433		12. REPORT DATE December 1979
		13. NUMBER OF PAGES
14. MONITORING AGENCY NAME & ADDRESS (if different from Controlling Office)		15. SECURITY CLASS. (of this report)
		15a. DECLASSIFICATION/DOWNGRADING SCHEDULE
16. DISTRIBUTION STATEMENT (of this Report) Approved for public release; distribution unlimited.		
17. DISTRIBUTION STATEMENT (of the abstract entered in Block 20, if different from Report)		
18. SUPPLEMENTARY NOTES Approved for public release; IAW AFR 190-17 JOSEPH P. HIPPS, Maj, USAF Director of Public Affairs		
19. KEY WORDS (Continue on reverse side if necessary and identify by block number) Phase Estimation Laser Line Scanning Fading Rayleigh Fading Viterbi Algorithm Maximum a Posteriori		
20. ABSTRACT (Continue on reverse side if necessary and identify by block number) An airborne laser line-scan imaging system can determine the relative range to a target by power modulation the illuminating laser and detecting the relative phase of the reflected signal with respect to the modulation phase reference. The amplitude of the reflected signal may fluctuate greatly due to such factors as speckle noise and the varying reflectivity of the target, resulting in the severe degradation of performance of commonly used		

block 20 continued:
phase detection circuitry.

In this report, a maximum-a posteriori (MAP) phase sequence estimator is developed based upon the Viterbi algorithm. The signal is observed in additive, zero mean, white Gaussian noise and the statistics of the amplitude are assumed to be Rayleigh. Perfect knowledge of each realization of the signal amplitude is assumed and the sensitivity to errors in the amplitude estimate is investigated. Expressions for approximate mean-squared error and a lower bound on mean-squared error are developed and verified by a Monte Carlo simulation of the estimator.

For quantization of the phase estimates to 15 levels and for a signal with constant amplitude, the estimator outperforms a first order phase-locked-loop (PLL) by 2-6 dB over the range of input signal to noise ratios of 3-17 dB.

For the case when the amplitude is rapidly fading, the estimator outperforms a first order PLL by greater than 10 dB. This performance margin is based on the Viterbi estimator's performance for a rapidly fading signal compared to PLL performance for a slowly fading signal. Note that as the amplitude fading bandwidth of the PLL signal is increased, the PLL will lose lock completely, so that the improvement margin presented is extremely conservative.

The Viterbi estimator is shown to be insensitive to errors in the estimate of the signal amplitude for input signal to noise ratios larger than 2 (3 dB). The MAP sequence estimator is also shown to reduce its mean-squared error with increasing decision depth (fixed lag of the Viterbi algorithm), and increasing number of discrete phase levels. The performance depends weakly on the match between the variance of the actual phase and the variance assumed by the estimator.